MAGNETIC RESONANCE IMAGING GUIDED NEUROMODULATION OF GASTRIC PHYSIOLOGY

by

Kun-Han Lu

A Dissertation

Submitted to the Faculty of Purdue University

In Partial Fulfillment of the Requirements for the degree of

Doctor of Philosophy

School of Electrical and Computer Engineering

West Lafayette, Indiana

May 2019

THE PURDUE UNIVERSITY GRADUATE SCHOOL
STATEMENT OF COMMITTEE APPROVAL

Dr. Zhongming Liu, Ph.D., Chair
Weldon School of Biomedical Engineering
School of Electrical and Computer Engineering
Dr. Terry L. Powley, Ph.D.
Department of Psychological Sciences
Dr. J. Paul Robinson, Ph.D.
Weldon School of Biomedical Engineering
Dr. Joseph V. Rispoli, Ph.D.
Weldon School of Biomedical Engineering

Approved by:
Dr. Pedro Irazoqui
Head of the Graduate Program

For my wife and family.

ACKNOWLEDGMENTS

I am sincerely grateful to those who have helped make me who I am today during my PhD Journey. Firstly, I would like to express my deepest gratitude to my advisor and mentor, Dr. Zhongming Liu, who has brought me into the field of MRI, neuroscience, and neural engineering. Without his guidance, encouragement, advice and exceptional support throughout the program, I would not have been able to achieve what I have accomplished so far. He not only mentors me in developing necessary scientific thinking and analytical skills in order to become a successful PhD, but also continuously cultivates me in building communication and writing skills that would have a life-long positive impact in my research career. Secondly, I would like to thank my thesis committee members, Dr. Terry L. Powley, Dr. J. Paul Robinson and Dr. Joseph V. Rispoli, for their encouragement, constructive feedback, and mentorship over these past few years.

I would also like to take this opportunity to thank my current and former colleagues in the Laboratory of Integrative Brain Imaging as well as other research collaborators. Thank you Dr. Haiguang Wen, Dr. Lauren Lynch, Mr. Jun Young Jeong, Mr. Junxing Shi, Mr. Steven Oleson, Mr. Nishant Babaria, Ms. Jiayue Cao, Ms. Yizhen Zhang, Mr. Ranajay Mandal, Mr. Jung-Hoon Kim, Mr. Kuan Han, Mr. Minkyu Choi, Ms. Xiaokai Wang and Ms. Yuanhanqing Huang for your insightful discussions, critical feedbacks, and experiments help throughout the past five years. Thank you Dr. Robert Phillips and Dr. Deborah Jaffey for the collaborative support and resources you offered in the SPARC project. Thank you Dr. Georgia Malandraki for engaging me in your cerebral palsy studies, which helps me see the critical need in providing engineering solutions to serious medical problems. I also appreciate the help from many others with whom I have worked during the past five years.

Last but not least, from the bottom of my heart, I would like to express my appreciation to my wife, Catharine Lory, for her love, support and patience during the ups and downs in my work and life, and to my parents, Che-Min Lu and Pi-Chuan Yu, who have provided me unconditional support and love for helping me become who I am today.

TABLE OF CONTENTS

LIST OF TABLES

LIST OF FIGURES

ABSTRACT

Author: Lu, Kun-Han. Ph.D.
Institution: Purdue University
Degree Received: May 2019
Title: Magnetic Resonance Imaging Guided Neuromodulation of Gastric Physiology
Committee Chair: Dr. Zhongming Liu, Ph.D.

The stomach is a digestive organ in the gastrointestinal tract that regulates food intake and paces digestion of nutrients and fluids. The emptying and motility patterns of the stomach are crucial rate-determining processes in maintaining energy homeostasis in the body. Dysregulation of gastric functions often leads to distressing conditions such as gastroesophageal reflux diseases, functional dyspepsia, gastroparesis and obesity. Gastric disorders affect more than 60 million people in the US, producing significant medical and economic burden. These diseases are often chronic and greatly compromise quality of life. As the causes of these diseases remain largely unknown, effects of current pharmacological, dietary, or surgical treatments are often dismal. In this regard, neuromodulation of peripheral nerves emerges as a promising electroceutical therapy for remedying gastric disorders. However, therapeutic effects were shown to be modest, largely due to the inability to validate or calibrate the efficacy and stability of neuromodulation methods with appropriate physiological readouts. To address these problems, here I developed a non-invasive, repeatable online high-resolution magnetic resonance imaging protocol, empowered with advanced image processing algorithms, to track gastric emptying, antral motility, pyloric motility, intestinal filling and absorption in a rat model. The protocol can be used to guide tuning and optimization of stimulation parameters of neuromodulation without perturbing ongoing and spontaneous physiology. The proposed technology and findings are expected to pave the way for the use of gastric MRI to evaluate the efficacy of therapeutics in treating gastric disorders under both preclinical and clinical settings.

1. INTRODUCTION

1.1 Overview

The stomach is a digestive organ in the gastrointestinal (GI) tract that regulates food intake and paces digestion of nutrients and fluids. The emptying and motility patterns of the stomach are crucial rate-determining processes in maintaining energy homeostasis in the body. Dysregulation of gastric functions often leads to distressing conditions such as gastroesophageal reflux diseases (GERD), functional dyspepsia, gastroparesis and obesity. In 2010, it was reported that gastric diseases collectively had affected more than 60 million people in the United States, producing significant medical and economic burden of over 97 billion dollars [1], [2]. These diseases are often chronic and greatly compromise quality of life. As the cause of these diseases remain largely unknown, effects of current pharmacological, dietary, or surgical treatments are often dismal [3]. With the alarming epidemic growth of gastric diseases, the need to develop next-generation diagnostic tools and biomedical treatments has become especially critical and urgent.

Proper functioning of the stomach requires the coordination of both regional enteric system and neural signals descending from the brain via the vagus nerve [4]–[6]. For this reason, researchers have begun to explore electrical stimulation of the gastric smooth muscle or the vagus nerve as an alternative strategy to remediate gastric disorders [7]. However, therapeutic outcomes remain modest largely due to inability to validate or calibrate the efficacy and stability of neuromodulation methods with appropriate physiological readouts. Such technical hurdles necessitate a comprehensive and ideally non-invasive method to characterize the stimulus-response relations. Notably, the assessment should be applicable to both human and preclinical animal models, as fundamental knowledge about the gastric physiology and pathology often results from animal studies, and new therapeutics are typically tested first in animal models before clinical trials.

The overarching objective of this dissertation is two-fold. First, a novel and reliable contrast-enhanced magnetic resonance imaging (MRI) technique was developed to advance assessment of GI functions in a rodent model. This MRI technique offers high spatial and temporal resolution and is further empowered by computer-assisted image processing pipelines to streamline the analysis of gastric MRI data for quantitative and objective characterization of gastric

functions. This imaging-based assessment provides an unprecedent opportunity to non-invasively monitor overall GI transit, gastric and its compartmental emptying, antral motility, pyloric motility, and intestinal filling and absorption. The MRI acquisition and analysis techniques are readily translational to humans. Second, this MRI-based assessment of gastric physiology was used to guide the tuning and optimization of stimulation parameters of neuromodulation without perturbing ongoing and spontaneous physiology. The proposed experimental protocol and findings are expected to pave the way for the use of gastric MRI to evaluate the efficacy of therapeutics in treating gastric disorders under both preclinical and clinical settings.

1.2 Introduction to Anatomy and Function of the Stomach

The stomach is a muscular, hollow organ in the gastrointestinal tract that connects between the esophagus and the small intestines (Figure 1.1). Anatomic regions of the stomach in humans include the fundus, corpus, antrum and pylorus. In small animal models like rodents, the stomach can be divided into the forestomach, the corpus, and the antrum (Figure 1.2). The stomach is distensible such that it can vary in volume. The volume of a near empty stomach in adult humans is about 75 ml, and it can expand to accommodate more than 1 liter of food [8]. There are two sphincters (ring of muscle) that keep the food within the stomach. The lower esophageal sphincter connects between the esophagus and the body of the stomach, and the pyloric sphincter is at the junction between the stomach and the duodenum. The role of lower esophageal sphincter is to prevent the gastric content from reflux back into the esophagus, whereas the function of the pyloric sphincter is to control the rate of food empty into the duodenum. Functionally speaking, the stomach can be coarsely divided into the gastric reservoir and the gastric pump. The fundus and the proximal corpus act as a reservoir that stores the ingested foodstuff, whereas the gastric pump includes the distal corpus and the antrum in which mechanical contractions waves are present. The physiological role of these two functionally distinct regions will be introduced in detail in the following section.

1.3 Physiology of the Stomach

After the food is being chewed and ingested in the mouth, the swallowed food enters the esophagus and is pushed into the forestomach by peristaltic contractions of the esophageal muscles.

This event happening in the mouth and the pharynx triggers neural reflexes into the central nervous system [9], [10], resulting in a downstream motor signaling to the gastric reservoir that causes relaxation in order to accommodate the incoming food. This process is primarily mediated by the vagus nerve, hence it is also termed vagovagal reflex [11]. This receptive relaxation allows the stomach to relax as it fills with food without stretching forcefully and increasing tension. By this regulation the gastric reservoir is prepared as a storage for the food. It is not until the food is thoroughly broken down into smaller particles (i.e. chyme) for emptying into the duodenum will the gastric reservoir exert a tonic contraction to evacuate the digesta.

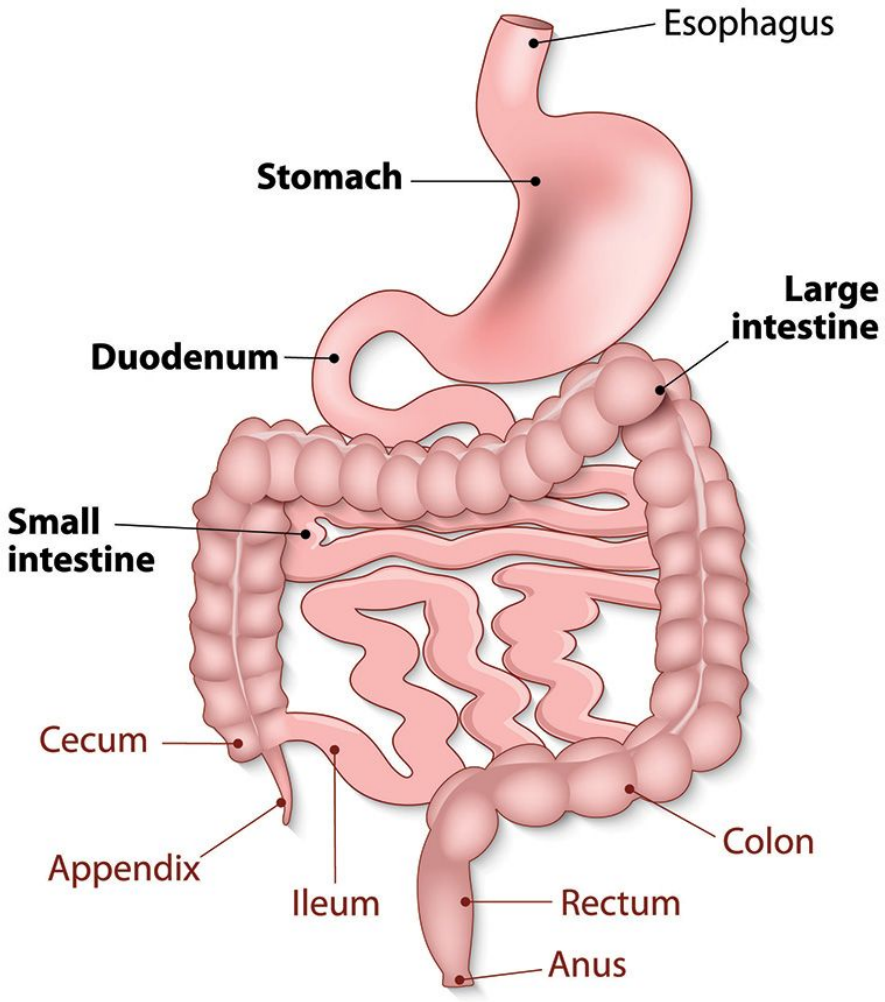

Figure 1.1 **Illustration of the human gastrointestinal (GI) tract.** The GI tract comprised of the esophagus, stomach, small intestine, large intestine, colon and the rectum (This figure is modified from an image created by MU Health Care from https://www.muhealth.org/conditions-treatments/surgical/bariatric-surgery/getting-started/anatomy-and-function-of-the-gi-tract).

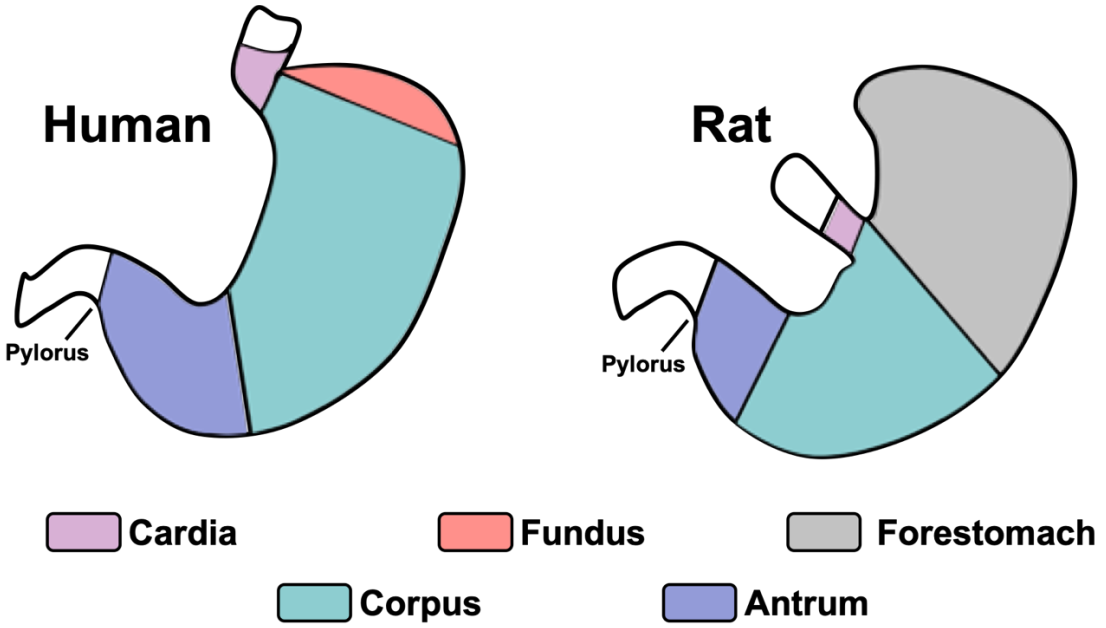

Figure 1.2 **Anatomic regions of the stomach of human and rat.**

While the motility of the gastric reservoir is mainly tonic, the gastric pump utilizes phasic, forceful peristaltic waves to grind large food particles into smaller chyme. When the chyme is sufficiently small, it will be propelled through the pyloric sphincter and enters the duodenum for further absorption. The peristaltic waves are induced by electrical events originating from a class of pacemaker cells, Interstitial cells of Cajal (ICC), situated on the gastric wall [12]. Due to the oscillations in the membrane potential of these interstitial cells, electrical pacesetter potentials are generated at certain frequency. The oscillatory frequency of the pacesetter potential differs among species. For humans, such frequency is about 2 to 3 cycles per minutes, whereas the frequency is about 5-6 cycles per minute in rodents. These pacesetter potentials generated from ICCs spread to surrounding smooth muscle cells and induce electrical events called the slow wave. The slow wave typically propagates from the proximal stomach to the distal stomach, regardless of the occurrence of peristaltic contraction waves (Figure 1.3). Nevertheless, slow wave determine the maximal frequency and the propagating velocity of the peristaltic contraction waves [13]. When the amplitude of the slow wave exceeds a certain threshold, spike potentials occur. This is due to activation of L-type voltage-gated calcium channels, which results in calcium influx to these smooth muscle cells and thus induces electro-mechanical coupling. The level of threshold is in part being modulated by excitatory neurotransmitters, one of which is known to be acetylcholine.

The higher the release of acetylcholine, the more pronounced the contractile activity will be. Generally, the peristaltic waves at the gastric corpus are shallow, and the waves become deeper as they propagate to the gastric antrum.

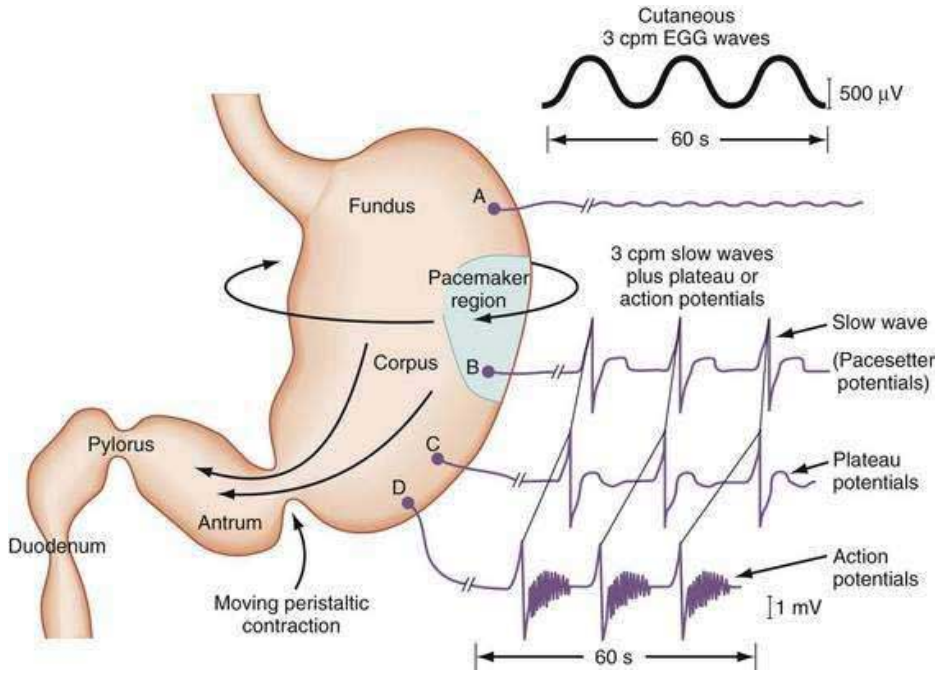

Figure 1.3 **Gastric slow wave recorded from electrodes positioned on the serosa of the stomach from the fundus (A) to the antrum (D).** The propagation of the slow wave is revealed as phase delays between signals recorded at different locations. The frequency of gastric slow wave in humans is approximately 3 cycles/minute. When the pacesetter potential exceeds a certain threshold, action potentials are generated and the smooth muscle cells are depolarized thus mechanical contractions occur (This figure is modified from Abdominal Key: https://www.abdominalkeys.com).

Both gastric reservoir and gastric pump play an essential role in digestion and emptying. When the digesta is present in the stomach, the parietal cells are activated and gastric acid is secreted into the gastric lumen. Gastric acid is necessary for protein digestion, elimination of allergenicity of food, prevention of bacterial overgrowth, and maintenance of stable intra-gastric environment [14]. When the digesta is thoroughly mixed with the secretory products, the chyme is formed. Then, the peristaltic waves propel chyme towards gastric antrum for further break down until it is sufficiently small to pass through the pyloric sphincter. This emptying process is achieved not only by the gastric pump but also from the tonic force exerted by the gastric reservoir. The tone of the gastric reservoir, the depth of the constriction of the peristaltic waves, the degree of pyloric opening, the resistance of the duodenum, and the coordination between all abovementioned

factors govern the rate of gastric emptying (Figure 1.4). In healthy humans, a coordinated gastric emptying pattern should consist of 1) fundic accommodation after food ingestion, 2) peristaltic propulsion of food from fundus to antrum, 3) trituration of food by the peristaltic waves, 4) tonic contraction of the reservoir coordinated by the enteric nervous system, 5) transpyloric flow by coordinated pyloric relaxation, and 6) antroduodenal coordinated emptying. Impaired fundic accommodation, gastric dysrhythmia, shallow peristaltic waves of antral motility, pylorospasm, to name a few, are factors that would eventually lead to delayed emptying.

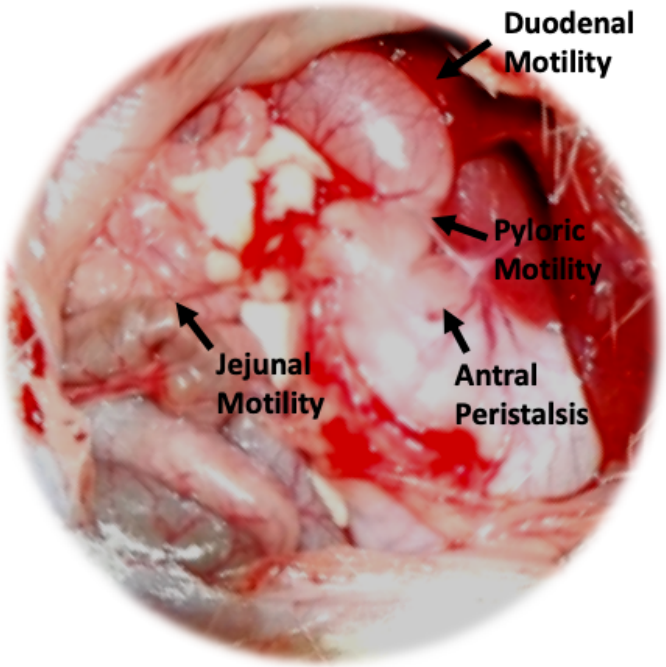

Figure 1.4 **Illustration of gastrointestinal motility in rats**

1.4 Past Methods to Assess Gastric Physiology

The assessment of motor function of the stomach is essential to understanding gastric physiology and pathophysiology. To date, evaluation of gastric functions can be broadly categorized into gastric accommodation, gastric emptying, gastric motor contractility, and myoelectrical activity. The currently available methods for measuring these gastric functions can be further classified into 1) invasive and noninvasive, 2) direct and indirect approaches. This section will review the methods that are most commonly employed in clinical and research settings [15].

1.4.1 **Gastric Barostat Technique**

As elaborated in the previous section, proper gastric accommodation requires the stomach to gradually relax during ingestion of a meal while maintaining low intragastric pressure (tone). Dysregulation of such process often leads to disease states such as functional dyspepsia. The gold standard for directly measuring proximal gastric tone is the gastric barostat technique [16]. To measure changes in gastric tone, a latex balloon that is attached to a double-lumen tube is inserted orally into the esophagus and placed in the proximal stomach (Figure 1.5). The barostat keeps a constant pressure in the balloon by infusion or aspiration of air/water in accordance to the relaxation or contraction of gastric tone. As such, the inflation or deflation in volume of the balloon can be used to estimate the gastric wall tension. Gastric barostat has not only been applied to humans but also to large animals (e.g. cats, pigs, rabbits, and horses) and rodents for studying the effect of neural and pharmaceutical compounds on gastric accommodation [17]–[20]. The major drawback of the barostat technique is its invasive intubation and the placement of the intragastric balloon in the stomach. The balloon by itself acts like a "bolus", which alters the true physiology of the stomach. The invasive nature of this test often makes patients stressful and uncomfortable.

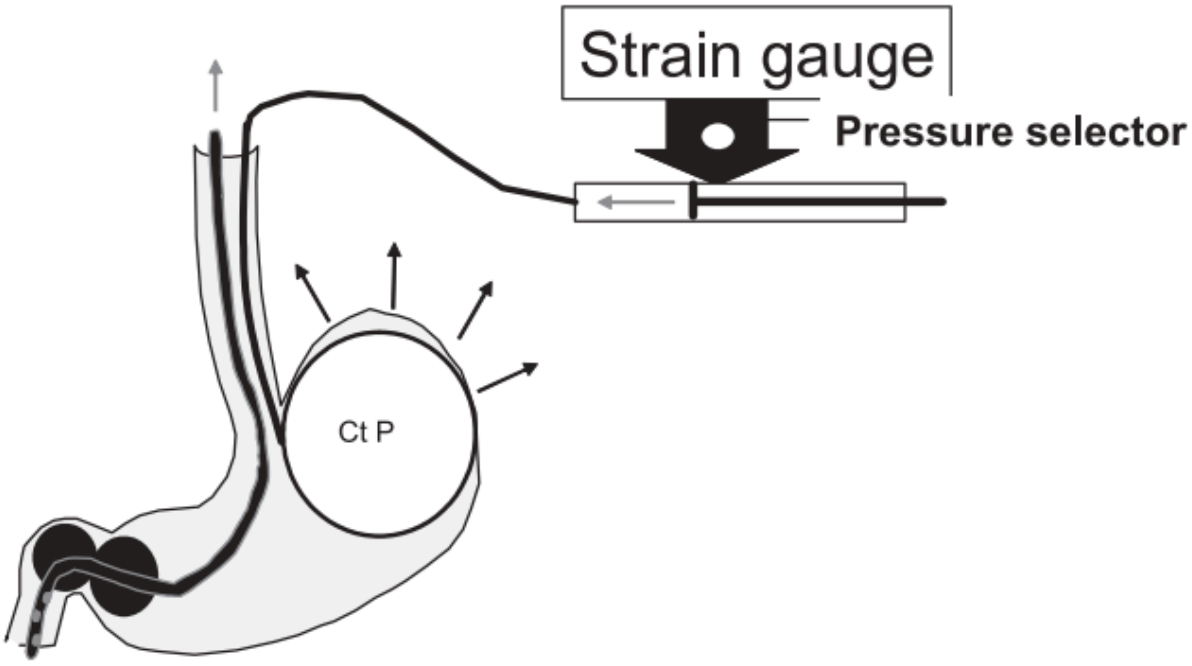

Figure 1.5 **Illustration of the gastric barostat device.** An intragastric balloon is intubated into the proximal stomach. The balloon is filled with air or water and maintained at constant pressure. Whenever the proximal contracts or relaxes, the deflation or inflation of the balloon will allow the user to readout the corresponding intragastric pressure change. This figure is adapted from [16].

1.4.2 **Gastric-emptying Scintigraphy**

Gastric-emptying scintigraphy is the most widely used method for measuring stomach's ability to empty food. It is also the current gold standard for diagnosing gastroparesis. To estimate gastric emptying rate, subject is required to consume a test meal that is labeled with radioactive isotope. The American Neurogastroenterology and Motility Society and the Society of Nuclear Medicine recommended a eating protocol that comprised of a low-fat, egg-white meal and scintigraphy imaging is performed at different times after meal ingestion [21]. The egg-white meal consists of 2 large eggs, 2 slices of bread, and jam with water that is labeled with technetium-99m sulfur colloid. After meal ingestion, two-dimensional gamma camera images are acquired to detect gamma radiation from the radiolabeled meal. Quantification of volume of gastric content is typically performed by manually drawing region of interests that cover all the radioactivity in the abdomen, as illustrated in Figure 1.6. Delayed gastric emptying is diagnosed if there is >90% gastric retention at 1 hour, >60% at 2 hours, and >10% at 4 hours [22]. Although gastric-emptying scintigraphy provides a direct and non-invasive measure of gastric volume, there are several drawbacks related to this approach. First, subjects are exposed to radiation, which in turn limits it use for repeated measures. Limited data points could be obtained over the course of several hours. Healthy children and pregnant women are advised to avoid undergoing scintigraphy. Second, the images are typically two-dimensional, making interpretation of the three-dimensional geometry of the stomach difficult. Lastly, the temporal resolution of this imaging technique is not sufficient to capture the motility of the gastric pump, thus limiting its use for measuring gastric volume only.

1.4.3 **^{13}C Isotope Breath Test**

The breath test can non-invasively monitor the gastric emptying rate without exposing the subject to radiation. The ^{13}C isotope is first bound to digestible compounds such as octanoic acid, then the ^{13}C isotope octanoic acid is mixed with either a solid or a liquid meal. After the ^{13}C isotope -labeled meal is ingested into the stomach and absorbed in the proximal small intestine, it will be metabolized by the liver and converted into ^{13}C-CO_2. The rate of gastric emptying is then estimated by a rise in the amount of ^{13}C-CO_2 excreted from the lungs. Although it is an indirect measurement, it has been demonstrated that the gastric emptying rate measured with ^{13}C isotope breath test is reliably similar to that obtained from gastric-emptying scintigraphy [23], [24]. However, the breath

test neither informs gastric anatomy nor gastric motility. Moreover, it has been suggested that patients with celiac disease or cirrhosis are not suitable for undergoing this test due to defect in metabolizing octanoate into CO_2 [22].

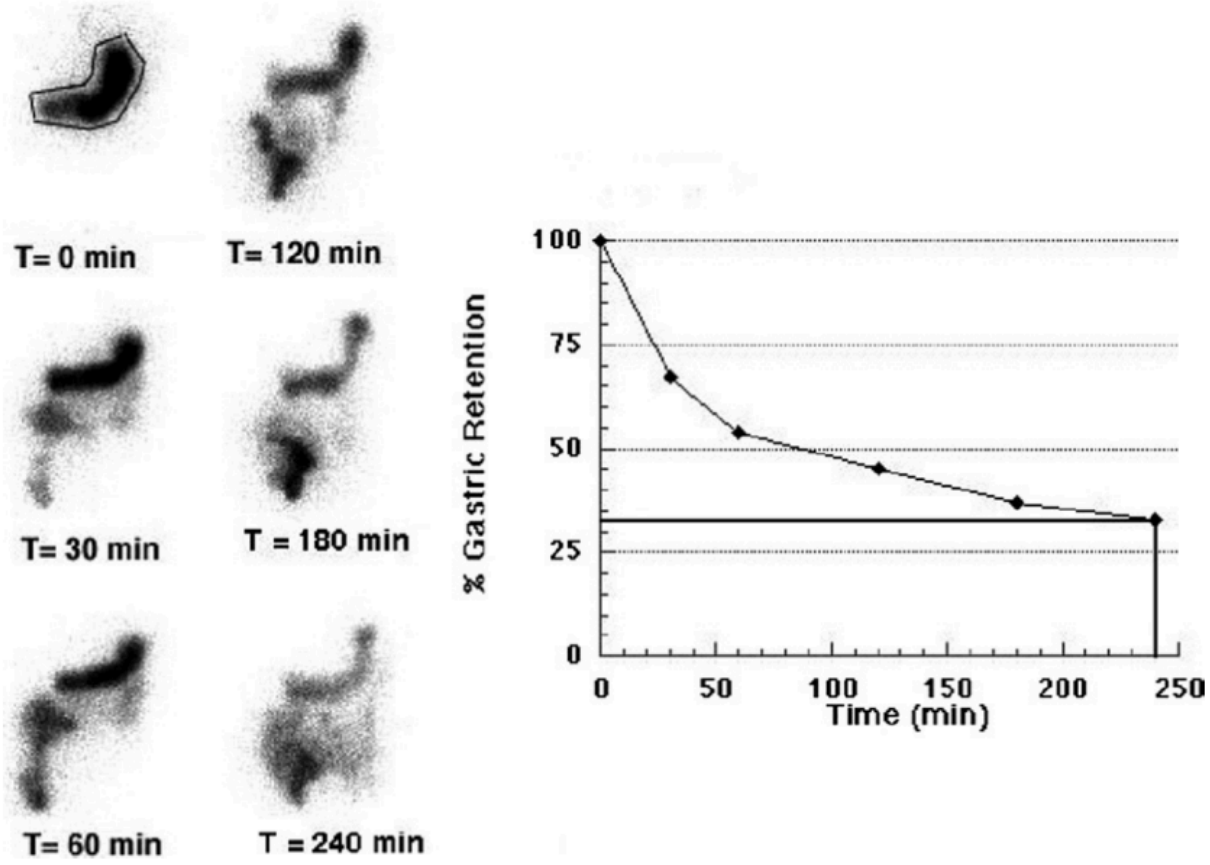

Figure 1.6 **Gastric scintigraphy images obtained from a patient with delayed emptying.** Left panel: gamma radioactive images outlining the geometry of the GI tract. At T = 0, the density of radiation is highest and the contour of the stomach can be manually delineated. As T progresses to later in the experiment, the density of radiation attenuates due to decay in the half-life of the radiolabeled material. This figure is adapted from [22].

1.4.4 **Antropyloroduodenal Manometry**

Manometric recordings is the most commonly used method for directly measuring antral, pyloric, and/or duodenal motility in pre-prandial or post-prandial states through pressure measurements [25]. With the aid of endoscopy, a water-perfused catheter with pressure sensors is properly positioned in the gastric antrum, pyloric sphincter, or the duodenal bulb to measure contractile activity [26]. The manometry could help identify any abnormalities in the coordination

and magnitude of muscle contractions in the stomach and the duodenum (Figure 1.7). The apparent disadvantage is its invasiveness and proper placement of the sensor is often technically cumbersome. Moreover, it is not unlikely that place the catheter in the antropyloroduodenal region would disturb normal gastric physiology, especially during the postprandial state when the stomach is loaded with food.

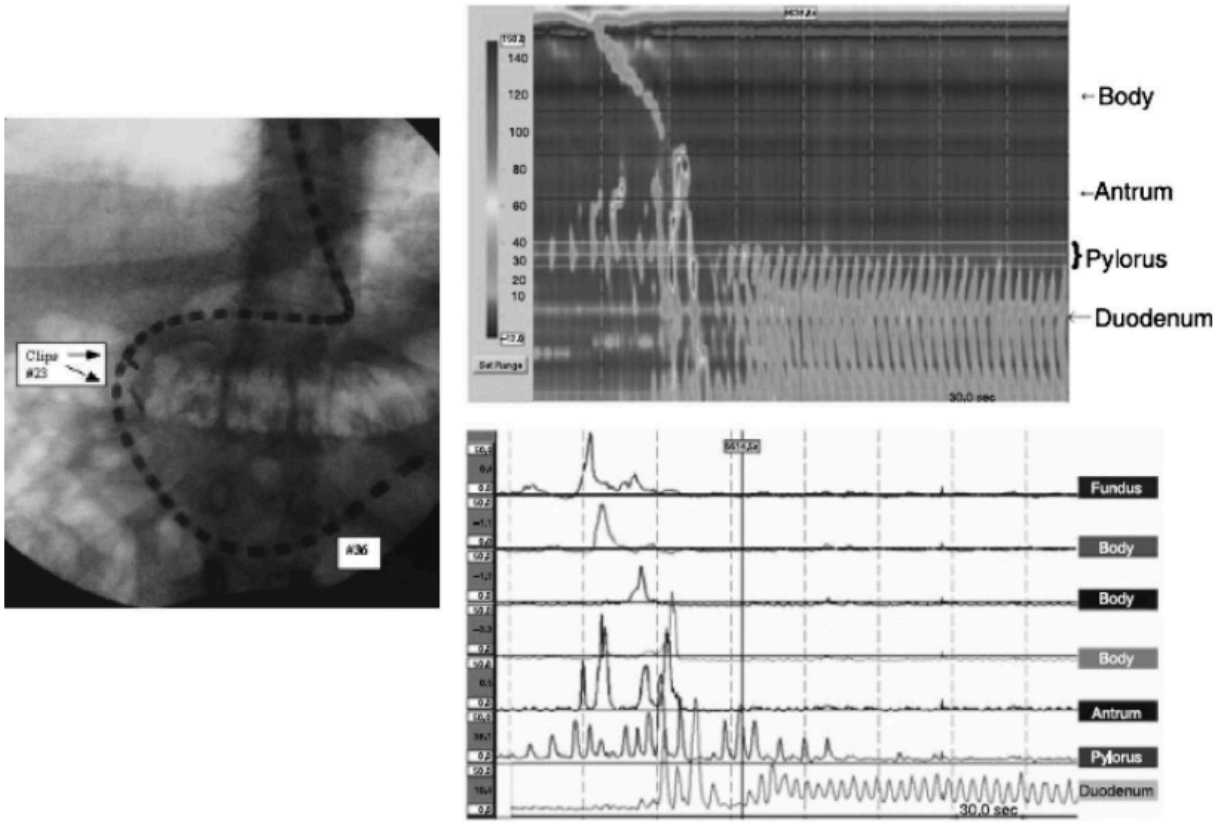

Figure 1.7 **Illustration of antropyloroduodenal manometry.** The panel on the left shows a fluoroscopic image that captures the position of the manometric catheter. The panel on the right shows the pressure events along the GI tract. This figure is adapted from [27]. The original figure was created by [26].

1.4.5 **Ultrasonography**

Transabdominal ultrasonography is a widely used non-invasive imaging method to assess anatomic and functional properties of abdominal organs. Two-dimensional ultrasonography has been used to capture antral motility by observing a cross-sectional change at the gastric antrum [28]. On the other hand, three-dimension ultrasonography has also been applied to calculate gastric

volume and intragastric meal distribution [29]. Further, the use of doppler ultrasound allows the physician to monitor transpyloric flow of the meal exiting the stomach [30] (Figure 1.8). Although ultrasonography is a simple, non-invasive, and widely available imaging tool, it suffers from a number of drawbacks. First, proper operation of the ultrasound probe and identification of gastric anatomy requires considerable technical experience. Second, the quality of ultrasonic images is often degraded by speckle noise and artifacts, making interpretation and quantitative assessment of gastric motility difficult.

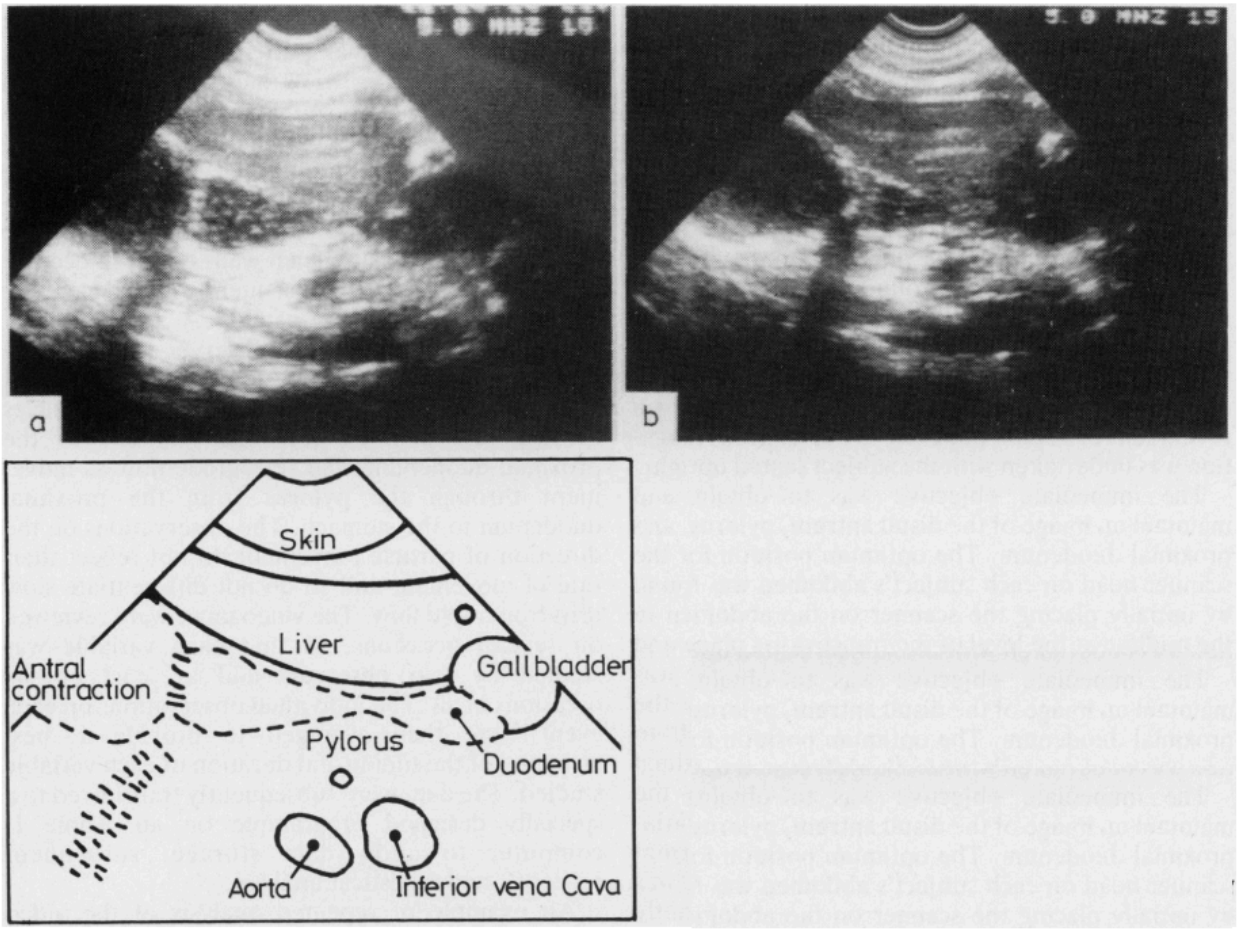

Figure 1.8 **Illustration of ultrasonography revealing antropyloroduodenal motility.** This figure is adapted from [30].

1.4.6 **Electrogastrography**

Electrogastrography (EGG) is a method to measure gastric myoelectrical activity. Electrogastrogram can be obtained from the gastrointestinal mucosa, serosa, or skin surface,

therefore the method itself can be invasive or non-invasive, depending on the placement of the electrode (Figure 1.9). The EGG signals reflect the frequency, amplitude and the power of the electrical slow wave activity. EGG recordings can be performed under both fasting or after a meal with the subject lying down without gross movements. For cutaneous EGG, a number of surface electrodes (typically 3~4 electrodes) is attached to the abdominal surface according to a standardized protocol [31]. However, there is no consensus on the optimal placements of the electrodes, because the location, displacement, and geometry of stomach highly vary across individuals. Moreover, the electrical conductivity profile further complicates the relationships between the electrical events on the gastric wall and the cuteneous EGG signals. Abnormality in slow wave activity such as bradygastria or tachygastria can be identified from frequency analysis of the EGG signals. More recently, by utilizing an array of surface electrodes, the propagation pattern and propagation velocity of the slow waves can be revealed by modeling the relationships between EGG signals measured with different electrodes [32]. However, EGG is an indirect measure of gastric motility, leaving the mechanical contractile activity undescribed, although a correlation between EGG and scintigraphy [33], manometry [34], or ultrasound [35] has been reported.

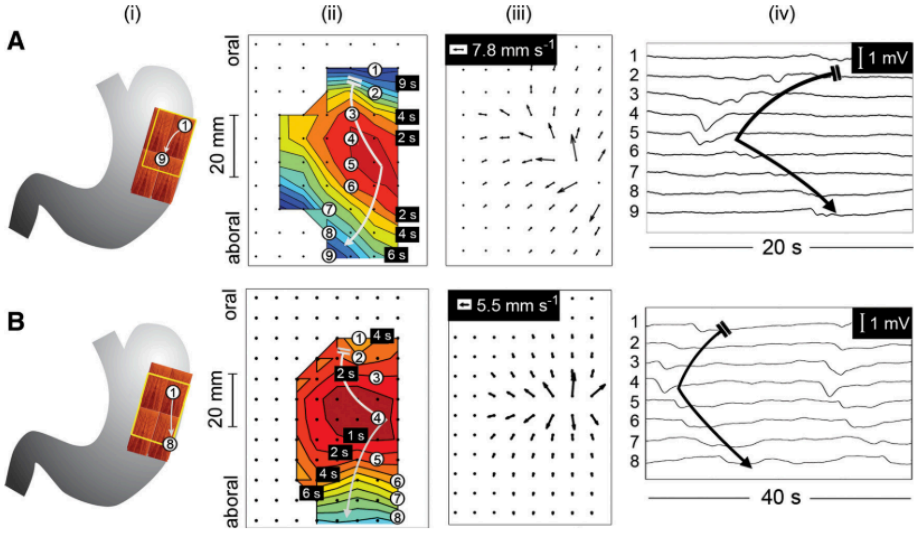

Figure 1.9 **Illustration of EGG recordings and analysis of propagation of the slow wave.** This figure is adapted from [32].

1.4.7 **Magnetic Resonance Imaging**

Magnetic resonance imaging is an emerging imaging modality to for direct imaging GI anatomy and function with excellent soft-tissue contrast and high spatial resolution, though it is yet frequently used in clinical practice. Initial applications of gastric MRI in humans have demonstrated its unique potential for non-invasive assessment of gastric emptying, intra-gastric distribution, and antral and duodenal motility, to name a few. A more detailed review on current application of MRI to assessing GI functions will be discussed in Chapter 2. The main disadvantages of this MRI-based assessment include 1) relatively high cost, 2) the imaging sequences and test meals used to evaluate gastric functions are not standardized, 3) quantitative analysis of large amount of imaging data still require a significant amount of manual processing, which is labor intensive and thus limits its throughput. Despite its expensive cost, one should also recognize the capability of MRI that multiple information could be obtained within a single study session (i.e. gastric emptying and gastric motility).

1.5 Concurrent Treatments for Gastric Disorders

Delayed emptying, also known as gastroparesis, is one of the most prominent gastric disorder that affects more than 25% of the US population [36]. Characterization of gastroparesis is by revealing slow emptying of food from the stomach to the small intestines without apparent mechanical obstruction. Gastroparetic patients often experience symptoms such as nausea and vomiting, early satiety, bloating, gastric pain and heartburn. Further complications of gastroparesis also include dehydration due to repeated vomiting, malnutrition due to poor absorption of nutrients, and weight loss, to name a few. The three main causes of gastroparesis are idiopathic, diabetic, and postsurgical etiologies [37]. Specifically, the etiologies reported by Soykan and his colleagues from 146 patients were: 36% idiopathic, 29% diabetic, 13% post-gastric surgery, 16.4% due to Parkinson's disease, collagen vascular disorders, intestinal pseudo-obstruction, or miscellaneous diseases [38]. Normal gastric emptying requires proper functioning of the autonomic nervous system, interstitial cells of Cajal, smooth muscle cells, and the enteric nervous system. In particular, impaired or denervation of the vagal nerve (i.e. by diabetic neuropathy and postsurgical vagotomy) often results in downregulation of parasympathetic activity, which leads to malfunction of fundic accommodation, shallow or none muscle contractility and prolonged closure of pyloric sphincter

[39]. Treatment and management of gastroparesis broadly includes dietary, pharmaceutical and surgical therapies. The proper choice of treatment highly depends on the cause of gastroparesis. A brief overview of current treatments for gastroparesis is introduced below.

1.5.1 **Dietary Treatment**

For patients with mild gastroparetic symptoms, changing eating habit, including adjustments to meal content and frequency, is the most common and simplest way to remediate gastroparesis-related symptoms. Gastroparetic patients are often asked to eat food of low fat and fiber; eat frequent, small, nutritious meals rather than large meals; eat soft, preferably liquid-based meal, etc. Meals of larger portion, higher calories, and higher fat are more likely to have longer gastric-emptying times [40], [41]. If the cause of gastroparesis is identified to be diabetic, blood glucose level requires further control (i.e. by injection of insulin) since hyperglycemia may further delay the emptying of food from the stomach [22], [42].

1.5.2 **Pharmaceutical Treatment**

For moderate to severe gastroparetic patients, dietary adjustment is typically not sufficient to alleviate symptoms. Therefore, several prokinetic medications have been suggested to promote gastric emptying by increasing smooth muscle contractility, correcting gastric dysrhythmias, and improving coordination between the segments of the GI tract. Common medicines for increasing contractions of smooth muscles in the gastric wall include Metoclopramide [43], Domperidone [44], and Erythromycin [45], [46]. On the other hand, antiemetic medicines such as Ondansetron [47], Prochlorperazine [48], Promethazine [49], and Mirtazapine [50] may help relieve nausea and vomiting but not overall gastric emptying. Taking Metoclopramide for example, Metoclopramide blocks dopamine D2 receptors and stimulates 5-HT4 receptors, leading to an increase in the release of acetylcholine within the gut wall [43]. As a result, the fundic tone and the amplitude of antral peristalsis is increased. However, these medications have only provided modest efficacy in treating gastroparesis. Moreover, it has been commonly reported that these drugs typically come along with adverse CNS side effects including dizziness, nervousness, headaches, anxiety, depression, and reduced mental acuity [22], [51].

1.5.3 Surgical Treatment

In more severe cases, where dietary and pharmaceutical treatments are not effective, surgical interventions such as oral/nasal tube feeding, jejunostomy tube feeding, venting gastrostomy may be taken into place [52]. To get the necessary amount of nutrients and calories, a special liquid food will be delivered directly into patient's small intestine for nutrient absorption through an oral/nasal tube (temporarily) or jejunal tube (more permanently). To relieve pressure from the stomach in case of severe gastric stasis after meal ingestion, a tube going through the gastrostomy into the patient's stomach will allow gastric content to flow out of the stomach via the tube [53]. Distressingly, these surgical operations are typically irreversible and do not fundamentally improve the function of the stomach but only help alleviate the symptoms. On the other hand, coordinated relaxation of pyloric sphincter is thought to be an important factor for normal gastric emptying. Therefore, pylorospasm is believed to contribute to gastroparetic symptoms. Injection of Botulinum, a known neurotoxin that can cause muscle paralysis through inhibition of release of acetylcholine from the nerve terminals, into the pyloric sphincter through endoscopic surgery is a common way to relax the pyloric sphincter [54], [55]. More recently, direct electrical stimulation of the gastric smooth muscle has emerged as a new therapy for treating gastroparesis [7]. A small, battery-powered device is implanted underneath the skin and attaches wires to multiple electrodes sutured on the gastric muscle wall. High intensity gastric electrical stimulation (GES) has been shown to pace slow wave activity in the gastric wall [56], while low intensity GES was shown to decrease long-term nausea and vomiting [57]. GES is currently applied to treat patients whose symptoms cannot be controlled with medicines. However, the stimulus settings for clinical GES often require trial and error, which highly vary across patients, and ironically, the stimulus settings are often adopted from preclinical trials.

1.6 Motivation and Problem Definition

To date, the therapeutic efficacy of concurrent treatments for gastric diseases remains dismal. These diseases are unfortunately either being refractory to medicines, and/or cannot be readily addressed with surgical interventions [58]. It is not until recent advancement in the development of electroceutical therapy that has begun to shed light on the potential of neuromodulation of gastric functions [18], [59]. The stomach not only possesses intrinsic neural plexuses that enable

autonomic control of gastric functions, but the enteric system also receives significant input from the CNS primarily via the vagus nerve and secondarily through the spinal nerve [5]. As elaborated previously, impairment or denervation of the vagus nerve often leads to dysregulation of GI functions. The vagus is the tenth cranial nerve that provides parasympathetic innervations to the heart, lungs, and the GI tract. It carries coordinated sensory information from visceral organs to the nucleus tractus solitarius (NTS) in the brainstem, and issues top-down signals from the dorsal motor nucleus of the vagus (DMV) back to these organs [5], [6], [60], [61]. Although initial promise of vagal nerve activation via electrical stimulation has been demonstrated for treating chronic heart failure [62], apnea [63], and inflammation [64], [65], the therapeutic potential of vagus nerve stimulation (VNS) on stomach-related disorders remains unclear and its mechanism-of-action is still elusive. Indeed, neuromodulation of the vagus has been tested to treat GERD [66], obesity [67], nausea and vomiting [68]. However, the therapeutic results turned out to be modest and inconsistent across studies. The reasons are likely multiple, but two stand out: First, the vagus is a heterogeneous nerve consisting of distinct fiber calibers that carries both efferent and afferent traffic [69], [70]. Different gastric regions are innervated by different vagal branches, thereby having differential responses to VNS, yet proper functioning of the GI tract is thought to require a coordinated choreography of all gastric regions [71], [72]. However, most existing neuromodulation protocols measure physiological responses to stimulation at discrete locations without considering the global state of the stomach. Second, the inability to calibrate and validate the efficacy of neuromodulation protocol is in part due to the lack of assessment tools. Concurrent assessments of meal-related GI motility are commonly based on radioactive imaging or measurements through invasive intubation, which are unsafe for repeated measurements, technically cumbersome, and/or physiologically confounding, making them unable to capture the true physiological gut patterns and severely limiting their throughput in tracking the effect of treatments for chronic pathophysiology.

The work presented in this thesis is motivated by recent progresses in understanding about the vagus-stomach connectome in rat [5], [6], [73]. The rat is an appropriate preclinical model for “proof-of-concept” test of the efficacy of neuromodulation on gastric functions. To evaluate the stimulus-response relations, MRI serves as an near ideal imaging tool for this purpose. MRI yields simultaneous, non-invasive surveys of many aspects of gastric functions with unprecedented spatial resolution and image quality. Although gastric MRI has been increasingly applied to

humans, it has rarely been used in small animal models for preclinical assessment. Fortunately, recent advancements in high-field animal MRI and imaging sequences have allowed researchers to combine MRI with a rich set of techniques that are more readily applicable to animals than humans for mechanistic insights into physiology, diseases, and therapeutics. Taken together, the purpose of my dissertation is to develop an MRI-based imaging and analysis protocol to assess a variety of gastric functions in rats (e.g. gastric emptying and motility, pyloric motility, intestinal filling and motility, and intestinal absorption, etc.). This assessment was later on being used to evaluate, calibrate, and validate the effect of neuromodulation (i.e. VNS) on gastric physiology. The proposed experimental protocol and findings are expected to shed light on the use of gastric MRI to evaluate the efficacy of therapeutics in treating gastric disorders.

1.7 The Organization of this Thesis

This thesis covers the research outcomes I have achieved with regard to the development of gastric MRI in rats and the application of this novel technology to advance our understandings about how vagus nerve stimulation could be a potentially useful therapeutic strategy to remediate gastric physiology.

In Chapter 2, I review the principles of magnetic resonance imaging, the state-of-the-art gastric MRI protocol and analytical protocols in humans, and the challenges and opportunities in back-translating this imaging technology to small animals.

In Chapter 3, I introduce the use of a contrasted-enhanced MRI protocol for quantitative measurement of gastric emptying, antral motility, pyloric motility, intestinal filling, and intestinal absorption in rats. The protocol I developed includes an animal feeding protocol, an animal preparation protocol, imaging strategies, and a computer-assisted image processing pipeline that aids the analysis of gastric MRI data.

In Chapter 4, I present the modulatory effect of left cervical VNS on gastric physiology. With a stimulus setting informed by electrophysiological studies, left cervical VNS was found to promote gastric emptying in rats by enlarging the pyloric opening assessed by the MRI protocol developed in Chapter 3.

In Chapter 5, I set out to disentangle the relative contributions of afferent versus efferent cervical VNS on gastric motility. A wide range of parameter settings were systematically tested in

a cohort of rats, during which antral motility and pyloric motility were evaluated as a function of different stimulus settings.

In Chapter 6, I summarize the contribution and findings of this work, identify the limitation of current work, and highlight future directions for further development of the technology.

2. GASTRIC MAGNETIC RESONANCE IMAGING

2.1 Introduction

The development of magnetic resonance imaging (MRI) has revolutionized diagnostic radiology in the past three decades. MRI can provide high-resolution anatomical and functional images with excellent soft tissue contrast in a non-invasive, non-ionization nature. Despite the influential impact of MRI in imaging static organs such as the brain, abdominal imaging of the gut has been particularly challenging for several reasons. First, the spatial distribution and morphology of the gut vary greatly across individuals (and even within individual if scanned at different times). The variability in the geometry of the gut poses difficulty in standardizing imaging sequence and image analysis. Second, abdominal images are often degraded by respiratory and peristaltic motion artifacts. Therefore, one way to reduce motion artifacts in the images is to ask subjects to take a breath-hold during image acquisitions. However, the peristatic motion is involuntary, thus it is relatively more difficult to fully remove artifacts caused by gut movements. Lastly, the long acquisition time has severely limited the use of MRI for studying GI motor functions. Fortunately, recent technical advancements in high-field MRI, new imaging sequences, accelerated acquisition methods, novel contrast agents, and dedicated hardware designs have altogether made gastric MRI practical and feasible for studying GI physiology and pathophysiology. In this chapter, I will first introduce the imaging principles of MRI and how contrast agent can aid delineate the lumen of the gut. Next, I will give a detailed review of major advancements and limitations in concurrent human gastric MRI studies, including imaging protocols and analysis. Finally, I will spell out the challenges and opportunity of back-translating gastric MRI to small animals for preclinical investigation of GI physiology.

2.2 Basics of MRI

The imaging principles of MRI will be reviewed in this section for readers who are not familiar with MRI. The mechanisms of MR contrast agent employed in this thesis will also be introduced.

2.2.1 **MRI Physics**

The fundamental source of MRI signals originates from hydrogen nuclei (^1H), which is the most naturally abundant element in the biological system (i.e. primarily the water and secondarily the fat). The hydrogen nuclei possesses a single proton that carries a positive charge. Due to the intrinsic presence of an angular momentum in the nucleus called spin, the spinning proton produces an electrical current that generates a small magnetic field. Thus, all spinning hydrogen nuclei behave like a small bar magnet where each of them has their own magnetic field. In the absence of an external magnetic field, these "small magnets" are randomly oriented and thus the net magnetic field from a bulk of hydrogen nuclei is near zero.

When a living subject, a piece of tissue, or a phantom that contains a bulk of hydrogen nuclei (i.e. protons) is placed in a strong external static magnetic field (B_0), that is, inside a MRI scanner, the protons begin to align with or against the B_0 field. According to quanto-mechanical nuclear magnetic resonance (NMR) theory, more protons would tend to align parallelly with the B_0 field than anti-parallelly with the field, because the latter condition requires the protons to maintain at a higher energy state. In addition, all protons would precess around the B_0 axis at a specific frequency in MHz called the Larmor frequency. Its value for the proton is 42.6 MHz/Tesla, which is proportional to the strength of B_0. Precession of protons about the B_0 axis results in a net bulk magnetization (M_0) along the longitudinal direction while cancelling out in all other directions due to their random and asynchronous precession phases. When a second magnetic field [radio frequency (RF) pulse] is applied in the transverse direction at the Larmor frequency, the energy can be transferred from the RF pulse to the protons. This phenomenon is known as resonance, hence termed magnetic resonance imaging. The RF pulse causes the protons to precess *in phase* and gradually move away from the B_0 direction, and will eventually be tipped down to the transverse plane. This process effectively produces a rotating transverse magnetization (M_{xy}) and a residual longitudinal magnetization (M_z). The resulting amplitude of M_{xy} and M_z depend on the strength and duration of the applied RF pulse. The angle between the net magnetization and the B_0 axis is called the flip angle. When a flip angle of 90° is achieved, the net magnetization will be fully converted to M_{xy} and that transverse magnetization would rotate about the longitudinal axis at the Larmor frequency. When a receive coil is placed in proximity, the varying magnetic flux generated by the rotating M_{xy} would induce an oscillating current in the coil according to the Faraday's Law. The oscillatory frequency of the induced current would also be at the Larmor

frequency. The dynamics of this induced current is described as the MRI signal. When the excitation pulse is switched off, the spins would begin to rotate *out of phase* and gradually return to their equilibrium state, where the net magnetization will eventually align with the B_0 axis. The processes under which the longitudinal magnetization recovers and the transverse magnetization decays are both approximately exponential, with the corresponding time constants known as T1 and T2, respectively. The values of T1 and T2 vary across tissue types, hence contrasts between tissues could be obtained by collecting images at different times during T1 and T2 relaxation.

To localize the MRI signals emitted from protons in the three-dimensional space, three orthogonal magnetic field gradients are typically used. First, a slice selection gradient is applied to alter the strength of B_0 such that protons at different locations along the gradient field would have different precession frequencies. Then, the RF pulse can be applied at a specific Larmor frequency so that only protons within a slice of certain thickness could be excited. After the slice is on resonance, a spatial-frequency encoding scheme is employed by utilizing the other two gradients (i.e. frequency-encoding gradient and phase-encoding gradient) to encode the MRI signals originated from this slice into the k-space. Finally, the actual MR image could be obtained by applying Fourier transformation to the k-space data.

2.2.2 **Contrast-enhanced MRI**

The contrast in the MRI images is governed by a number of factors. First, the higher the proton density within a volume, the stronger the signal and therefore the brighter the image intensity would be. Increasing or decreasing the numbers of protons within a tissue segment can modify the proton density within a voxel. In many body areas, GI tract being one of them, it is possible to artificially change the proton density thereby improving the luminal contrast. As shown in Figure 2.1, CO_2 was used as a negative contrast agent for the stomach, small bowel or colon by substituting the luminal content thereby reducing the proton density [74], [75]. Conversely it is possible to obtain positive contrasts by using oral water alone, to increase the proton density [76]. The image intensity is also highly dependent on the T_1 and T_2 relaxation times. Water protons in different tissues have different T_1 and T_2 values, thus taking images at different times during the recovery and/or decay of T_1 and T_2, respectively, could result in different image contrasts. Notably, the T_1 or T_2 relaxation times of a tissue compartment (or oral media) can be reduced by the

administration of paramagnetic agents such as a chelate of the metal ion gadolinium (Gd^{3+}) or super-paramagnetic iron oxide (SPIO) particles, respectively [77].

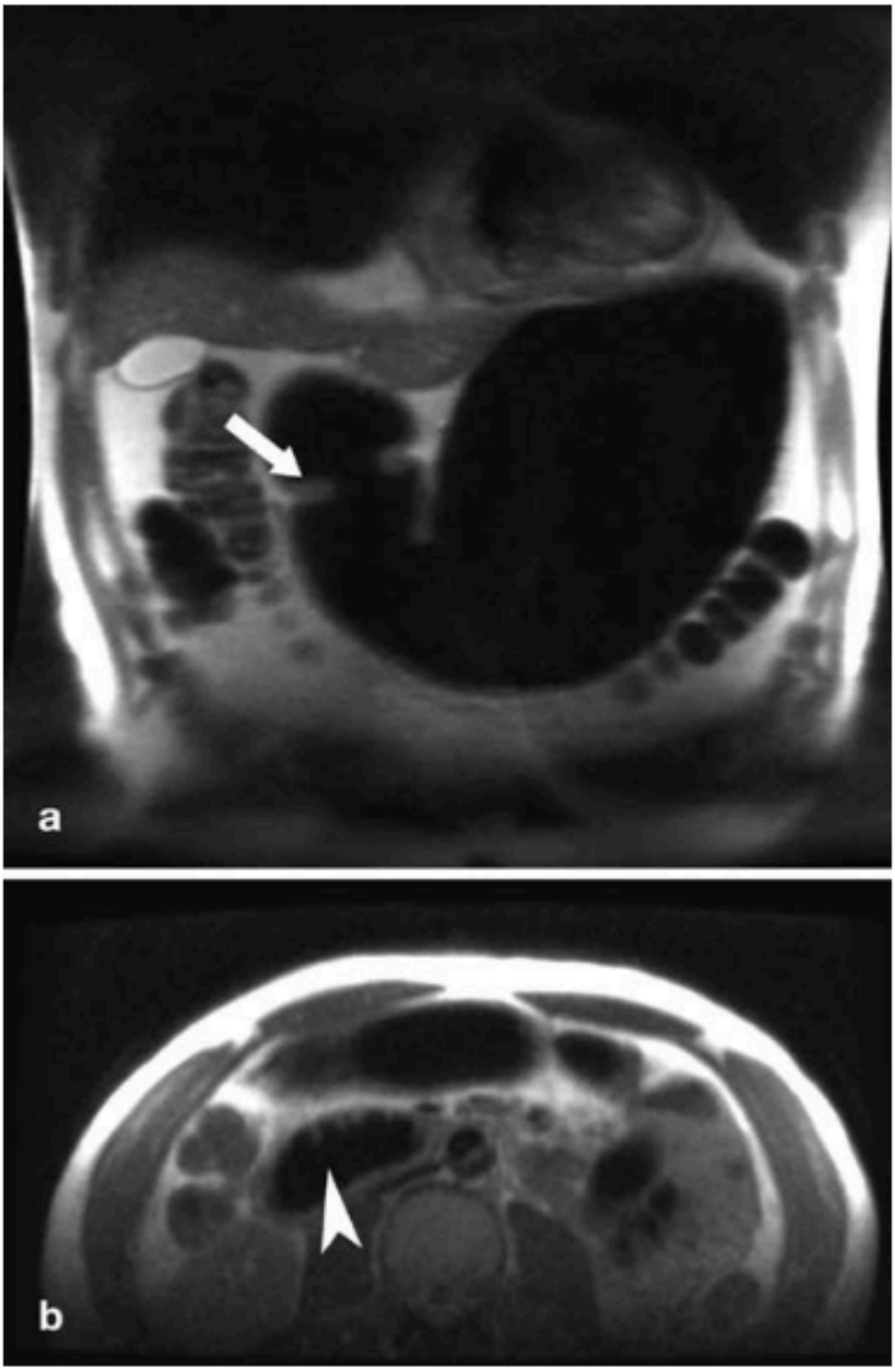

Figure 2.1 **Breath-hold images of the CO_2-distended stomach and the small intestines.** Top panel: the negative contrast clearly delineates the contour of the stomach, highlighting the peristaltic wave as indicated by the white arrow. Bottom panel: distended duodenum as indicated by the white arrow. This figure is adapted from [75].

Gadolinium is strongly paramagnetic so that it can become temporarily magnetized when placed in an external magnetic field. This is due to the unpaired electrons in shells or bonding orbitals of the Gadolinium ions, thus the unbalanced spins can produce a strong magnetic moment. Metal ion gadolinium has the same spin but of a much smaller size than protons, thus their gyromagnetic ratios are 657 times larger [78]. Given this strong magnetic moment, it can facilitate magnetic relaxation in nearby water protons. As a result, gadolinium can shorten both T_1 and T_2 of neighboring water protons, making them more apparent than other surrounding tissues on T_1- or T_2-weighted MRI images (Figure 2.2). Contrast agents have been used in NMR since the earliest days when Bloch added paramagnetic ferric ions in solution to shorten T_1 of protons in water [79]. Development of the first commercially available contrast agent (Gd-DTPA) for MRI was first introduced at around 1980's [78], followed by the first reported use in humans in 1984 [80].

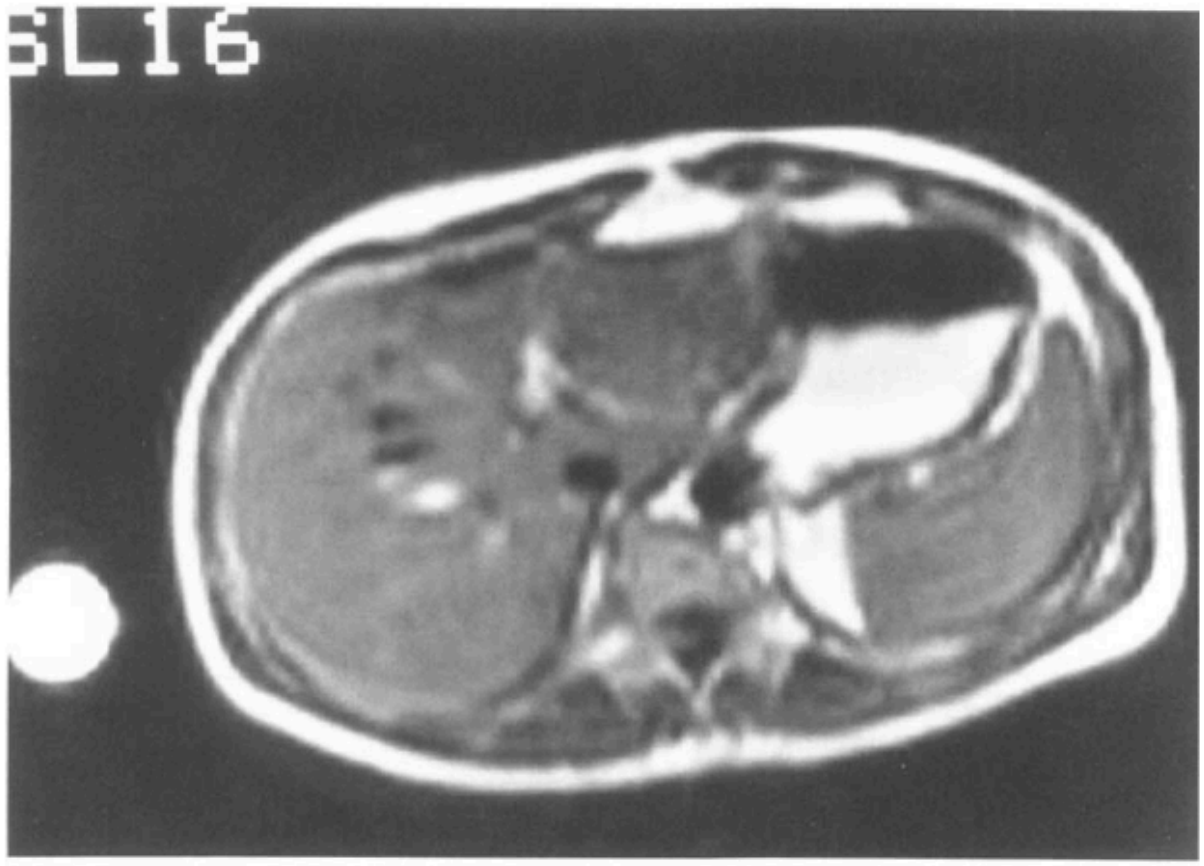

Figure 2.2 **Contrast-enhanced gastric MRI of fundic lumen labeled with Gd-DOTA.** The stomach was divided into gastric air and the gastric content. This figure is adapted from [81].

2.3 Gastric MRI in Humans

The earliest use of MRI in imaging gastric emptying, antral motility, and intestinal motility can date back to 1988 [82], [83]. During that time, echo-planar imaging (EPI) was their primary sequence because of its fast scan time. However, EPI images are susceptible to artifacts and the spatial resolution is typically low, thus limiting its capability in monitoring GI physiology [84]. Subsequent development of rapid imaging sequences such as fast spin-echo sequence and spoiled gradient sequence has substantiated the application of MRI in functional GI imaging. Multiple stacks of images of the stomach can be taken under two or three separate breath-holds, depending on the imaging sequence used. Human gastric MRI has allowed researchers to investigate the effect of different meal types (e.g. liquid vs. solid food, calorie load, meal viscosity) [85]–[87], different body positions (e.g. lying or sitting) [85], [88], and pharmaceutical compounds [89], [90] on gastric emptying. By specifying appropriate sequence parameters (T_1 or T_2-weighted, the property of the test meal, and/or the type of paramagnetic contrast agent used), total gastric volume, gastric air volume, gastric content volume, and intragastric distributions can be calculated from the gastric MRI images [88], [91]. Schwizer and his colleagues used Gd-DOTA as an oral contrast media to enhance the lumen of the GI tract, and the gastric emptying rate was assessed in healthy humans [81]. They found that the emptying curve measured with MRI was highly correlated with the double-indicator techniques. Later validations of gastric volume MRI was performed against other conventional approaches such as intragastric balloons [92] and gastric-emptying scintigraphy [93], [94]. A good correspondence in gastric measurements between these techniques was reported. MRI has also been applied to evaluate the effect of intragastric dilution by secretion [86], [95], [96]. To estimate gastric secretion volume, these studies utilized *in vitro* calibration of either the T_1-weighted signal intensity or T_1 values of the gadolinium-labeled meal with respect to different levels of dilution of hydrochloride acid. The resulting calibrated dilutive profile of the test meal allowed them to estimate the proportion of meal content and gastric juice based on the *in vivo* signal intensity measurements. However, this approach was only applicable to liquid meal so that a homogeneous luminal image is ensured for quantification of secretory volume. Gastric MRI could not only be used to assess postprandial volume but is also able to evaluate gastric juice volume in the fast state [97]. Gastric MRI has also been applied to assess antral motility at rapid intervals by utilizing single-slice imaging techniques or multi-slice 3D imaging methods. The

assessment of antral motility with MRI has been used to validate the effect of pharmacological compounds such as metoclopramide [98], erythromycin [90], and cisapride [99].

Although the development and use of gastric MRI has come to a point where clinical applications are in sight, there are several practical constraints that prevent gastric MRI from being routinely conducted in clinical settings. One of the major technical hurdles that impedes the widespread translation of gastric MRI is the lack of automated segmentation and analysis software. Despite several software applications available for automated segmentation of MRI images, they are mostly application-specific to static, homogeneous, or anatomically well-defined structures such as the brain [100]–[103] but not applicable to the gut. There are practical and technical challenges unique to the segmentation of gastric MRI images. First, the stomach is a highly deformable organ. Its size, shape and location in the abdomen can vary highly within (i.e. if scanned at different time points) and across individuals. Second, the signal intensities of the lumen are not homogeneous within the stomach. For example, the luminal intensities are often dimmer near the gastric wall than at the center of the stomach, because gastric juice secreted from the gastric wall dilutes the meal and lowers the concentration of the contrast agent. Such heterogeneity in signal intensity poses challenges in accurate segmentation. Lastly, there is currently no standardized protocol for gastric MRI acquisitions (e.g. imaging sequence parameters, test meal, type of contrast agent, concentration of contrast agent, etc.). At present gastric MRI is typically carried out by individual units, thus the image contrast and quality (e.g. partial volume effect) often vary from research site to research site, which poses additional difficulties in generalizing the automation of data analysis. As a result, current quantification of gastric volume and motility is still often performed by hand, which can be a burdensome and daunting task given that vast quantities of data (>1000 images) can be collected within one imaging session. Although several semi-automated gastric MRI processing algorithms have been proposed in the past few years [104]–[108], they are not accessible to other research groups. Moreover, these methods require manual tracing of the contour of luminal content that is then subsequently refined by automated algorithms (Figure 2.3). Problems with these methods include intensive labor and variation in results due to erroneous or biased image interpretation. Taken together, there is a critical need in developing and disseminating an automated segmentation process and more generalizable data analysis software. To address this need, I have developed an analysis pipeline that allows automated segmentation of the GI tract as elaborated in section 3.2.6.

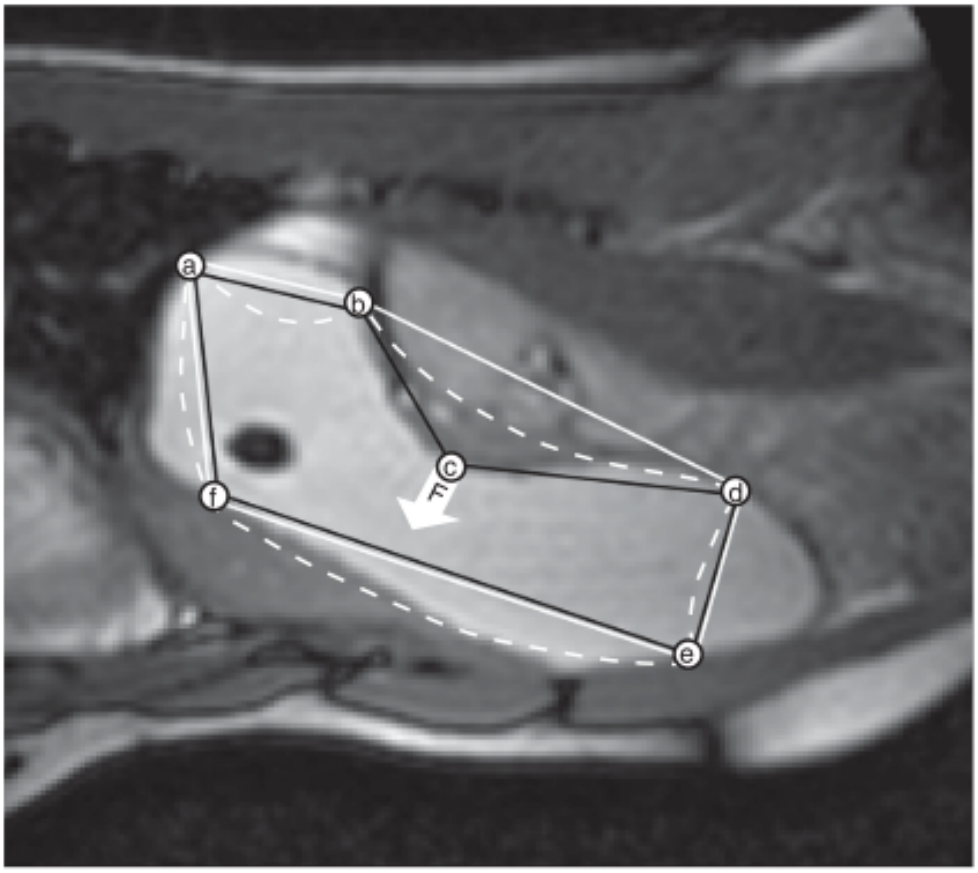

Figure 2.3 **Semi-automatic segmentation of the gastric lumen.** First, a number of anchor points needs to be placed around the contour of the gastric lumen. Then, the polygon would iteratively expand or shrink until it reaches the edge of the gastric lumen. This figure is adapted from [104].

2.4 Challenges and Opportunity of Gastric MRI in Animal

Despite its increasing applications in humans, gastric MRI has rarely been applied to small animals [109]–[112]. However, fundamental knowledge about the GI physiology and pathology often results from animal studies, and new therapeutics are typically tested first in animal models (especially rodents) before clinical trials. It is thus of interest to establish gastric MRI in rodents for basic science and preclinical studies. Doing so would also pave the way to combine MRI with a rich set of techniques that are more readily applicable to rodents than humans for mechanistic insights into GI physiology, diseases, and therapeutics. For example, one of such avenues is to combine gastric MRI with electrophysiology [56], [113], hormone [114]–[116], and behavioral [117] essays to evaluate the emerging bioelectric therapeutics [113], [118]–[120]. Nevertheless,

gastric MRI is still premature for animal studies, and it is lack of standardized routines for either image acquisition or analysis.

Establishing gastric MRI in rodents is not simply a backward translation from humans. There are practical and technical challenges unique to rodents. *In vivo* gastric imaging is generally more difficult in rodents given their much faster gastric motility [121]. Besides, rodents, unlike humans, are not compliant to self-directed food ingestion or breath-holding, both of which are critical requirements for gastric MRI in humans, thus calling for adaptation of the MRI protocols to avoid otherwise poorly controlled experiments and severe motion artifacts. As elaborated earlier, the complex GI geometry and inhomogeneous lumen contrast also place challenges to image processing [122]. Therefore, automated image processing is piecemeal for gastric MRI, severely limiting its throughput, dissemination, and application in both humans and animals [123].

3. CONTRAST ENHANCED MAGNETIC RESONANCE IMAGING OF GASTRIC EMPTYING AND MOTILITY IN RATS

3.1 Introduction

Gastric emptying, motility, and intestinal transit are essential aspects of gastrointestinal (GI) function [125]. Impairment of such responses may cause gastroparesis [51], [126], obesity [127], and gastroesophageal reflux diseases [128]. Understanding and diagnosis of gastric disorders require direct and accurate assessment of gastric emptying and motility. In this regard, current tools are mostly based on radioactive imaging [94], [129], or measurements through invasive intubation [130]–[133], which are unsafe for repeated measurements, technically cumbersome, and/or physiologically confounding. In contrast, magnetic resonance imaging (MRI) is emerging as a likely more favorable alternative for imaging GI anatomy and function with excellent soft-tissue contrast and high spatial resolution [91]. Initial applications of gastric MRI in humans have demonstrated its unique potential for comprehensive assessment of gastric emptying [93], [105], [134], [135], intra-gastric distribution [85], [86], and antral and duodenal motility [85], [136], to name a few. However, gastric MRI has rarely been applied in small animals, though new therapeutics are typically tested first in animal models before clinical trials. Such technical hurdles necessitate the development of gastric MRI in animals in order to characterize gastric physiology and pathophysiology for better calibration and validation of the efficacy of new therapeutics.

The goal of this study is to bridge the gap between preclinical and clinical gastric MRI by establishing a robust, standardized, and quantitative imaging technique for assessing gastric functions in rats. Specifically, I introduced an animal feeding protocol to train rats for voluntary consumption of a Gadolinium-labeled test meal right before MRI. This protocol served to control food ingestion for consistency across animals, and to enhance GI contrast in T_1-weighted and high-field MRI. With the enhanced contrast/signal to noise ratios, I optimized the MRI acquisition to assess either gastric emptying or motility with relatively high spatial or temporal resolution, respectively. I further developed computer-assisted image processing pipelines to streamline the

analysis of gastric MRI data for quantitative and objective assessment of gastric anatomy, emptying and motility, etc.

3.2 Materials and Methods

3.2.1 Subject

Eleven rats (Sprague-Dawley, male, adult, 229-330g) were studied according to a protocol approved by the Institutional Animal Care and Use Committee at Purdue University. The animals were housed individually in a ventilated cage with lifted stainless steel wire floor, and maintained on a 12:12h light-dark cycle (lights on at 6AM and lights off at 6PM).

3.2.2 Animal Training

Each animal was trained to consume a fixed quantity of palatable dietgel (DietGel Recovery, ClearH_2O, ME, USA). The diet training took about 7 days. In the first 2 days, the animal was supplied with both regular rat chow and ~10g dietgel (the dietgel was put in a dish in the cage at 11AM) to accustom itself to the dietgel. In the following days, the animal was fasted for 18 hours (5PM to 11AM) and then was fed with the dietgel only at 11AM. The animal was given 30 minutes to consume 10g dietgel; then regular meals were supplied to the animal afterwards regardless of whether it finished the dietgel or not. After the diet training (~2 to 3 repetitions), each animal was able to naturally consume the dietgel following overnight food restriction.

3.2.3 Labeling Test Meal with Gadolinium-DTPA

3.2.3.1 Preparation of Test Meal

On the day for gastric MRI, each animal was given a test meal with a mixture of the dietgel (Figure 3.1) and an MRI contrast agent - Gadolinium (Gd). Specifically, 10g dietgel was liquefied by double-boiling in the warm water, and then it was mixed with 22.4 mg powder-form of Gd-DTPA (#381667, Sigma Aldrich, St. Louis, USA) to obtain a 4mM-quivalent solution. The liquefied dietgel was cooled to the room temperature to reform itself to the gel state.

3.2.3.2 Properties of the Test Meal

The ingredients in the dietgel include Purified Water, Corn Syrup, Vegetable Oil, Vegetable Protein, HydroColloids, Electrolyte Mix, Food Acid, Mineral Mix. The dietgel is a

nutrient-fortified gel that contains 60% water, calories and electrolytes. Ten grams of the dietgel is about 21.4kcal. After labeling the dietgel with the specific amount of Gd-DTPA as aforementioned, both unlabeled and Gd-labeled dietgel were scanned in a vial with a Fast Low Angle Shot gradient echo (FLASH) sequence in a Bruker 7T small animal magnet (see Gastric MRI section for a more detailed description of the apparatus), with imaging parameters being: repetition time (TR) = 124.131 ms, echo time (TE) = 1.364 ms, flip angle (FA) = 90º, 5 coronal slices, slice thickness = 2 mm, FOV = 60 × 60 mm^2, in-plane resolution = 0.23 × 0.23 mm^2, and 4 averages. Figure 3.2 shows the difference in image intensity before and after labeling the dietgel with Gd-DTPA.

Figure 3.1 **The nutrition-fortified dietgel used as the test meal in this study.** This figure is modified from an image created by Datesand from http://datesand.com/index.php/product/dietgel-recovery/.

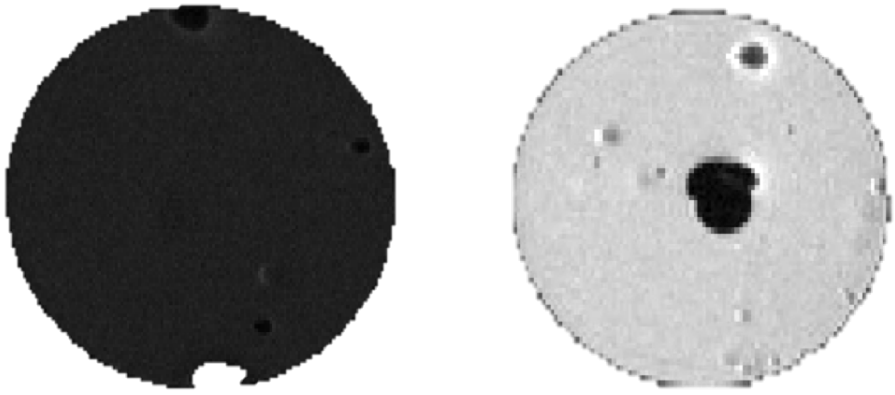

Figure 3.2 **T1-weighted images of unlabeled (Left) and Gd-labeled dietgel (Right).**

Relaxometry measurements (T_1 and T_2) were also performed on the unlabeled and Gd-labeled dietgel. The same dietgel samples were scanned under a Fast Spin-Echo sequence with variable repetition time (for measuring T_1) and variable echo time (for measuring T_2). Specific imaging parameters are listed below: TR = [80, 200, 400, 800, 1500, 3000, 5500] ms, Effective TE = 35 ms, Echo spacing = 7ms, FA = 90º, 1 coronal slice, slice thickness = 2 mm, FOV = 60 × 60 mm^2, matrix size = 256 × 256, and RARE factor = 2. To estimate voxel-wise T_1 values, the relationship between the nominal TRs and the signal intensity measured at respective TR was fitted by the Bloch equation (Equation 3-1):

$$SI = A + B \times (1 - \exp(-\frac{TR}{T_1})) \qquad \text{(Equation 3-1)}$$

where TR and SI are the nominal repetition times and their corresponding measured signal intensities, and A, B and T_1 are parameters to be estimated. Similarly, voxel-wise T_2 values were computed by fitting an exponential function (Equation 3-2) to the T_2-relaxation decay with respect to multiple echo times:

$$SI = C + D \times \exp(-\frac{TE}{T_2}) \qquad \text{(Equation 3-2)}$$

where TE and SI are the nominal echo times and their corresponding measured signal intensities, and C, D and T_2 are parameters to be estimated. After obtaining the T_1 and T_2 maps for the two samples, a 10-by-10 window was randomly sampled within the gels to obtain average T_1 and T_2 values within the window.

3.2.4 **Animal Preparation**

Given the over-night food restriction, every animal was able to consume the Gd-labeled test meal in several minutes. Then, it was anesthetized with 4% Isoflurane mixed with oxygen at a flow rate of 500ml/min for 5 minutes, and it was then placed on a water-heated cradle in prone position. On the cradle, the animal received a subcutaneous (SC) bolus injection of 0.01mg/kg dexmedetomidine solution (0.05mg/ml, Zoetis, NJ, USA). About five minutes later, 0.3-0.5% isoflurane mixed with oxygen at a flow rate of 500ml/min was continuously delivered through a nose cone. About fifteen minutes after the bolus, continuous SC infusion of dexmedetomidine at 0.03mg/kg/hour was administered. An MRI-compatible system (SA Instruments Inc., Stony Brook, NY, USA) was used to monitor the animal's respiration, cardiac pulsation, and body temperature to ensure a stable physiological state throughout the experiment.

3.2.5 **Gastric MRI**

The animals were scanned in a 7-tesla horizontal-bore small-animal MRI system (BioSpec 70/30; Bruker Instruments, Billerica, USA) equipped with a gradient insert (maximum gradient: 200mT/m; maximum slew rate: 640T/m/s), and a volume transmit/receive ^{1}H RF coil (86 mm inner-diameter).

The MRI protocol started with an abdominal localizer to acquire T_2-weighted scout images to reveal the long axis of the stomach (Figure 3.3B). Along this long axis, two sets of T_1-weighted coronal images were acquired using a two-dimensional FLASH sequence: one for assessing gastric volume with higher spatial resolution and larger spatial coverage (herein referred to as the "volumetric" scan, Figure 3.3C), and the other for assessing gastric motility with higher temporal resolution and more targeted spatial coverage (referred to as the "fast" scan, Figure 3.3D). As the Gd-labeled test meal initially filled the stomach and progressively entered the intestines, the GI volumes were rendered with much higher T_1-weighted intensities, providing greatly enhanced contrast against other visceral organs.

The volumetric and fast scans were repeated in an interleaved manner (Figure 3.3A) for a total of 4 hours. The volumetric scans were acquired with TR = 124.131ms, TE = 1.364ms, FA = 90º, 30 oblique slices, slice thickness = 1mm, FOV = 60 × 60 mm^2, in-plane resolution = 0.23 × 0.23 mm^2, 4 averages, and no repetition. The fast scans were acquired with TR/TE = 11.784/1.09ms, FA = 25º, 4 oblique slices, slice thickness = 1.5mm, FOV = 60 × 60 mm^2, in-plane resolution 0.47 × 0.47 mm^2, no averaging, and 150 repetitions. The four fast scan slices were positioned and adjusted to cover the antrum, pylorus and duodenum based on the immediately preceding volumetric images to account for the stomach displacement during gastric emptying. To mitigate motion artifacts, both volumetric and fast scans were respiration-gated such that images were acquired during end-expiratory periods while the chest volume stayed roughly unchanged. With the respiratory gating, the volumetric scan took about 4 minutes; the fast scan took ~2 seconds per repetition and lasted about 6 min for 150 repetitions.

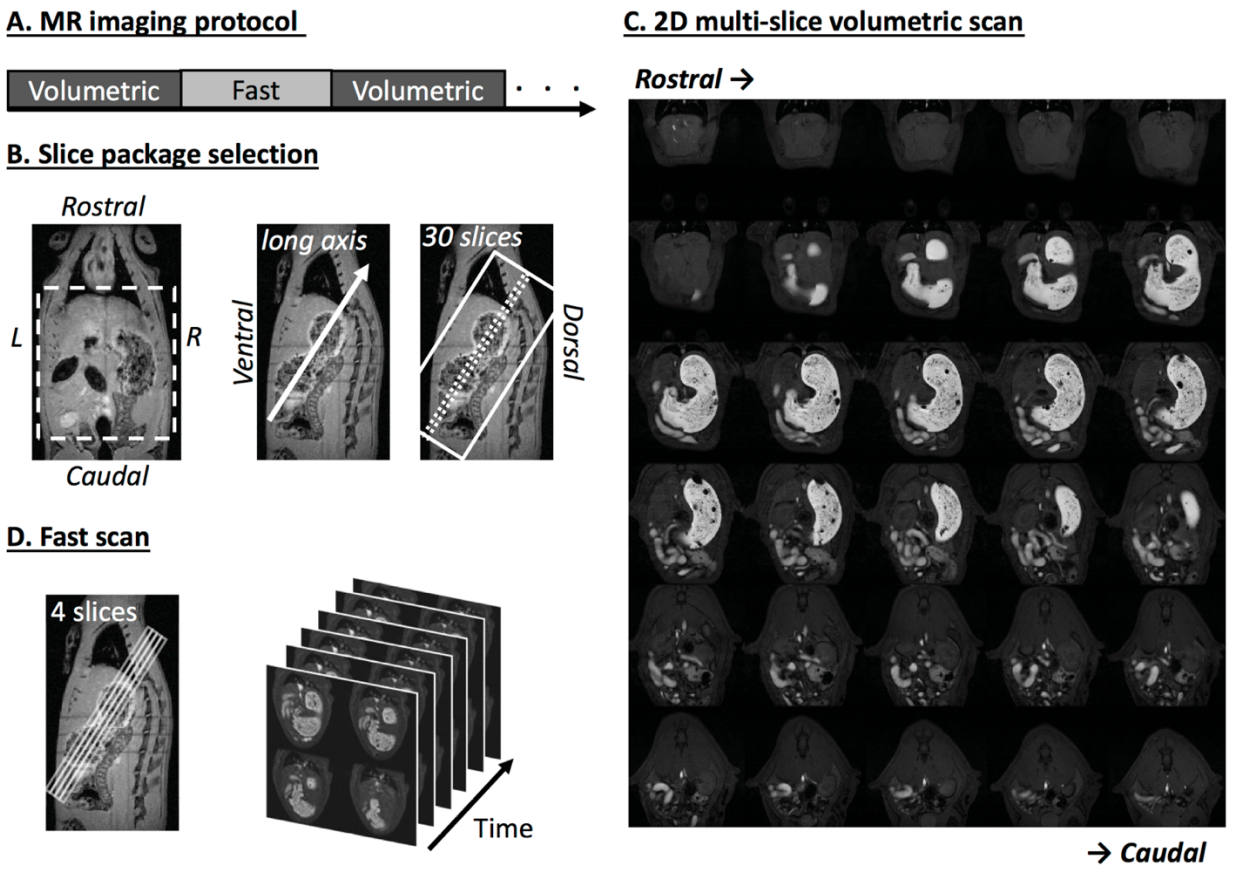

Figure 3.3 **Imaging sequence and slice package selection.** **A.** 2D multi-slice volumetric scan (denoted as "Volumetric") and fast antral motility scan (denoted as "Fast") were performed interleaved throughout the experiment. **B.** Two example T_2-weighted images (left: coronal view, right: sagittal view) acquired from a multi-slice localizer sequence. An oblique 30-slice package was placed along the long axis of the stomach from the sagittal image. **C.** Example semi-coronal view images from the 2D multi-slice volumetric scan. **D.** Fast scan of the antrum with four slices. The position of the slice package was determined from images acquired from the volumetric scan.

3.2.6 **Assessment of Gastric Volume, Compartments, and Emptying**

The stomach volume was assessed both as an entire quantity and by compartments approximately every 15 mins for 4 hours. As illustrated in Figure 3.4, the volumetric images were processed using a customized and automatic pipeline in Matlab (Mathworks, Massachusetts, USA) to segment the contrast-enhanced lumen volume of the GI tract.

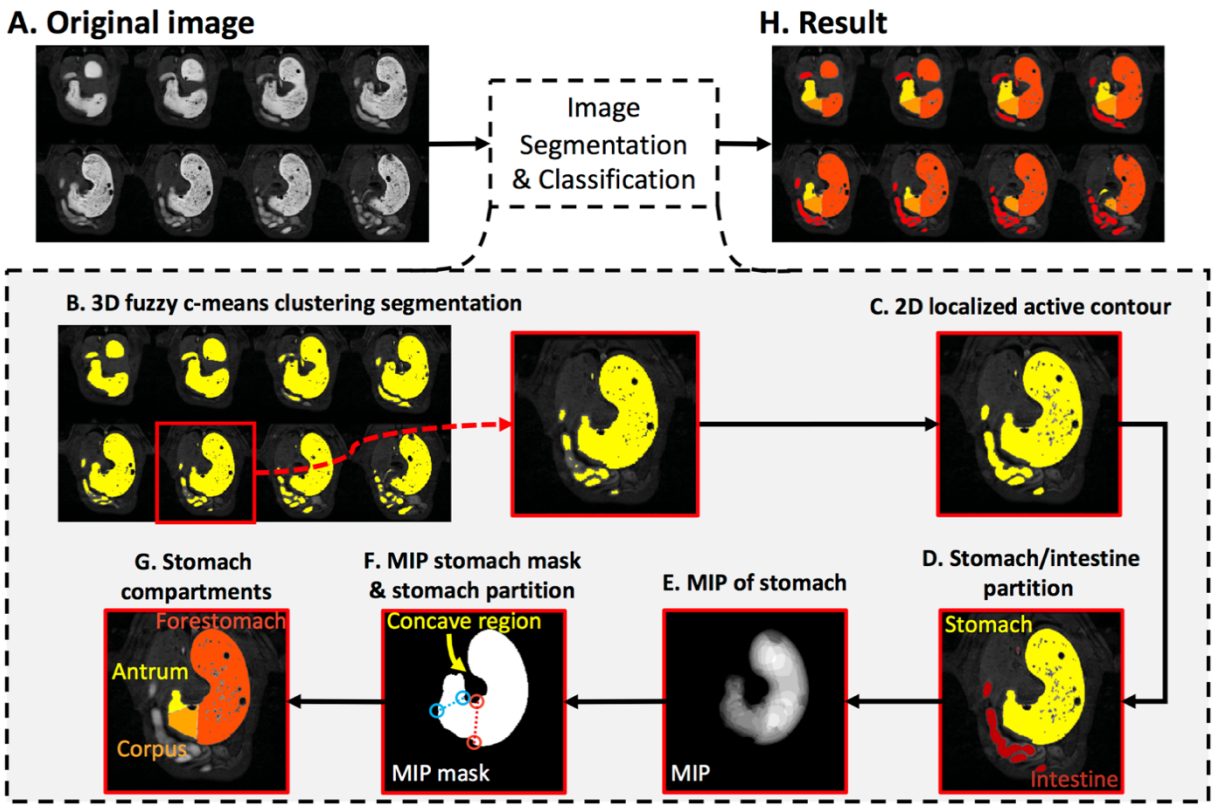

Figure 3.4 **Image segmentation and classification of the GI tract. A.** Contrast-enhanced gastric MRI with volumetric scans. **B.** Preliminary segmentation of the GI tract with 3D fuzzy c-means clustering algorithm. **C.** Refinement of the segmentation result with 2D localized active contour method. **D.** Partition of the stomach and the intestine. **E.** Maximum intensity projection (MIP) of the stomach. **F.** A stomach mask obtained from all non-zero voxels from the MIP of the stomach. The forestomach and the corpus was separated along the red dotted line, and the corpus and the antrum was separated along the blue dotted line. **G.** Partition of the forestomach, the corpus, and the antrum on an example slice. **H.** Partition of the forestomach, the corpus, the antrum, and the intestine on 8 example slices.

First, a 3D fuzzy c-means clustering algorithm (fuzziness: 2.2) [137] was applied to the unprocessed images (Figure 3.4A) to initially partition all voxels into two clusters: the higher-intensity Gd-labeled meal and the lower-intensity tissues (Figure 3.4B). The former yielded an initial segmentation of the GI tract filled with the meal. To refine the segmentation, a localized region-based active contour segmentation algorithm [138] was further applied to each slice to correct for the heterogeneity in lumen intensities and to smooth the contour (Figure 3.4C). Briefly, the algorithm operated upon a rectangular window (15-by-15 pixels) sliding across each slice; the segmentation was optimized separately for each instance of the sliding window by using the

gradient-descend method to minimize the intensity inhomogeneity in both the segmented and non-segmented regions while regularizing the arc length of the contour of the segmented regions. It is important to note that some voxels outside the GI tract might be mistakenly included in the above segmentation. These included the voxels in large veins with much shortened T_1 and those in the renal medulla due to systemic Gd absorption roughly 2 hours after the start of the experiment. However, such spurious voxels were identified and excluded from the GI segmentation.

Following the segmentation, the GI was divided into two compartments (the stomach and the intestines) based on an automatic image analysis. Specifically, the segmented volume (Figure 3.4C) was eroded with a disk (using a Matlab function *imerode* with a kernel size of 7 pixels) to disconnect the stomach and the intestines at the pylorus. After identifying the stomach and the intestines, the eroded segmentation was dilated with the same disk (using a Matlab function *imdilate*) to restore its original size, yielding separate stomach and intestinal segmentations (Figure 3.4D). The segmented stomach volume was further sub-divided into the forestomach, the corpus, and the antrum [139]. Specifically, the forestomach and the corpus were separated by the limiting ridge, while the corpus and the antrum were separated by a line connecting the angular incisure with a point located at the highest convexity on the greater curvature of the distal stomach. To define such morphological landmarks, all the voxels inside the stomach were projected onto a planar shadow through maximum intensity projection (MIP) (Figure 3.4E). A 2-D mask of the stomach contour was extracted from non-zero pixels in the MIP of the stomach (Figure 3.4F). Based on this mask, a convex hull of the stomach mask was identified by first using the Matlab function (*bwconvhull*), followed by subtraction of the stomach mask. This resulted in the concave region of the stomach mask. One set of eight extrema points was calculated for the concave region, and another set of eight extrema points was obtained for the entire stomach mask. These were calculated using the Matlab function (*regionprops* with option '*Extrema*'). The bottom-right and the bottom-left extrema points of the concave region were considered to be the upper-endpoint of the limiting ridge and the angular incisure, respectively. Similarly, the bottom-right and bottom-left extrema points of the stomach mask corresponded to the lower-endpoint of the limiting ridge and the landmark on the greater curvature of the distal stomach, respectively. The bottom-right point from each region was connected and represented the limiting ridge. Similarly, the bottom-left point from each region was connected. These connections separated the stomach into the forestomach, the corpus, and the antrum (Figure 3.4F, red dotted line, blue dotted line). Such

compartment-wise masks were further used to partition the originally segmented stomach into 3 different compartments for all slices (i.e. forestomach, corpus and antrum, Figure 3.4G, H).

The volume of the segmented GI was quantified as a whole and by regions. This provided the imaging-based measurements for the GI volume, the intestinal volume, the stomach volume, and the volumes of different compartments of the stomach (i.e. the forestomach, the corpus, and the antrum). The volumetric MRI scans at different times were segmented, quantified separately, and then normalized as the ratios over the total GI volume at time 0. This allowed us to observe the relative volume change over time for each animal, while the normalization additionally accounted for the varying amount of the meal intake for different animals. The time series of gastric volumes were resampled at 15-min intervals for every animal and then averaged across animals to characterize gastric emptying in the group level.

3.2.7 **Assessment of Gastric Motility**

Similarly, the images from the fast scans were processed by using a custom-built pipeline in Matlab (Figure 3.5). First, the fast scans were aligned to their immediately previous volumetric scans with rigid body transformation. Next, a rectangular region of interest (ROI) was set up to cover the antrum on every slice of the fast scans (Figure 3.5A). Within this ROI, high-intensity voxels (i.e. the Gd-labeled meal) were segmented by using an automatic clustering-based image thresholding method as described elsewhere [140] (Figure 3.5B). To obtain the antral motility representation from the peristaltic wave (Figure 3.5C), I implemented an algorithm similar to one previously developed for human antral imaging [141]. Specifically, perpendicular to the antral axis, cross-sectional planes were defined at different positions at the axis. The segmented voxels within each cross section were summed over all slices to quantify the cross-sectional area along such axis. As a result, the antral volume was expressed as a line profile, where each intensity value represented the antral area in a cross section at the specific position along the axis. The line profiles were then stacked over times and graphed (herein referred to as the antral motility representation) (Figure 3.5D), in which the horizontal axis represents time and the vertical axis represents the distance from the proximal antral to the distal antrum. The antrum contraction terminated at the pylorus opening, where there was no (or at least minimal) contractile activity represented by the cross-sectional area change. The antral contraction frequency, velocity and amplitude were obtained from the antral motility representation. The middle of the peristaltic pathway was

automatically determined, which resulted in a horizontal line that was passed through this location. The intensity profile was then sampled along the line and plotted as shown in Figure 3.5E. The sampled signal intensity represented the temporal change of the cross-sectional areas over time. The peaks (marked as *) and the valleys (marked as o) of the time series were automatically detected, which corresponded to the maximal and minimal size of the antrum corresponding to the antral distension and contraction, respectively. The percentage occlusion of the antrum (herein referred to the contraction amplitude) was obtained by calculating the ratio of the peak-valley difference over the peak size. This was repeated and then averaged across all the peak-valley pairs on the motility representation, yielding an average percentage occlusion of the antrum. To estimate the frequency of the antral contraction, the Fourier transformation was applied to the time series of the antral contraction, followed by the peak detection in the magnitude of the frequency spectrum. For computing the propagating velocity of the antral peristaltic wave, two intensity profiles were sampled at two voxels above and below the middle of the peristaltic pathway. The distance between the two lines was 5 voxels, which corresponded to 2.344 mm with my imaging protocol. The valleys on each sampled line were computed and plotted as the white dots on the motility diagram (Figure 3.5F). Therefore, the gradient (Δdistance/Δtime) was computed by calculating the distance and time difference between two paired white dots, reporting the propagating velocity of the peristaltic wave.

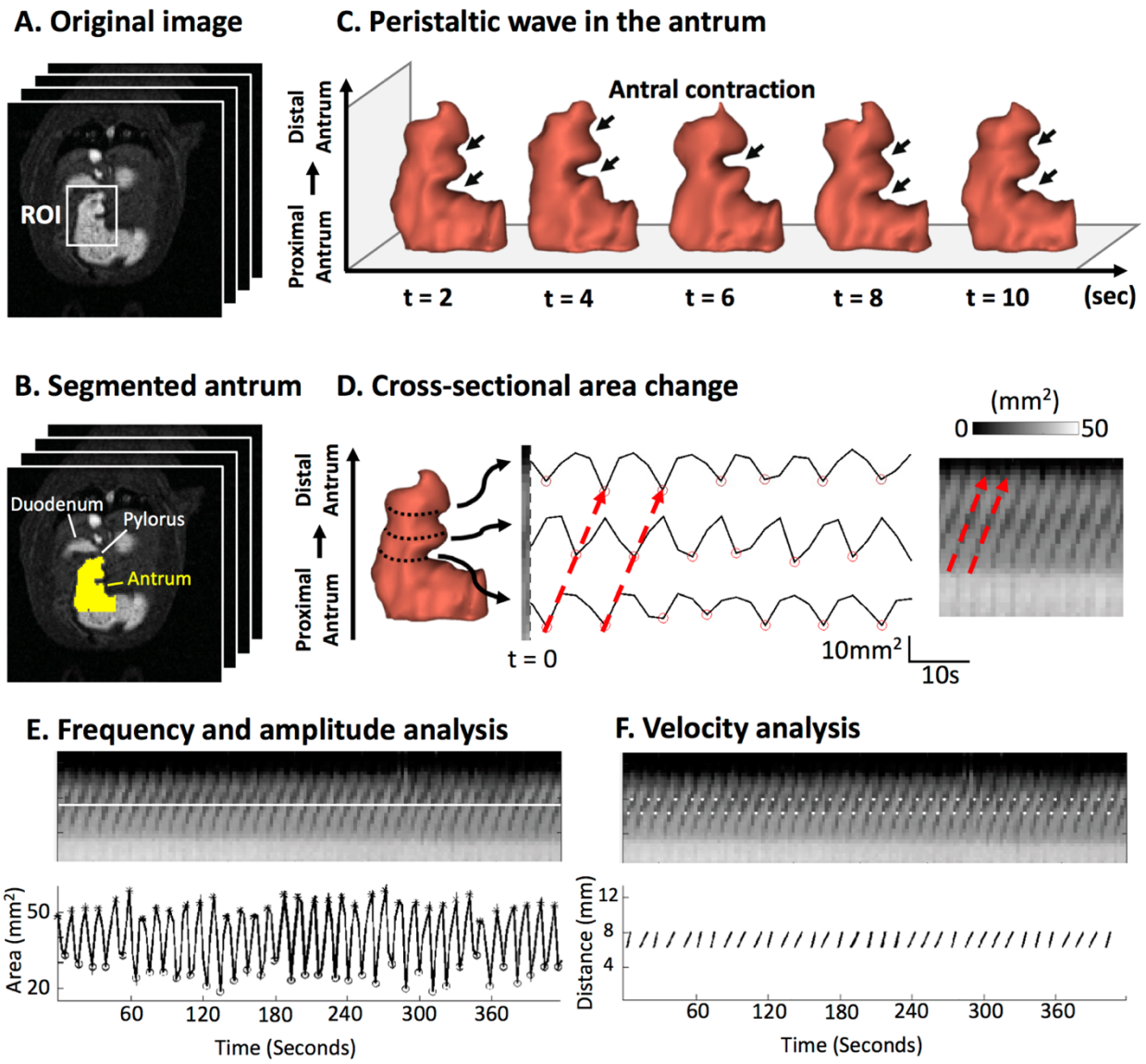

Figure 3.5 **Image analysis of antral motility.** **A.** Contrast-enhanced gastric MRI with fast sampling. **B.** Segmentation of the antrum. **C.** Temporal progression of the 3-D antral volume reveals the peristaltic wave. **D.** Changes in the cross-sectional area at different locations along the long axis of the antrum (from the proximal to the distal) are shown as time series or an image, both characterizing the antral motility. The red arrows mark the occurrence and progression of an antral contraction. **E.** The frequency and amplitude of the antral motility time series reveals the contraction frequency and amplitude. The distensions are marked with * and the contractions are marked with o. **F.** The spatial gradient of the phase of the motility time series reports the velocity of the peristaltic wave.

3.3 Results

3.3.1 Contrast-enhanced Gastric MRI

After a 7-day diet training followed by an 18-hour fast, each of the 11 animals was able to naturally consume a Gd-labeled test meal (Mean±S.D=6.90±1.33g; 5.43±1.05ml). Immediately after the meal, the animal was sedated and scanned with MRI for 4 hours (Figure 3.3). None of the animals showed any abnormal behavior or syndrome either during the diet training or after recovery from MRI. Repeated measurement was plausible on the same animal. *In vitro* calibration of T_1 and T_2 values of unlabeled and Gd-labeled dietgel is shown in Table 3.1. In T_1-weighted abdominal MRI, the test meal showed much higher intensity than surrounding tissues (Figure 3.3C). The contrast enhancement was pronounced during the entire experiment. As the ingested meal initially filled the stomach and then the intestines, it delineated the gastric lumen and revealed the gastric emptying and intestinal filling with high contrast and resolution for robust and quantitative analysis.

Table 3.1 ***In vitro*** **calibration of T_1 and T_2 measurements of the unlabeled and the Gd-labeled dietgel.**

	T_1		T_2	
	Unlabeled gel	Gd-labeled gel	Unlabeled gel	Gd-labeled gel
Value (ms)	1043.22	76.95	35.04	22.07

3.3.2 Gastric Emptying

Figure 3.6A shows the high-definition 3D-rendered gastric volumes for different compartments automatically segmented from the MRI images (as illustrated in Figure 3.4). The regional volumes in the stomach and the intestines were normalized against the total GI volume at time 0 within each animal, and then averaged across animals. At time 0, the stomach (Figure 3.6C) and intestinal volumes (Figure 3.6D) were 84.81±1.92% and 15.19±1.92%, respectively (n=11), summing up to 1 for the total GI volume. The stomach volume progressively decreased due to gastric emptying (Figure 3.6C), which was notably faster during the first 30 minutes than during the rest of the experiment. Along with this observation, the intestinal volume increased as the labeled meal filled the intestines, especially during the first 30 minutes (Figure 3.6D). Afterwards,

the intestinal volume decreased due to intestinal absorption from 30 to 60 minutes, and stayed roughly unchanged from 60-240 minutes, reflecting a balance between intestinal filling and absorption. Note that the total GI volume increased during the first 30 minutes (Figure 3.6B). This observation was likely attributed to gastric secretion. The total GI volume monotonically decreased from 30 to 240 minutes (Figure 3.6B), suggesting that there was a higher rate of gastric absorption than secretion during this period. After four hours in a sedated condition, the stomach volume decreased by 27% on average. This was mostly attributable to the progressive emptying of the forestomach (Figure 3.6E), whereas the corpus and the antrum had relatively minor volume changes (Figure 3.6F and Figure 3.6G). Quantitatively, the forestomach volume decreased from 64.20±3.43% to 47.60±3.71% (Figure 3.6E); the corpus volume decreased from 17.84±1.85% to 12.33±1.82% (Figure 3.6F); and the antral volume decreased from 5.34±0.62% to 4.07±0.61% (Figure 3.6G). The volume and morphological changes of the stomach and its compartments were apparent in multi-slice MRI images, showing high-resolution and high-contrast depiction of the lumen content in the GI tracts (Figure 3.7).

3.3.3 **Antral Motility**

When sampled with high temporal resolution around 2 seconds, the contrast-enhanced gastric MRI captured the gastric motility as a wave of antral contraction propagating along the long axis of the antrum. As shown in Figure 3.5, this antral peristaltic wave could be quantitatively characterized to accurately measure the frequency, amplitude, and velocity of the antral contraction. Averaged across animals, the frequency and velocity of antral contraction as well as the amplitude of antral occlusion was 6.34±0.07 contractions per minute, 0.67±0.02 mm/s and 30.58±1.03%, respectively.

I also evaluated the correlation between antral motility and stomach emptying across animals. As shown in Figure 3.8, no correlation was observed between stomach emptying and antral contraction frequency (r=0.0056) or amplitude (r=0.0555), whereas there was a weak correlation with the contraction velocity (r = 0.2709).

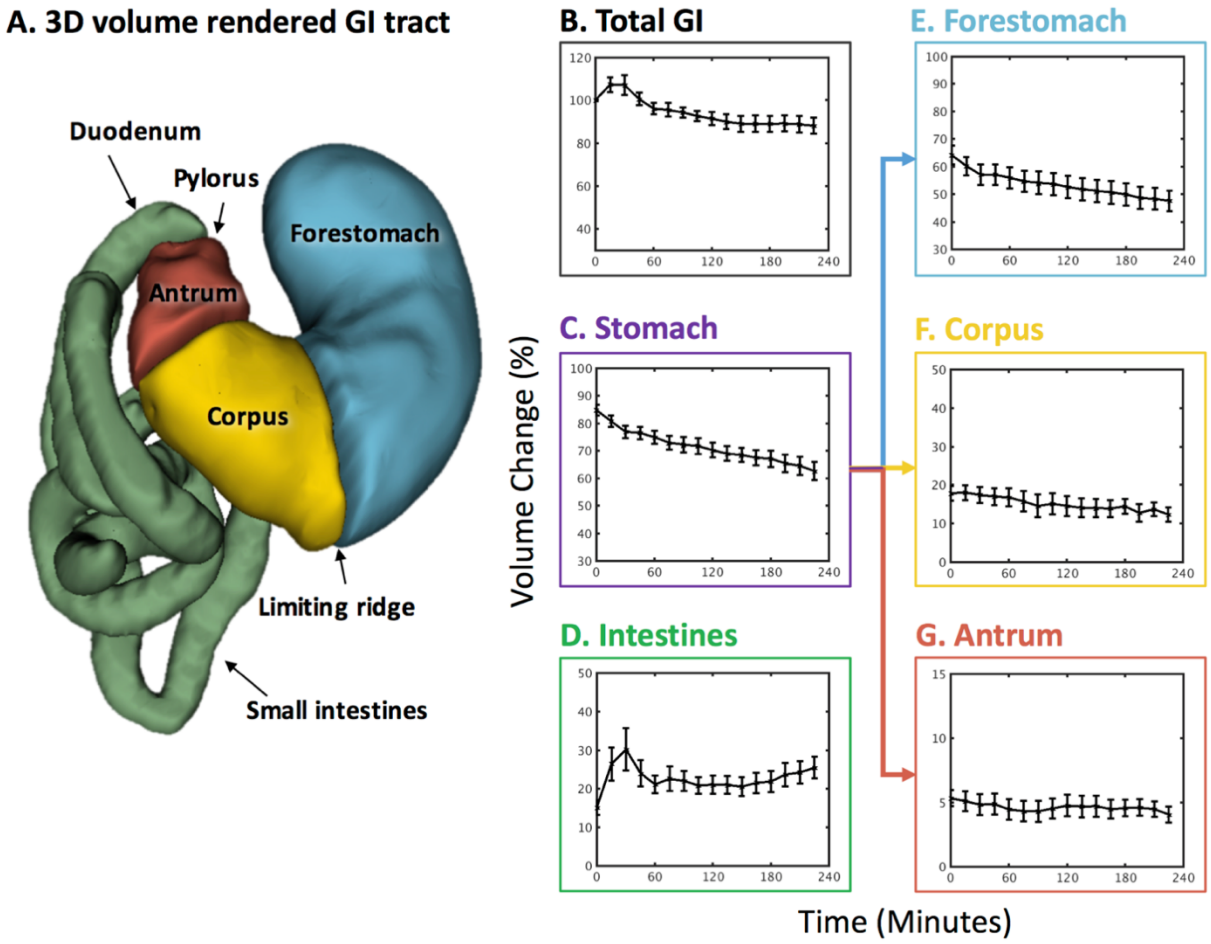

Figure 3.6 **Total and compartmental gastric emptying profiles. A.** 3D volume rendering of the GI tract. **B.** Change of the total GI volume. **C.** Stomach emptying profile. **D.** Intestinal filling profile. **E.** Forestomach emptying profile. **F.** Corpus emptying profile. **G.** Antrum emptying profile. All volumes were normalized against the total GI volume at time 0. Values are mean±standard error of the mean.

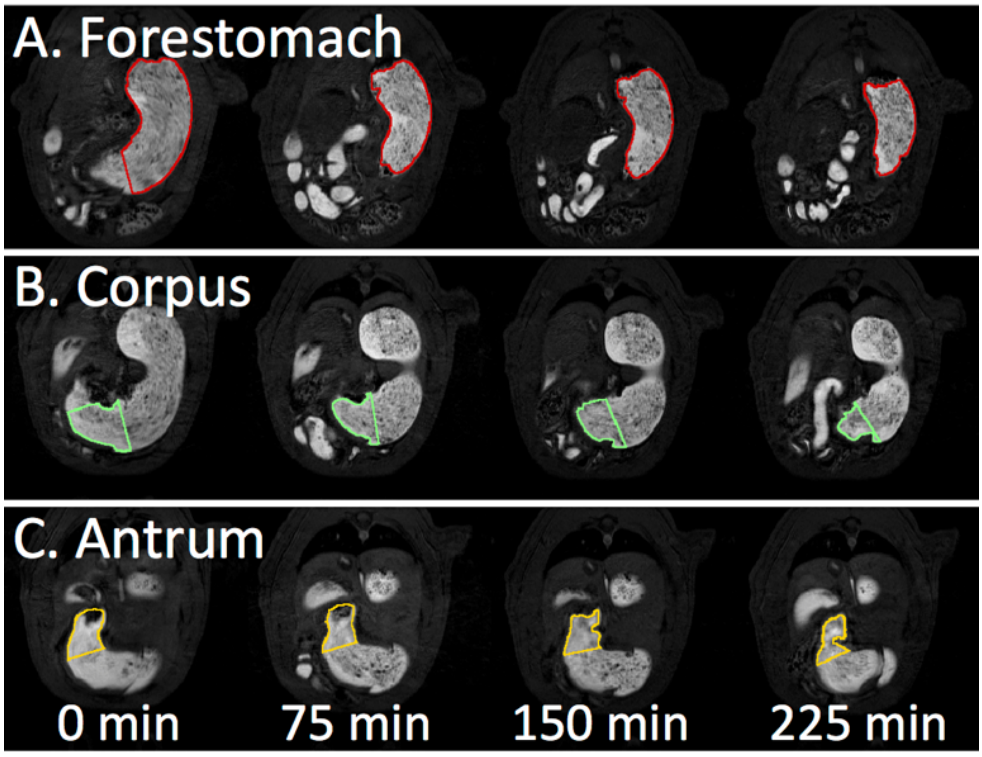

Figure 3.7 **Representative slices of temporal progression of gastric emptying in different stomach compartments. A.** Forestomach emptying. **B.** Corpus emptying. **C.** Antrum emptying.

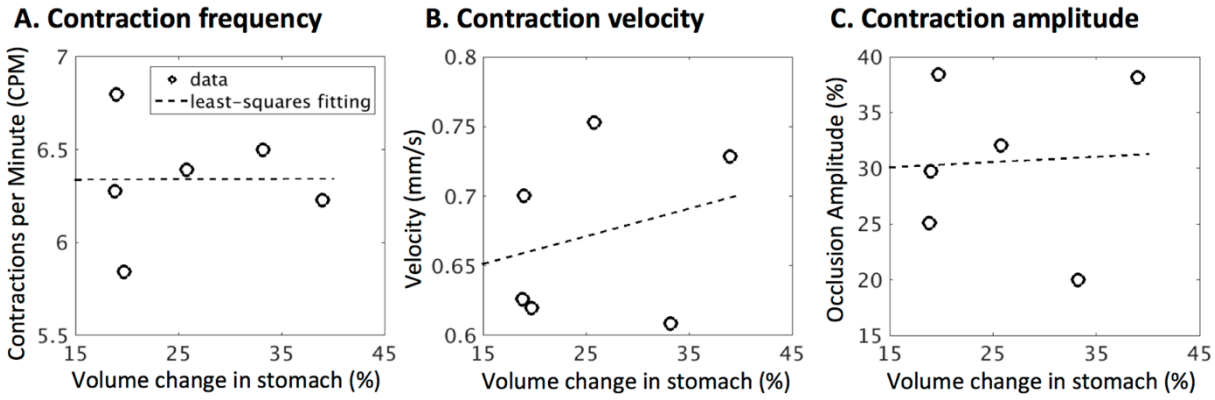

Figure 3.8 **Correlates of gastric emptying rate and antral motility. A.** Correlation between volume change in the stomach (%) and the antral contraction frequency (r = 0.0056). **B.** Correlation between volume change in the stomach (%) and the antral contraction velocity (r = 0.0555). **C.** Correlation between volume change in the stomach (%) and the antral contraction amplitude (r = 0.2709).

3.3.4 **Intestinal Absorption**

Along with my observation that the total GI volume decreased during the period from 30 to 240 minutes, there was a progressively emerging signal intensity enhancement in the renal medulla roughly 2 hours after the start of the experiment (Figure 3.9). This was likely due to the systemic accumulation of circulating Gd absorbed from the mucosa of the intestinal walls. The kinetics of how the kidney handled the systemically circulating gadolinium provided an indirect measurement of the intestinal absorption of nutrients.

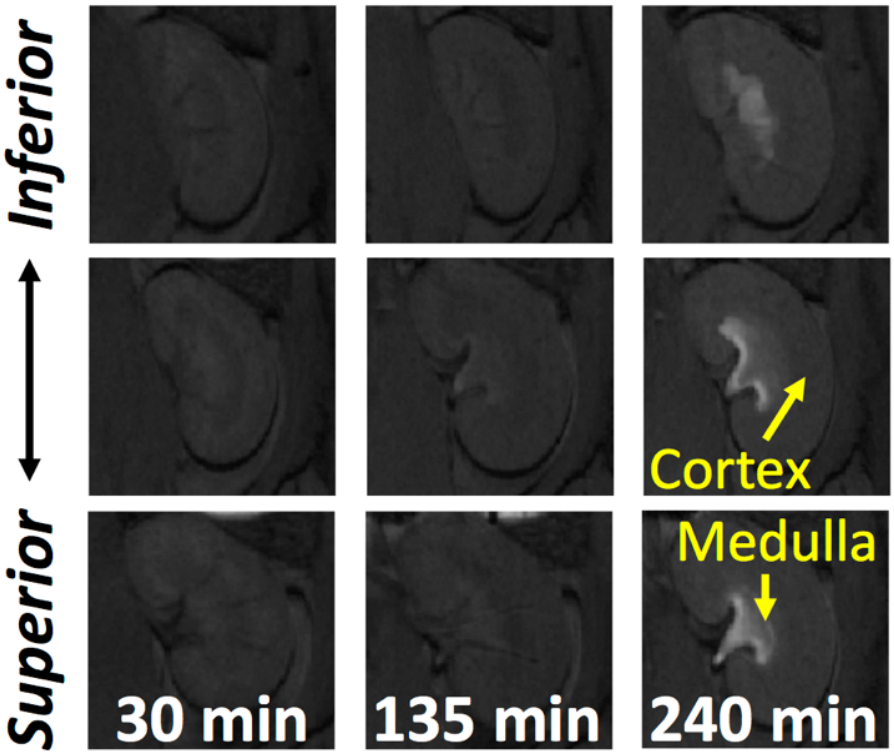

Figure 3.9 **The extent of absorption of nutrients measured in terms of kidney handling of systemically circulating gadolinium.** Representative slices of temporal progression of signal intensity enhancement in the renal medulla.

3.4 Discussion

Here, I present a robust and effective contrast-enhanced MRI method to image and characterize gastric emptying and motility in rats. This method includes animal training and MRI imaging protocols as well as image analysis pipelines. My results demonstrate the promise of using gastric MRI to non-invasively and quantitatively assess the emptying of the stomach and its compartments. It also allows quantitative evaluation of the antral motility in terms of the frequency, amplitude, and velocity of the antral peristaltic wave. This technique not only allows for repeated assessment within animals, but also shows consistent assessment across animals. It is thus well-suited for basic-science and preclinical studies of gastric physiology and diseases.

3.4.1 Highly Benign and Effective Animal Feeding Protocol

In this study, the animals were trained for one week to spontaneously consume a post-fast meal laced with trace amounts of gadolinium [the concentration was adapted from human feeding protocols [142]]. This allowed me to define gastrointestinal organs with high-resolution and high-contrast MRI. Although free gadolinium ion (Gd^{3+}) is a toxic lanthanide heavy metal, the compound is considered to be biologically safe when combined with other chelates such as DTPA and DOTA [143]. Adverse effects of oral or intravenous administration of gadolinium-based contrast agent were only recently found in patients with severe renal impairments [144]. This was likely due to impaired clearance of gadolinium by the kidney, which led to tissue accumulation of dissociated Gd^{3+}. A potential alternative to Gd-DTPA is Gd-DOTA, which is a more stable contrast agent in acidic gastric environment. Additionally, Gd-DOTA would not be easily absorbed by the GI tract, thus reducing the amount of systemically circulating gadolinium that kidneys need to handle [81]. A notable advantage of this protocol is that it bypasses the need of oral gavage. Oral gavaging introduces a major non-physiological simplification and considerable stress to the animal. Additionally, it may alter the physiological gut-brain coordination with normal food ingestion, in which the natural interaction between dietary exposure and oral mucosa is necessary for proper cognitive and sensory processing as well as gastric accommodation reflexes [145]–[147].

3.4.2 Gastric Emptying and Secretion

The ingestion volume, the secretion volume, and the volume that empties out of the stomach account for the total stomach volume change. This differs for the intestine, where the

volume that transits from the stomach and the volume of chyme that is absorbed through the intestinal mucosa account for the change in the intestinal volume. Given the fact that the animal did not ingest any additional food during MRI scans, the change in the gastric volume was strictly determined by the decrease throughout the emptying process and the increase in secretion volume.

My finding that the gastric emptying rate was largely attributed to the emptying rate of the forestomach is consistent with previous findings that emptying rates were higher in the forestomach than in the glandular stomach in rats [148], [149]. Therefore, the MRI-enabled compartment-wise analysis offers the sensitivity and specificity in detecting regional differences in emptying within the stomach, and may potentially be useful for examining different pathological disorders (i.e. gastroparesis).

In this study, I could not differentiate the remaining meal and the gastric secretion in the stomach, because the latter also appeared with high contrast in MRI. One way to separate meal and gastric juice may be based on in vitro calibration of either the T_1-weighted signal intensity [94], T_1 [105], [150], or T_2 value [86] for these two substances, for example by diluting the test meal with different amounts of hydrochloric acid to simulate the meal-juice mixture in vivo. This strategy assumes a homogeneous mixture of the meal, gastric juice and the contrast agent, and typically requires the test meal to be in the liquid state. Such assumption or requirement was not met in this study since my test meal was a viscous semi-solid dietgel that appeared heterogeneous in the gastric lumen with small intra-gastric air cavities. Moreover, the dilution and mixture of a viscous test meal with secretion juice is slow and uneven in the stomach, mostly occurring at the wall of the lumen [86]. Future methodological development is much desired to accurately assess gastric secretion for various types of test meal.

3.4.3 **Confounding Effect of Anesthetic Agent**

One of the major limitations of doing gastric MRI in animals is the need of anesthetics for restraining them from body movement. As a result, the choice of anesthetic(s) is critical, given that different anesthetics alter the GI functions differently. Here, I chose to use a combination of dexmedetomidine and low dose of isoflurane. The reasoning behind this choice is twofold; although it has been reported that dexmedetomidine delays gastric emptying, the effect is weak compared to saline placebo [151]. In contrast, using isoflurane alone would significantly impact the activity of the gut by a reduction of 50% in GI transits [152]. Further, it is also critical to

understand the biochemical and bioelectrical signaling processes in between the enteric and central nervous systems. In this regard, MRI serves as a versatile imaging tool to investigate brain functions (i.e. functional MRI), especially because there is an emerging interest in examining the functional network in the rodent brain [153], [154]. A common anesthetic protocol that could serve both needs is advantageous because it could potentially be used for imaging both the GI tract and the rodent brain. As such, I adopted and adapted the anesthetic protocol from [154] for neural imaging in rats. This has previously been shown to better preserve the functional activities in rodent's central nervous system (CNS) under longitudinal experiments [155], as compared to using isoflurane alone. By combining the use of these two anesthetics, my dosage for each of them was well below what has been reported in the earlier studies. However, I do not rule out the possibility that the gastric functions are (at least minimally) affected by the anesthetics. It might be possible to adopt the animal protocol developed in animal brain imaging [156], [157] to train animals to stay still during gastric MRI in future studies.

4. VAGUS NERVE STIMULATION PROMOTES GASTRIC EMPTYING BY INCREASING PYLORIC OPENING MEASURED WITH MAGNETIC RESONANCE IMAGING

*Modified and formatted for dissertation from the article published in *Neurogastroenterology & Motility* [158]

4.1 Introduction

Dysregulation of GI functions is associated with gastroparesis [48], [51], obesity [127], gastroesophageal reflux disease and other GI disorders [128]. These diseases are often chronic, idiopathic, and to date, not readily mitigated by surgical, pharmaceutical, and/or dietary treatments [3]. For this reason, researchers have begun to explore electrical stimulation of the vagus nerve as an alternative strategy to remedy gastric disorders [66], [159]–[162].

The vagus nerve plays an important role in mediating the interaction between the central nervous system (CNS) and the gut. It carries coordinated afferent information from the GI tract to the nucleus tractus solitarius (NTS) in the brainstem, and issues efferent signals from the dorsal motor nucleus of the vagus (DMV), primarily to the lower third of the esophagus and the stomach to modulate their functions [5], [6], [113], [163], [164]. Different branches of the vagus innervate different parts of the GI tract. Therefore, fiber-selective or feedback-controlled stimulation of the vagus is potentially a favorable and effective approach to treat targeted gastric disorders.

Substantial efforts have been made in mapping the topographical and functional organization of the vagus nerve [70], [72]. Initial promise of VNS has also been demonstrated for treating epilepsy [165], anxiety disorders [166], chronic heart failure [167], apnea [168] and inflammation [169], [170]. However, the therapeutic potential of VNS on gastric disorders remains unclear and its mechanism-of-action is still elusive. The reasons are likely multiple, but two stand out: First, the GI tract is not only innervated by the extrinsic vagovagal neurocircuits, but also by its intrinsic enteric network. The interplay of extrinsic and intrinsic innervations are rather complex [5]. Second, different gastric regions are innervated by different vagal branches, thereby having differential responses to VNS, yet proper functioning of the GI tract is thought to require a coordinated choreography of all gastric regions [72].

Most existing neuromodulation protocols measure physiological responses to stimulation at discrete locations without considering the global state of the stomach [171]–[173]. In this regard, magnetic resonance imaging (MRI) yields simultaneous surveys of many tissues, making it an ideal tool to study various aspects of gastric motility. While gastric MRI has been increasingly applied to humans [105], [174], [175], it has rarely been used in small animal models for preclinical assessment. Here, I set out to evaluate the effects of left cervical VNS on antral contraction, pyloric opening and gastric emptying in heathy rats by using the imaging-based assessment I developed in the previous chapter. The proposed experimental protocol and findings could offer new insights in the use of animal gastric MRI to evaluate the efficacy of therapeutics in treating gastric disorders.

4.2 Materials and Methods

Briefly, a gadolinium-based contrast agent was mixed with the animal's meal in order for chyme to appear "bright" in MRI scans, thereby delineating the gastric and intestinal volume. A multi-slice MRI sequence was used to scan the GI volume with high spatial resolution, and a similar sequence with a smaller spatial coverage was used to scan antral contractions with high temporal resolution. Measurements of gastric functions and physiology included the overall change in GI volume, gastric emptying, forestomach volume, corpus volume, antral volume, antral contraction frequency, antral peristaltic wave velocity, antral contraction amplitude, pyloric opening size, intestinal filling and, indirectly, absorption.

4.2.1 Animal Protocol

Thirty rats (Sprague-Dawley, male, 228-330g) were included in the study. All study procedures were approved by the Purdue Animal Care and Use Committee. Rats were housed individually in ventilated cages with elevated stainless steel wire floors during all time to prevent the animals from accessing their feces. The environment was maintained on a 12:12h light-dark cycle (lights on at 6AM and lights off at 6PM).

4.2.2 Animal Preparation and Surgical Protocol

According to the feeding protocol described in section 3.2.2, each animal was trained until (approximately 7 days) it would voluntarily consume a fixed quantity (10g) of dietGel (DietGel

Recovery, ClearH_2O, ME, USA). On the day for gastric MRI, each animal was given the test meal with a mixture of dietgel and Gadolinium.

Following an over-night food restriction (18 hours, 5PM to 11AM), rats were able to voluntarily consume the Gd-labeled test meal in 14±5 minutes. Then, each animal was anesthetized with 4% isoflurane mixed with oxygen at a flow rate of 500ml/min for 5 minutes. Rats were allocated into 3 groups as follows: 1) an unoperated control group including the rats that did not receive surgery (n=11); 2) a sham control group including the rats that only received sham surgery (n=9); 3) a VNS group including the rats that received both surgery and vagus nerve stimulation (n=10). Rats in the sham and VNS groups underwent the identical neck surgery for implantation of a bipolar cuff electrode around the left cervical vagus nerve.

After administering a pre-operative bolus of carprofen (10mg/kg, IP; Zoetis, NJ, USA) and performing a toe-pinch to assure adequate anesthesia, a ventral midline cervical incision was made between the mandible and sternum. Anesthesia was maintained by 2.5-3.0% isoflurane mixed with oxygen at a flow rate of 1000ml/min throughout the electrode implant and sham implant surgery. The subcutaneous tissue of the ventral neck was then bluntly dissected and retracted laterally together with the mandibular salivary glands to reveal the trachea and the left carotid artery. Upon exposure of the left carotid artery, the left cervical vagus nerve, which sits lateral and runs parallel to the carotid artery above the level of the carotid bifurcation, was identified. The connective tissues surrounding the left cervical vagus nerve were carefully dissected so that a 10-15 mm portion of the cervical vagal trunk was isolated from the carotid artery. A custom-designed bipolar cuff electrode (MicroProbes, Gaithersburg, MD, USA) with a platinum-iridium wire lead was wrapped and secured on the isolated vagus nerve. The lead was externalized prior to suturing the incision site.

The animal was then placed in prone position on a water-heated MR-compatible cradle. On the cradle, the animal received a bolus injection of 0.01mg/kg dexmedetomidine solution (0.05mg/ml, SC; Zoetis, NJ, USA). Five minutes later the isoflurane dose was reduced to 0.3-0.5% isoflurane mixed with oxygen at a flow rate of 500ml/min. Fifteen minutes after the initial bolus, a continuous subcutaneous infusion of dexmedetomidine was administered (0.03mg/kg/hour, SC). An MRI-compatible system (SA Instruments Inc., Stony Brook, NY, USA) was used to monitor respiration, cardiac pulsation, and body temperature to ensure a stable physiological state throughout the experiment. The two leads of the vagal electrodes were connected to a pair of

twisted wires that ran from the MRI bore to the console room, and the wires were further connected to a constant-current stimulator (A-M Systems Model 2200). Upon the start of the first MRI acquisition, electrical pulses (monophasic pulses with alternating polarity, inter-pulse duration (IPD) = 50ms; pulse amplitude (PA) = 0.6mA; pulse width (PW) = 0.36ms; frequency = 10Hz; 20 seconds on and 40 seconds off) were delivered to the cervical vagus throughout the 4-hour experiment.

4.2.3 **Gastric MRI**

The animals were scanned in a 7-tesla horizontal-bore small-animal MRI system (BioSpec 70/30; Bruker Instruments, Billerica, USA) equipped with a gradient insert (maximum gradient: 200mT/m; maximum slew rate: 640T/m/s) and a volume transmit/receive ^{1}H RF coil (86mm inner-diameter).

As elaborated in section 3.2.5, after the long axis of the stomach was localized with the initial MRI scans, the MRI protocol was performed with a series of alternating volumetric scans and fast scans; the former was for quantifying gastric volume with higher spatial resolution and larger spatial coverage, whereas the latter was for assessing antral motility with higher temporal resolution and more targeted spatial coverage. The volumetric scans were acquired using a two-dimensional FLASH sequence with TR = 124.131ms, TE = 1.364ms, FA = 90º, 30 oblique slices, slice thickness = 1mm, FOV = 60 × 60 mm^2, in-plane resolution = 0.23 × 0.23 mm^2, and 4 averages. The fast scans were acquired using a two-dimensional FLASH sequence with TR/TE = 11.784/1.09ms, FA = 25º, four oblique slices, slice thickness = 1.5mm, FOV = 60 × 60 mm^2, in-plane resolution 0.47 × 0.47 mm^2, no averaging, and 150 repetitions. The four fast scan slices were positioned and adjusted to cover the antrum, pylorus and duodenum, based on the immediately preceding volumetric images to account for the stomach displacement during gastric emptying.

To minimize motion artifacts, both volumetric and fast scans were respiration-gated such that images were acquired during end-expiratory periods, while the chest volume stayed roughly unchanged. With the respiratory gating, the volumetric scan took about 4 minutes; the fast scan took ~2 seconds per repetition and lasted ~6 min for 150 repetitions. The volumetric and fast scans were repeated in an interleaved manner for a total of four hours.

4.2.4 **Assessment of GI volume, Compartmental volume, and Emptying rate**

The GI volume was assessed globally and compartmentally, which included the gastric volume and intestinal volume. The intestinal volume comprised the duodenal, jejunal, and ileal volumes. The gastric volume was further partitioned into forestomach, corpus and antral volumes. The volumes were sampled approximately every 15 minutes for 4 hours. Specifically, the contrast-enhanced lumenal volumes of the GI tract at different times were segmented, partitioned, and quantified separately from the volumetric scans by using the image processing pipeline described in section 3.2.6. Note that some voxels in large veins with much shortened T_1 and those in the renal medulla due to systemic Gd absorption might be mistakenly included in the above segmentation. Such spurious voxels were manually identified and excluded from the analysis. In addition, the heterogeneous image intensity (e.g. feces with unenhanced and/or partly enhanced image intensity) in the colon raised difficulty in proper quantification of the colonic volume; hence voxels in the colon were removed as well. The processing time for a 4-hour volumetric dataset was about 1.5 hours. The volume of each compartment measured at intervals was further normalized as a percent of its initial volume at time 0. This normalization step allowed us to observe the relative volume change over time for each animal, while accounting for the varying amount of the meal intake and the preparation time for different animals. The time series of gastric volumes were resampled at 15-min intervals for every animal and then averaged across animals to characterize gastric emptying at the group level. Note that the VNS began at the start of the first volumetric scan ($t = 0$). Since the scan took about 4 minutes to acquire, a 4-minute delay was added to all time series.

4.2.5 **Assessment of Gastric Motility**

The frequency, amplitude and velocity of the peristaltic wave in the gastric antrum were quantified from the fast scans by using the custom-built Matlab image processing pipeline. Briefly, the antrum was first delineated from a stack of 4 slices, and the proximal-to-distal antral axis was determined. The cross-sectional areas perpendicular to the proximal-to-distal antral axis were then calculated by summing the number of antral voxels within each cross-sectional plane. By iteratively doing so for each volume, I obtained a time series that represented the cross-sectional area (CSA) change of the antrum at different locations distant to the pylorus. In the CSA time series, the maxima of the time series indicated antral distension and the minima antral contraction

(i.e. the lumen was largely occluded by the depth of the constriction of the antral wall). The antral contraction frequency, occlusion amplitude and velocity were computed from the time series. In this study, the antral motility indices were obtained from the middle antrum, which was 4.7mm distant from the pylorus. This process was repeated for each volume. A time series that characterized the antral motility was obtained and resampled at 15-min intervals for every animal and then averaged across animals. Since VNS began at the start of the first volumetric scan (t = 0) and the volumetric scan and the fast scan took about 4 minutes and 6 minutes, respectively, a 10-minute delay was added to all time series. Of the 11 animals in the unoperated control group, 5 animals were excluded from the study due to either disoriented antrum or the presence of gastric air in the antrum. One animal in the VNS group was excluded from the study using the same exclusion criteria.

4.2.6 **Measurement of the Size of the Pyloric Sphincter Lumen**

To measure the size of the pyloric sphincter, I manually determined a cross-sectional plane that was perpendicular to the outflow direction of the terminal antrum on the segmented GI tract from the volumetric scans. The CSA of the pyloric sphincter was calculated by counting the number of lumenal voxels in the determined plane, as shown in Figure 4.3A. This process was repeated for each volume, and a time series that characterized the pyloric opening was obtained for each animal. The time series were resampled at 15-min intervals for every animal and then averaged across animals for analysis at the group level. A 4-minute delay was added to all time series for the same reason mentioned in the gastric emptying analysis.

4.2.7 **Statistical Analysis**

Unless otherwise stated, all data are reported as mean±standard error of mean (SEM). A probability (p-value) < 0.05 was considered significant to reject the null hypothesis. To evaluate the significance of the difference in the gastric emptying profile between the two conditions, the emptying curve from each subject was modeled by a Weibull distribution expressed as in Equation 4-1, for which the two parameters (t_{const}, β) were estimated by the least-squares method [176],

$$V(t)(\%) = 100exp^{-(\frac{t}{t_{const}})^{\beta}} \quad \text{(Equation 4-1)}$$

where V(t) is the remaining volume at experiment time t (min), β is the shape parameter of the curve, and t_{const} is the emptying time constant (min). The fitting was done by using the *fit* function

in Matlab. Only the estimated parameters with goodness of fit (R^2) metrics greater than 0.85 were subject to the subsequent statistical analysis. One-way ANOVA was performed to assess the significance of the differences between the fitted parameters for the unoperated control, the sham control, and the VNS conditions, followed by Fisher's least significant difference (LSD) post-hoc tests. To further assess the difference of the remaining volume in each compartment, one-way ANOVA with LSD test was conducted on individual time points between the three conditions. One-way ANOVA with LSD test was also applied to determine whether there were statistically significant differences in antral motility indices and the degree of the pyloric opening between the three conditions.

4.3 Results

4.3.1 Gd-labeled Meal Revealed the Gastric Lumen in MRI

All animals voluntarily consumed the Gd-labeled dietgel on the day of imaging following 7 days of training. Specifically, the unoperated control rats consumed 6.90±0.40g meal in 14±5 minutes; the sham rats consumed 8.45±0.43g meal in 15±3 minutes; the VNS rats consumed 8.62±0.59g meal in 13±7 minutes. The overall preparation time (the interval between the finish of eating and the start of the first MRI acquisition) for the unoperated control rats, the sham rats and the VNS rats was 22±7 minutes, 83±15 minutes and 75±10 minutes, respectively. Eleven unoperated control rats were scanned for gastric MRI under low dose anesthesia; Nine sham rats were scanned for gastric MRI after sham surgical operations, whereas the remaining 10 rats were scanned with their left cervical vagus nerve being electrically stimulated for 4 hours after the surgery (Figure 4.1A). Figure 4.1B shows the electrical stimulation paradigm. Adding gadolinium to the meal shortened the T_1 relaxation. The meal thus appeared with much higher image intensity on the T_1-weighted images compared to the surrounding tissues (Figure 4.1C & Figure 4.1D). The gastric volume and motility were quantified according to my image processing pipeline. Animals that underwent acute electrode implant surgeries prior to imaging were euthanized at the end of the experiment.

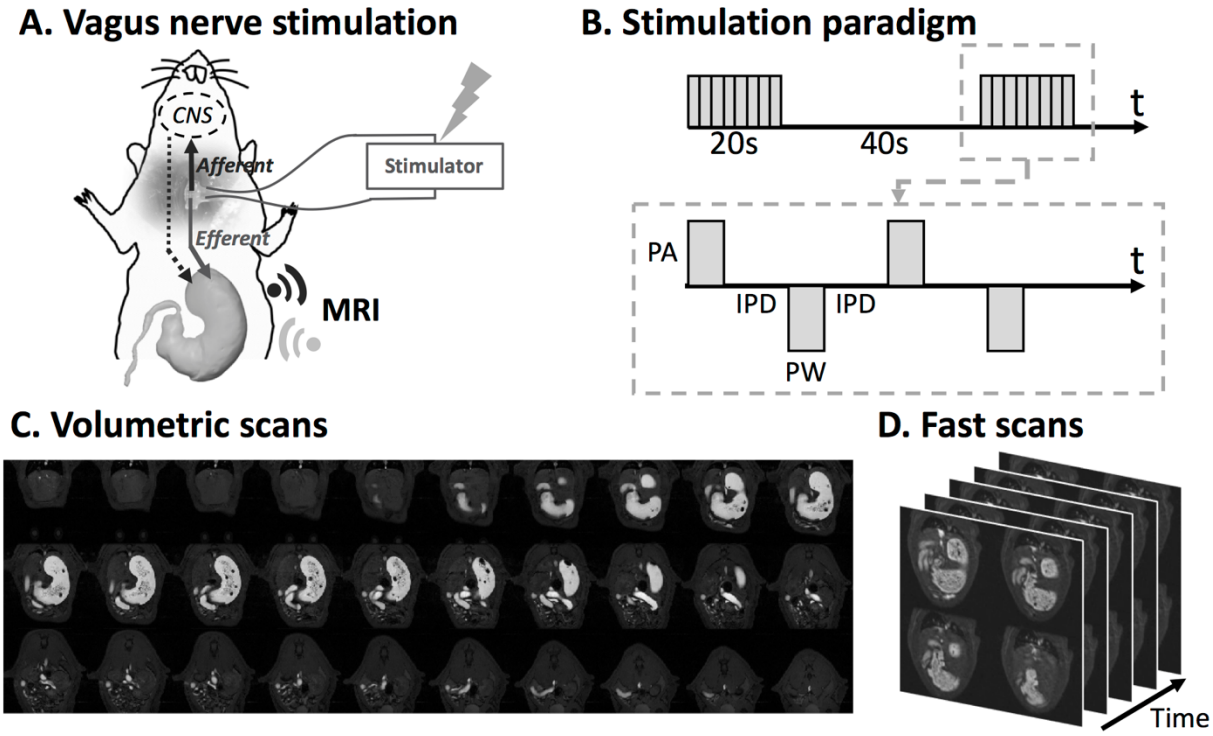

Figure 4.1 **Vagus nerve stimulation and imaging sequence. A.** Schematic diagram of the experiment protocol. A bipolar cuff electrode was implanted at the left cervical vagus of a rat. Vagus nerve stimulation was performed during the 4-hour MRI scans. **B.** Stimulation waveform, paradigm and parameters used in this study. (inter-pulse duration (IPD) = 50ms; pulse amplitude (PA) = 0.6mA; pulse width (PW) = 0.36ms; frequency = 10Hz; 20 seconds on and 40 seconds off) **C.** Example semi-coronal view images from the 2D multi-slice volumetric scan. The gastrointestinal tract is highlighted by the Gadolinium-labeled meal. **D.** Fast scans of the antrum with four slices. The position of the slice package was determined from images acquired from the volumetric scan.

4.3.2 Vagus Nerve Stimulation Promoted Gastric Emptying

Figure 4.2 shows the modulatory effect of VNS on gastric emptying. All volumes were normalized against the volume within each respective GI compartment at time 0 – which indicates the emptying rate with respect to their initial volume – and then averaged across animals. Figure 4.2A illustrates the 3D GI tract rendered from the high resolution volumetric scans.

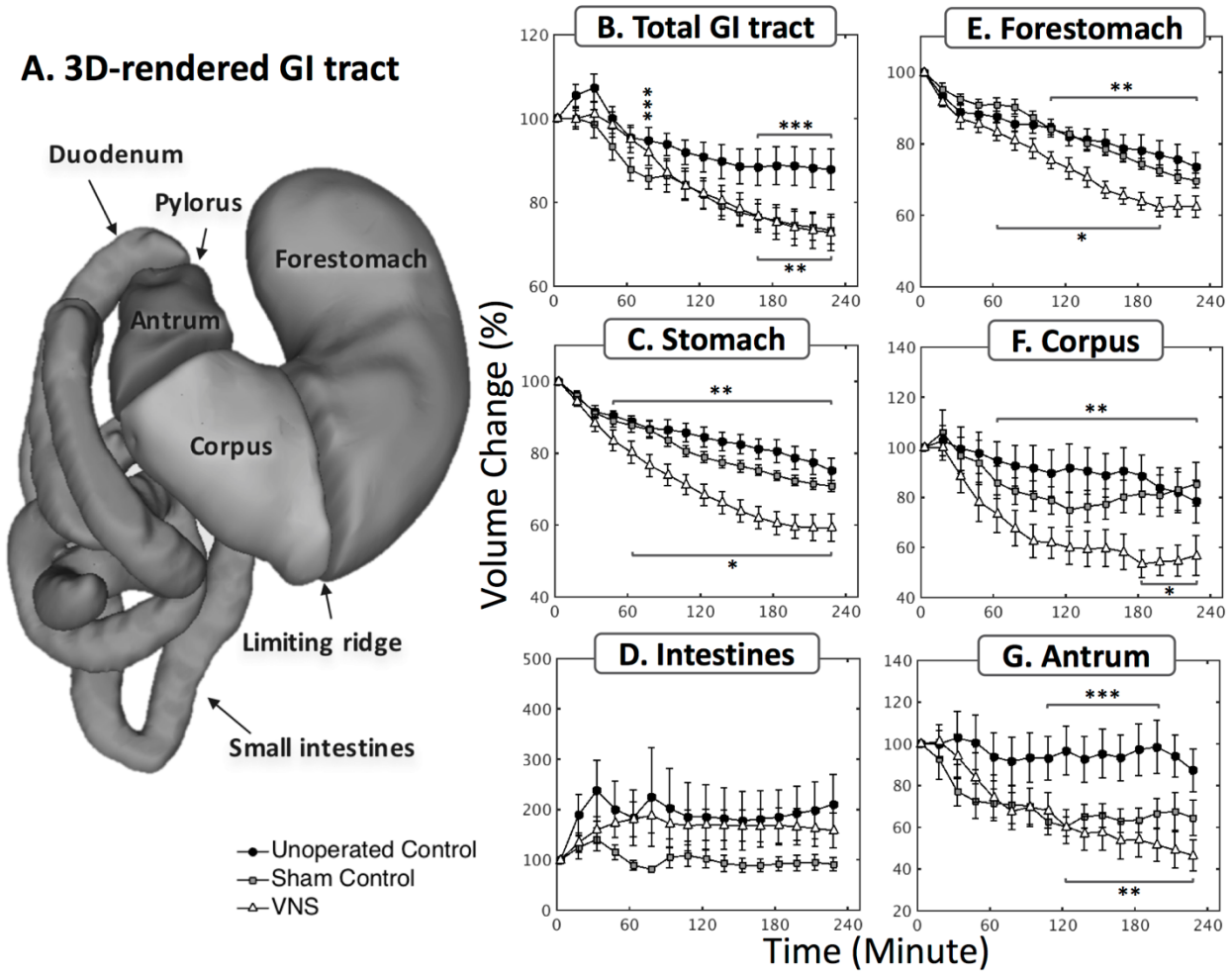

Figure 4.2 **Vagal stimulation significantly enhances the rate of gastric emptying. A.** 3D volume rendering of the lumen of the gastrointestinal tract. The profiles of volume change were quantified at a global scale including **B.** total GI tract, **C.** stomach, **D.** intestines, as well as at a compartment-wise scale including **E.** forestomach, **F.** corpus, **G.** antrum. *: $p<0.05$: sham vs. VNS, **: $p<0.05$: unoperated control vs. VNS, ***$p<0.05$: unoperated control vs. sham.

Different compartments of the GI tract were separated and labeled by the processing pipeline. Figure 4.2B shows the volume change (%) of the GI tract (gastric volume plus small intestinal volume). The volume changes in the GI tract is strictly determined by the meal volume, secretion volume, and the volume absorbed by the intestines. In the first 30 minutes, there was an increase in the total GI volume in the unoperated control group (likely due to secretion) but not in the sham and the VNS groups. After approximately one hour, the rate of volume change was faster in both sham group and VNS group than in the unoperated control group. Although no significant difference in total GI volume change was found between the sham group and the VNS group,

gastric emptying was significantly faster with VNS compared to the sham condition (Figure 4.2C). A compartment-wise analysis showed that the emptying rate in the forestomach (Figure 4.2E) and corpus (Figure 4.2F) was increased by VNS but not in the antrum (Figure 4.2G). Note that the antral volume stayed almost unchanged in the unoperated control condition, suggesting a balance between secretion, the delivery of chyme to the antrum and the transfer of chyme to the duodenum. Such a balance was not observed in the sham and VNS condition. In Figure 4.2D, the intestinal volume (i.e., duodenum, jejunum and ileum) increased as the chyme filled the intestines, especially during the first 60 minutes. The intestinal filling rate was greater with VNS than in the sham condition, consistent with the accompanying difference in gastric emptying rate. The intestinal volume stayed roughly unchanged from 60-240 minutes, which suggests a balance between intestinal filling and absorption.

The gastric emptying curves were quantitatively characterized by a shape constant (β) and a time constant (t_{const}). No significant difference in shape constant was found between the three conditions [unoperated control (n=8) vs. sham (n=9) vs. VNS (n=9): 1.08±0.22 vs. 0.80±0.09 vs. 0.89±0.10]. The time constant [unoperated control (n=6) vs. sham (n=9) vs. VNS (n=9): 822.2±134.8 vs. 1011.9±134.0 vs. 437.1±40.7 minutes] was significantly less in the VNS condition than in the sham condition ($p<0.05$), suggesting that VNS increased the rate of gastric emptying. No significant difference in time constant was found between the unoperated control group and the sham group ($p=0.2419$). The differences of volume change within each compartment were also statistically evaluated as illustrated in Figure 4.2B-G. Specifically, there was a significant difference between the sham and the VNS group in the overall (i.e. 4-hour) volume change in the stomach (sham vs. VNS: 29.1±1.5% vs. 40.7±3.9%, $p<0.05$), in the corpus (sham vs. VNS: 14.7±8.8% vs. 43.2±7.9%, $p<0.05$), and a non-significant difference in the forestomach (sham vs. VNS: 30.3±2.1% vs. 37.6±3.0%, $p=0.14$). A significant difference in volume change was also found between the unoperated control and the sham group in the total GI volume and the antral volume ($p<0.05$).

4.3.3 **Vagus Nerve Stimulation Increased the Size of the Pyloric Lumen**

The lumenal CSA of the pyloric ring was defined as shown in Figure 4.3A. Figure 4.3B shows how the size of the pylorus size changed during the 4-hour experiment for VNS animals and their controls. With VNS, the lumenal CSA of the pylorus was on average significantly greater

than that without VNS (sham vs. VNS: 1.5±0.1 vs. 2.6±0.4 mm^2; $p<0.05$; Figure 4.3C), particularly at t = 4, 19, 34, 79, 169 and 184 minutes ($p<0.05$). The increase in the pyloric lumenal size was further correlated with the increase in stomach emptying. The overall volume change (%; four-hour difference) in the stomach was significantly correlated with the CSA of the pyloric lumen ($r = 0.5887$, $p < 0.001$). Note that VNS in general led to a larger volume change in the stomach and to a greater size of the pylorus as shown in Figure 4.3D.

4.3.4 **Vagus Nerve Stimulation Promoted Antral Motility**

Next, I examined whether VNS modulated antral motility in terms of the frequency, amplitude and velocity of antral contractions. When sampled every ~2 seconds, the contrast-enhanced gastric MRI captured the gastric motility as a wave of antral contraction propagating along the long axis of the antrum. I found that surgical operations resulted in a non-significant decrease in antral contraction amplitude (unoperated control vs. sham: 30.6±3.0 vs. 23.3±3.0 percent occlusion; $p=0.1667$; Figure 4.4B) and a significant decrease in the propagating velocity of contraction waves (unoperated control vs. sham: 0.67±0.03 vs. 0.50±0.02 mm/s; $p<0.05$; Figure 4.4C). With VNS, the antral contraction amplitude was on average significantly greater than the sham condition (sham vs. VNS: 23.3±3.0 vs. 32.5±3.0 percentage occlusion; $p<0.05$; Figure 4.4B, right panel), particularly during the first two hours of the experiment (Figure 4.4B, left panel). Similarly, the propagating velocity of contraction waves was on average significantly greater with VNS than without VNS (sham vs. VNS: 0.50±0.02 vs. 0.67±0.03 mm/s; $p<0.05$; Figure 4.4C, right) throughout the 4-hour experiment. However, no significant differences were found in contraction frequency between the three conditions (unoperated control vs. sham vs. VNS: 6.3±0.1 vs. 6.1±0.2 vs. 6.4±0.2 cpm; $p=0.4482$; Figure 4.4A, right panel), except that differences were found during the first 30 minutes and the last 30 minutes of the experiment ($p<0.05$; Figure 4.4A, left panel).

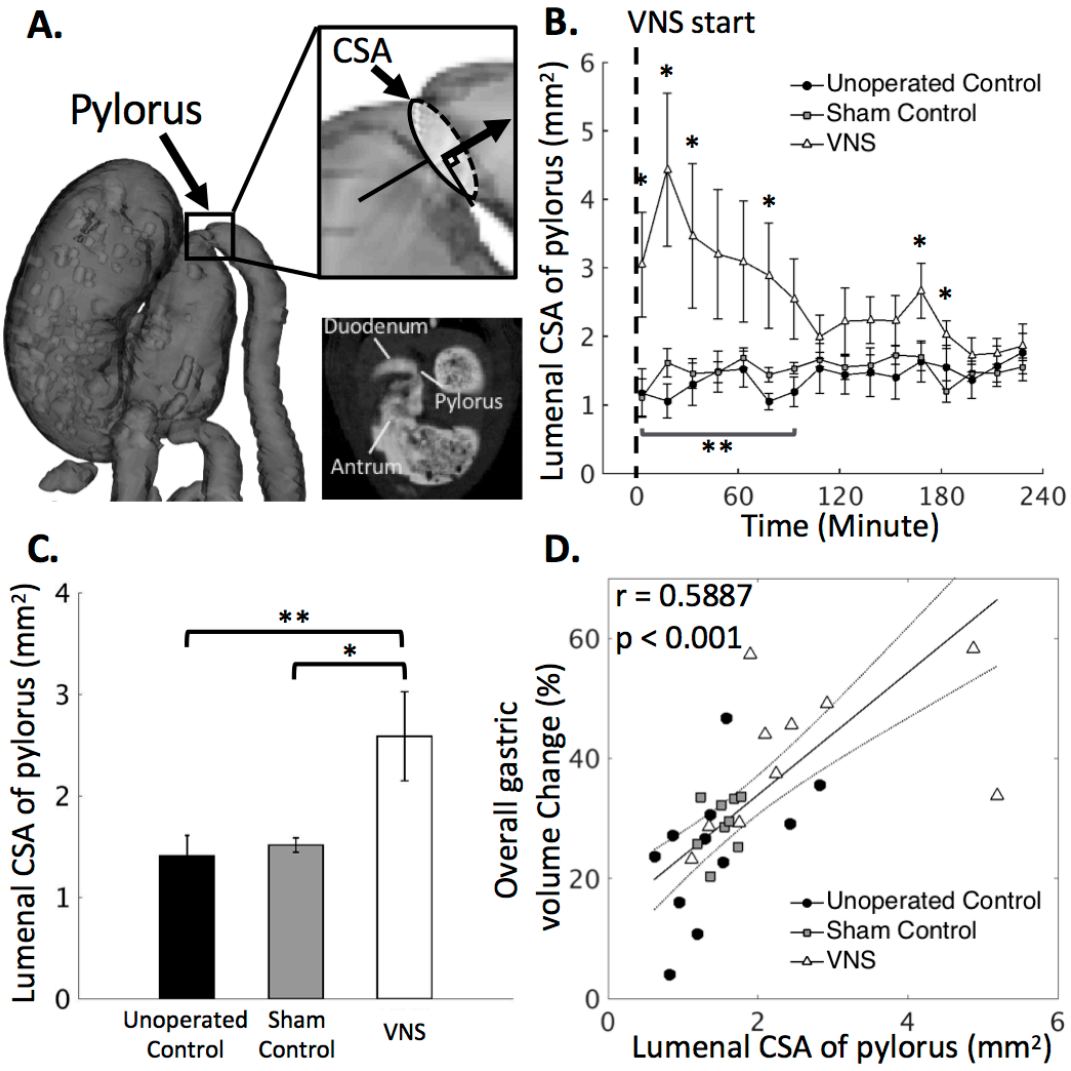

Figure 4.3 **Quantification of the extent to which the pyloric ring opened under unoperated control, sham and VNS conditions. A.** Illustrates the location of the pylorus from a 2D slice and from a rotated 3D rendered volume. The degree to which the pyloric ring opened was measured in terms of the cross-sectional area (CSA) of the lumenal content in the pyloric canal from the high spatial resolution scans. **B.** The CSA of the pyloric ring is on average greater with VNS than without VNS, with notable and significant differences during the first 1 hour of the experiment. **C.** In general, VNS significantly increases the size of the pylorus. **D.** The overall gastric volume change (%; four-hour difference) is significantly correlated to the CSA of the pyloric ring. Noted that VNS in general leads to a larger volume change in the stomach and to a greater CSA of the pyloric ring. *: $p<0.05$: sham vs. VNS, **: $p<0.05$: unoperated control vs. VNS, ***$p<0.05$: unoperated control vs. sham.

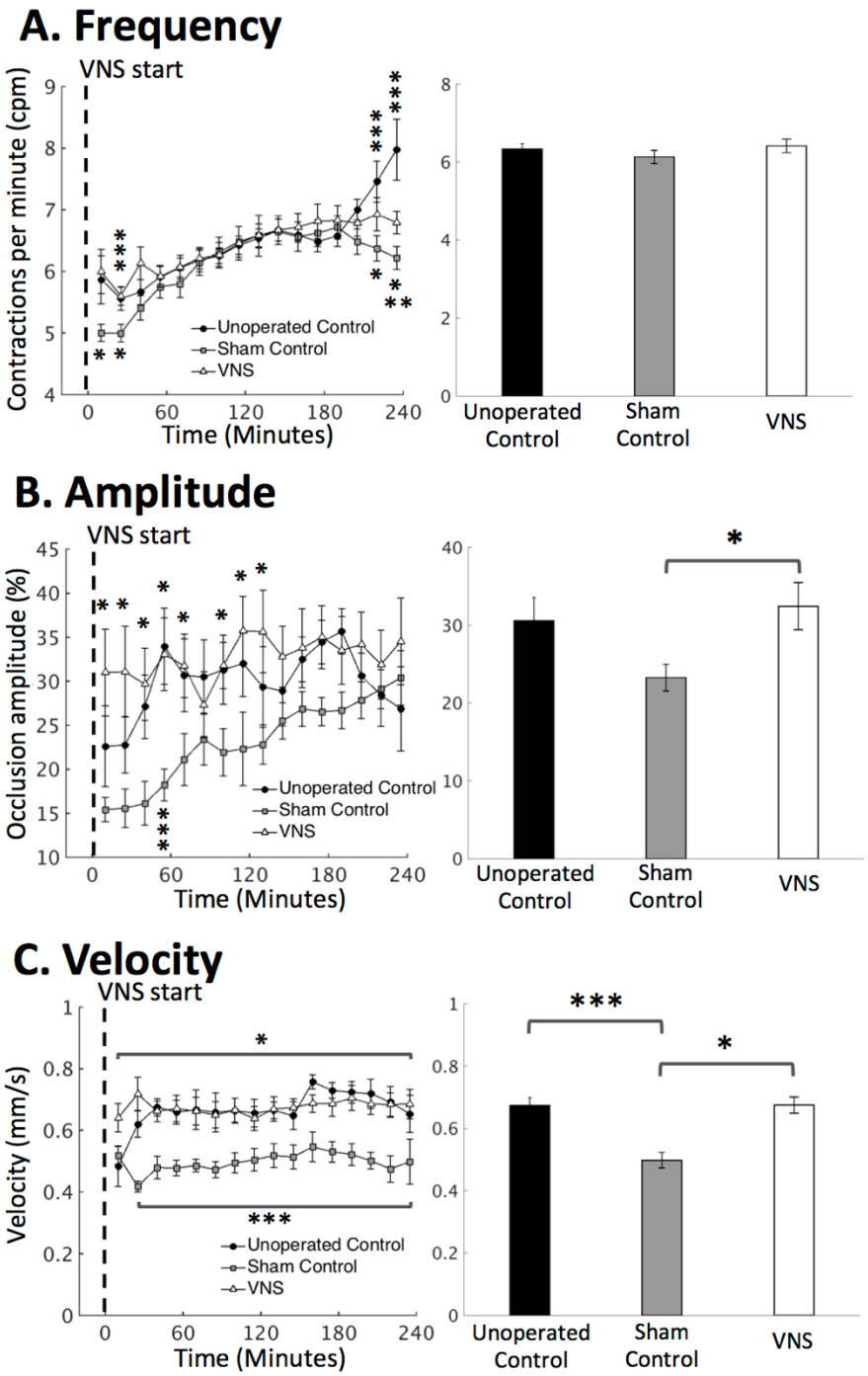

Figure 4.4 **Quantification of antral motility under unoperated control, sham and VNS conditions.** Antral motility was characterized as both time series and the mean over time. **A.** Antral contraction frequency. **B.** Antral contraction amplitude. **C.** Propagating velocity of antral contraction waves. *: $p<0.05$: sham vs. VNS, **: $p<0.05$: unoperated control vs. VNS, ***$p<0.05$: unoperated control vs. sham.

4.4 Discussion

Here, I used a contrast-enhanced MRI protocol to assess the effects of VNS on gastric motility and emptying in rats. By using the effective feeding protocol, the animals could voluntarily consume a Gd-labeled meal circumventing the need of oral gavage. The Gd-labeled meal, which could be adopted for human applications, allowed gastrointestinal organs to be clearly defined. The present paradigm makes it possible to non-invasively track how the GI tract handles a voluntarily taken Gd-labeled test meal by measuring total gastric and even regional stomach emptying, antral motility (i.e., frequency, amplitude and velocity), the extent of pyloric opening, and intestinal filling.

Stimulation of the left cervical vagus nerve with the selected parameters was found to significantly enhance the rate of gastric emptying by a factor of ~1.4. The increased emptying rate was found to relate to the tonic relaxation or dilation of the pyloric sphincter, as VNS significantly enlarged the pyloric lumenal CSA (or equivalently reduced its tone). Surgical operation of electrode implantation on the vagal nerve was found to cause a confounding reduction in antral contraction amplitude and velocity. However, VNS significantly promoted antral contraction amplitude and velocity as compared to its sham controls. Although antral hypomotility was observed in the sham rats, no significant difference in gastric emptying was found between the unoperated control rats and the sham control rats. Therefore, the degree to which the pyloric ring opens appears to be the primary contributor to the increase in gastric emptying. In sum, the experimental protocol used in this work opens an avenue for non-invasive assessment of the efficacies of neuromodulation protocols that might be used for further tuning and optimizing stimulation parameters in the future.

4.4.1 Effect of Vagus Nerve Stimulation on Gastric Emptying

A major finding in this study was that VNS promoted gastric emptying by increasing pyloric relaxation or opening. Two accepted driving forces pace gastric emptying. The first driving force is the transient transpyloric flow generated by antral contraction, where the peristaltic wave propagates toward the pyloric sphincter and a coordinated sequence of pyloric opening and receptive relaxation of the duodenal bulb [177], [178] leads to the forceful propulsion of chyme through the pyloric opening. The second driving force is from the transpyloric steady flow caused by the gastroduodenal pressure gradient and maintained by the tone of the proximal stomach [179],

[180]. To disentangle the potential mechanisms that may underlie the VNS effect that I observed, I quantified compartmental gastric volume change, which served as an indirect index of the gastric tone in different compartments. Antral motility indices and the degree to which the pyloric ring opened (i.e. the CSA of the lumenal content in the pyloric canal) were also obtained.

Central to the regulation of the transpyloric flow is the extent to which the pylorus relaxes and opens. It has been suggested that it is the opening of the pylorus, not the intraluminal pressure per se, that dominates the continuation and cessation of flow [181]. Results in this study show that the chosen VNS parameter (0.6mA, 0.36ms, 10Hz) increased the degree to which the pyloric ring opened, therefore leading to a potential increase in transpyloric flow. The extent of relaxation of the pylorus was further found to correlate with gastric emptying rate. With unprecedented spatial and temporal resolution, these present MRI observations are consistent with earlier studies showing, in broad outline, that stimulation of efferent vagal fibers decreases pyloric resistance and thus increases transpyloric flow in cat [182], [183], dog [184] and pig [185] models. However, the elicited response appears to depend critically on the stimulation parameters. It is well accepted that efferent vagal fibers carry both excitatory and inhibitory stimuli to the GI smooth muscles including the pylorus. When the excitatory pathway is activated, a greater release of excitatory neurotransmitters (e.g. acetylcholine and substance P) from the vagal nerves terminating on the enteric plexus depolarizes the slow wave and produces stronger contractions. On the other hand, when the inhibitory pathway is activated, a greater release of inhibitory neurotransmitters such a vasoactive intestinal peptide and nitric oxide relax the smooth muscle [186]. When stimulating at comparatively low threshold parameters, the excitatory (cholinergic) pathway could be selectively activated to upregulate the tone of the pyloric sphincter. At higher threshold stimulation parameters, activation of the inhibitory (non-adrenergic non-cholinergic, NANC) pathway – which in turn relaxes the pylorus [163], [171], [187] – can be superimposed on the excitatory effect of the cholinergic pathway. Martinson et al. showed that short stimulation pulse width induced excitatory effects on GI motility, while increasing the duration of the stimulatory pulses to higher values elicited inhibitory effects as well [188]. Moreover, Allescher et al. demonstrated that stimulation of the vagus nerve at low (0.2-0.5Hz) vs. high frequency (>0.7Hz) elicited excitatory and inhibitory pyloric response, respectively, in anesthetized dogs [189]. Taken together, both the present MRI study and the prior observations with less spatial and temporal resolution suggest that the pyloric response (i.e., relaxation of the pylorus) I observed is due to the direct innervation of

efferent vagal fibers to the pyloric sphincter. Since the afferent vagal pathways were not blocked, I cannot rule out the possibility that afferent stimulation of vagus may be differentially processed in the brainstem, thus recruiting different subpopulation of efferent fibers (i.e., either excitatory, inhibitory, or both) to evoke the appropriate pyloric response.

Based on my findings and previously established factors that govern the pyloric sphincter and gastric emptying, I evaluated whether VNS elicited any excitatory or inhibitory effects on antral motility. My results showed that surgical operations [e.g. injection of carprofen, manipulation of vagal nerve and a higher dose (2.5-3.0%) of isoflurane used during the surgery] compromised antral contraction amplitude and velocity, whereas VNS turned out to promote antral contraction amplitude and velocity back to a level similar (or more) to those observed in the unoperated control rats. The antral hypomotility was most likely due to the use of analgesic agent and anesthesia [112], [152]. Nevertheless, we do not rule out the possibility that manipulating the vagal nerve (i.e. mechanical stimulation) during the surgery could also have an impact on antral motility.

It is not surprising that the frequency of antral contraction remains virtually unchanged. Intrinsic gastric pace-setter potential (associated with the interstitial cells of Cajal network) sets the basic electrical rhythm (BER) of the contractions in mono-gastric animals, whereas the level of vagal discharge influences the amplitude and propagating velocity of the contractions [190], [191]. The VNS settings used in this study resulted in different effects on the pyloric sphincter and the gastric antrum. The same settings relaxed the pyloric sphincter but imposed an excitatory effect on the gastric antrum, resulting in an increased strength and a higher propagating velocity of the antral contractions. The positive correlation between the amplitude and the propagating velocity of antral contractions is consistent with recent findings based on slow wave recordings in humans [192]. I speculate that stimulation at the cervical vagus may release different neurotransmitters at different terminals of gastric vagal branches. However, additional investigations, for instance, stimulating at different gastric vagal branches, will be required to disentangle the effect of VNS on different gastric regions.

The responses of gastric motility to VNS may also be attributed to the specific pattern of stimulation employed. Grundy et al. showed that efferent stimulation in bursts (10 times faster for one-tenth of the time as the constant frequency stimulation) elicited significantly greater antral contractions than with a constant frequency (i.e., the same pattern as I used in this study) in the

ferret antrum [172]. Speculatively, the main difference between these two types of stimulation is that when stimulating at continuous frequency, both excitatory and inhibitory pathway are activated, and the latter may overshadow the former effect. However, when stimulating at bursts, successive post-synaptic events are likely superimposed due to temporal summation of the fast-delivered electrical pulses, therefore resulting in a dominating acetylcholine output within the enteric plexus that could elicit stronger antral contractions.

4.4.2 Naturalistic Feeding Protocol and Non-invasive Imaging Ensures Undisturbed Vagovagal Reflex

A noteworthy feature of this study is that the animals were trained to voluntarily consume the test meal. Naturalistic food ingestion allows for interaction between meal and oral mucosa to properly activate cognitive and sensory processing in the brain [145], [147]. These processes presumably take place in the brainstem as well as higher brain areas (e.g., amygdala), thereby supplying synaptic input to modulate the DMV neurons that control the vagal outflow to the gut. Further, meal-associated, swallow-induced esophageal distention activates vagovagal reflexes, thus triggering receptive relaxation of the forestomach and the corpus. Receptive relaxation allows the expansion of the gastric reservoir to accommodate the ingesta with minimal change of intra-gastric pressure [193]. In contrast, oral gavage typically introduces stress [194], [195]. In addition, artificial delivery (i.e., oral gavage) of the food directly to the stomach bypasses vagovagal reflexes and increases intra-gastric pressure [146].

This study highlights the capability of animal gastric MRI in assessing physiological functions of the stomach. In-vivo assessment of natural GI functions in small animals is more challenging given their smaller body size, much faster gastric motility, and the need for voluntary meal consumption. Existing methods are often invasive (or even lethal) [196], radioactive [121] and indirect [196], or employ other imaging methods [29], [197] that offer limited spatial, temporal, or quantitative resolution. For example, the gastric barostat method requires intubation of a balloon in the proximal or distal stomach to measure gastric motility. Such invasive intubation in fact acts like a bolus, which could be physiologically confounding and greatly interrupts vagal innervation to the gut. Another example is ultrasound, which allows for non-invasive imaging of the gastric reservoir [197]. However, ultrasound images possess limited spatial resolution and their image quality are typically degraded by speckles. The use of ultrasound in quantifying gastric functions is technically cumbersome, and the analysis is labor intensive and often observer dependent. Lastly,

radioactive imaging (i.e., gastric scintigraphy) has been mainly applied to quantify gastric volumes, but the inability of repeated measurements and the relatively low sampling rate limits its use in simultaneous assessment of contractile motility. In summary, MRI overcomes the above-mentioned challenges and provides a unique opportunity to assess the gastric response to therapeutic treatments without perturbing the ongoing and spontaneous physiology. More importantly, recent advances in standardizing experimental protocols and developing computer-assisted software for processing gastric MRI data have made gastric MRI increasingly accessible to research and clinical practices [104], [106], [123].

5. DIFFERENTIAL EFFECTS OF AFFERENT AND EFFERENT VAGUS NERVE STIMULATION ON GASTRIC MOTILITY ASSESSED WITH MAGNETIC RESONANCE IMAGING

5.1 Introduction

The parasympathetic innervation to the GI tract plays a key role in regulating, modulating, and controlling GI motility and maintaining energy homeostasis [5], [6]. As such innervation is predominantly supplied by the vagus nerve [69], [70], it has been of great interest to modulate motor neural signaling to the gut via electrical stimulation of the vagus nerve [59], [198], [199]. However, several morphological and functional studies have suggested that the vagus is a heterogeneous nerve consisting of distinct fiber calibers that carries both efferent and afferent traffic [10], [72]. The stimulus-response relations often vary according to the site of stimulation and also the choice of stimulus parameters. As a result, the complete extent of vagal innervation to the enteric neural plexuses remains incompletely characterized.

The vagus is comprised of about 75% sensory afferent and 25% motor efferent fibers [72]. Previous studies have uncovered that, depending on the choice of stimulus parameters, electrical stimulation of efferent fibers could impose both excitatory and relaxatory effect to gastric tone and motility [171], [200], [201]. Because of this mixed, opposite effect, it remains unclear whether stimulating the efferent vagal fibers could result in choreographic gastric motility that can be used to remedy gastric symptoms. Stimulation of efferent fibers has also been shown to induce gastric acid secretion, which depends, at least in part, on the stimulus frequency [172], [202], [203]. While a majority of VNS-gastric studies attempted to program the motor limb (i.e. efferent) of the vagovagal circuitry, the effect of stimulating the reflex arc (i.e. afferent) of the circuitry on gut motility is less understood. The significance of afferent stimulation could be evidenced by the fact that reflex vagal excitation by intra-gastric distension has been shown to promote antral motility [204]. Moreover, patients with epilepsy or depression treated with chronic VNS experienced substantial weight loss [205], [206]. The influences of VNS on the central nervous system (CNS) may therefore affect appetite control [207], [208], food intake [209], or potentially lead to downstream modulation on gastric tone and motility. As such, elucidating the potentially differential impact of efferent versus afferent VNS on gastric physiology is necessary for better calibration of neuromodulation efficacy.

To evaluate the efficacy and stability of stimulus settings, most studies employed invasive methods, such as intubation of intra-gastric balloon, in fasted animals. However, it is not unlikely that the stimulus-response relations might be confounded by such unphysiological intervention. Moreover, as electroceutical therapeutic outcomes in humans are largely derived during meal digestion, the importance of characterizing the stimulus effect under postprandial states should also be underscored.

Here, I sought to disentangle the impact of left cervical VNS with different settings (i.e. afferent, efferent, or combined afferent and efferent VNS) and parameters (i.e. pulse amplitude, pulse width and pulse frequency) on antropyloric motility in anesthetized rats. Dynamic gastric MRI was performed continuously before and during VNS. The occlusive amplitude of antral contraction waves and the luminal size of pyloric opening were measured as a function of stimulus settings. The findings from this study could shed lights on the selection of VNS settings for better modulating gastric functions.

5.2 Materials and Methods

5.2.1 Subjects

Thirteen Sprague-Dawley Rats (Male; Envigo RMS, Indianapolis, IN), ranging from 266 to 338g body weight were used in this study. All experimental procedures were approved by the Purdue Animal Care and Use Committee (PACUC) and the Laboratory Animal Program (LAP). The animals were housed individually in ventilated cages under a strictly controlled environment (temperature:70±2°F, and 12 h light-dark cycle: lights on at 6:00 AM, lights off at 6:00 PM). The floor was elevated by a stainless-steel wire frame during all time to prevent the animals from accessing their feces. All experiments were performed acutely, after which the animals were euthanized according to a standard approved protocol.

5.2.2 Test Meal

All animals were trained to voluntarily consume a fix quantity (about 10g) of nutrient-fortified water gel (DietGel Recovery, ClearH_2O, ME, USA) under a re-feeding condition following an overnight (18 hours, 5PM to 11AM) fast. The training protocol consisted of 2 stages. During the first stage, an aliquot (~10g) of the Dietgel was placed in a cup in animal's home cage overnight for two times, with the regular rat chow being supplied ad libitum. Once the animal got

used to the test meal, their usual feeds were deprived for 18 hours followed by re-feeding of the Dietgel. At the end of the 7-day training, all animals were compliant to the naturalistic feeding paradigm in order for us to investigate gastric functions in a physiologically fed condition.

5.2.3 **Animal Preparation and Surgical Implantation of Stimulating Electrode**

On the day of imaging, the animal was fed with 10g of Gadolinium (Gd)-labeled test meal after the 18-hour overnight fast. Soon after ingestion, the animal was anesthetized with Isoflurane followed by implantation of a bipolar cuff electrode (Pt/Ir electrode; MicroProbes, Gaithersburg, MD, USA) onto the left cervical vagus nerve with a surgical procedure identical to that described in section 4.2.2. The specification of the bipolar cuff electrode is illustrated in Figure 5.1A. The animal was then setup in prone position in the scanner. Respiration and body temperature were monitored with an MR-compatible system (SA Instruments Inc., Stony Brook, NY, USA) to ensure stable physiology. The leads of the electrode were connected to a pair of twisted wires that were connected to a current stimulator (A-M Systems Model 2200; A-M Systems, Sequim, WA, USA) placed outside of the MRI room. A bolus injection of 0.01 mg/kg dexmedetomidine solution (0.05 mg/mL, Zoetis, NJ, USA) was administered subcutaneously (SC). Fifteen minutes after the bolus, dexmedetomidine was infused (SC) continuously throughout the experiment (0.03 mg/kg/h). The dose of Isoflurane was lowered to 0.3-0.5% as soon as the animal's respiratory rate began to decrease.

5.2.4 **MRI Data Acquisition**

Dynamic gastric MRI images were acquired with a 7-Tesla horizontal-bore small-animal system (BioSpec 70/30, Bruker, Billerica, MA, USA) and the imaging protocol described in section 3.2.5. Briefly, an abdominal localizer was first applied to reveal the long axis of the stomach from T_2-weighted sagittal images. Then, a FLASH sequence with 4 slices was prescribed along the long axis of the stomach. The 4 slices were carefully positioned and adjusted to cover the antrum, pylorus and the duodenum (Figure 5.1D). The MRI scans were acquired with TR/TE = 11.78/1.09ms, FA = 25°, 4 oblique slices, slice thickness = 1.5mm, FOV = 60 × 60 mm^2, in-plane resolution = 0.4688 × 0.4688 mm^2, and no averaging. To reduce motion artifact in the images, the MRI scans were respiratory-gated such that images were acquired only during the end-expiratory phase with minimum diaphragmatic motion. Readout gradient triggers were recorded

to adjust acquisition times between volumes due to varying respiratory rates. The resulting sampling rate was typically between 2 to 3 seconds per volume, depending on the respiratory pattern of the animal.

5.2.5 **Experimental Protocol**

After about 5 minutes of stable, baseline dynamic MRI images were obtained, cervical VNS was delivered simultaneously with MRI acquisition. The rats were allocated into 2 groups as follows: (i) a group of rats (N=8) that received afferent VNS (i.e. action potential propagates rostrally to the brain) and (ii) a group of rats (N=5) that received efferent VNS (i.e. action potential propagates caudally to end organs). The directionality of the stimulation was determined by the placements of anode and cathode along the nerve. According to the principle of anodal blocking effect [210], the nerve tissue at the cathode depolarizes and evokes compound nerve action potential (CNAP), while the nerve tissue at the anode hyperpolarizes and may block the propagation of CNAP. Therefore, as illustrated in Figure 5.1B, afferent stimulation can be favored by placing the cathode rostrally to the anode and passing rectangular pulses of current between the two electrodes. Meanwhile, placing the cathode caudally to the anode may preferentially result in efferent stimulation. In addition to evaluating the effect of afferent versus efferent VNS on gastric motility, I further applied bidirectional VNS (i.e. combined afferent and efferent stimulation) to the rats in the afferent VNS group, immediately after which afferent VNS was performed. The bidirectional VNS was achieved by delivering rectangular pulses of current in alternating directions between the two electrodes.

For each VNS group, the stimulus parameters were varied in terms of pulse amplitude (PA: 0.13, 0.25, 0.5, 1mA), width (PW: 0.13, 0.25, 0.5ms), and frequency (PW: 5, 10Hz). The frequency of afferent or efferent VNS was defined as the number of electrical pulses delivered per second. The frequency of bidirectional VNS was defined as the number of paired cathodal and anodal pulses delivered per second. Low, medium, and high values were selected for each parameter settings, all of which are frequently used in clinical and preclinical settings. Here, a stimulus dose was defined as the area under individual electrical pulse [product of pulse amplitude (mA) and pulse width (ms)], representing the electrical charge [Q; micro coulomb (μC)] delivered to the nerve tissue. For bidirectional VNS, the stimulus dose for a pair of cathodal and anodal pulses was defined as the charge under the cathodal pulse, because the effect of cathodal and anodal pulses

were treated separately (i.e. alternating afferent and efferent). As illustrated in Figure 5.1C, each stimulation setting comprised of a duty cycle of 1-minute ON and 1-minute OFF, and different VNS settings were performed in a randomized order to eliminate any causal effect of one setting on the other. No stimulus was delivered during the OFF period. As a result, every rat in each group underwent VNS with 24 different sets of parameters.

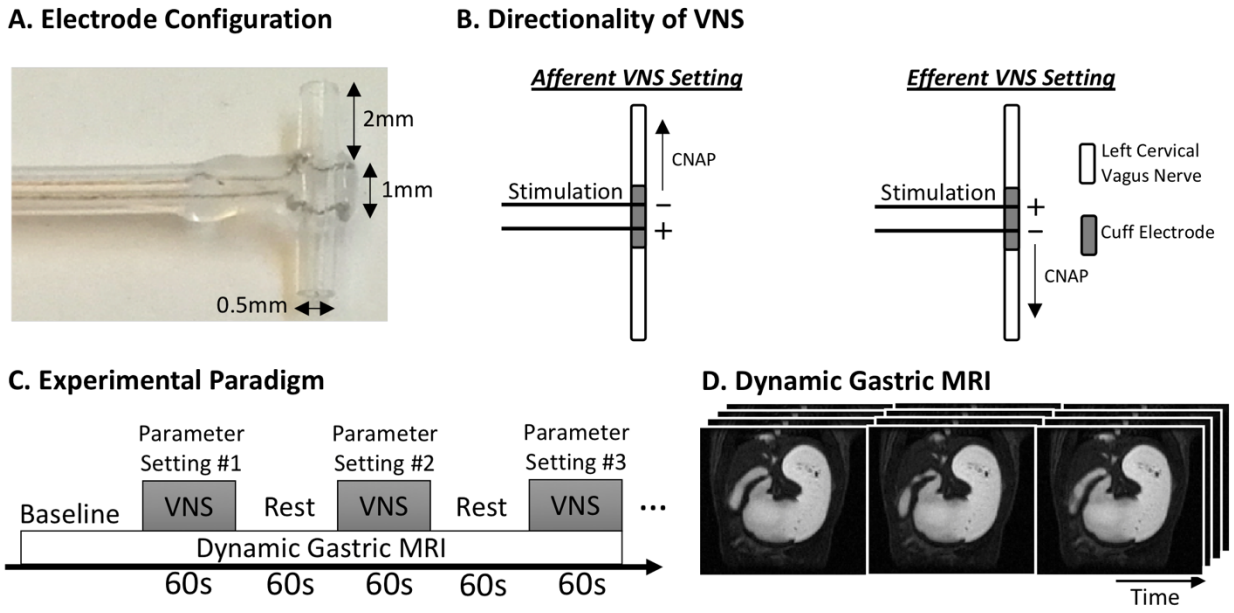

Figure 5.1 **Illustration of instrumentation and experimental design. A.** The specification of the bipolar cuff electrode. **B.** The propagating direction of stimulation-evoked compound nerve action potential was controlled by the placement of the anode (+) and cathode (-) along the nerve. **C.** Dynamic gastric MRI images were collected before and during VNS. Every VNS setting was performed for 1 minute followed by another minute of rest. The sequence of different VNS settings was randomized within and across animals. **D.** Example images obtained from dynamic gastric MRI.

5.2.6 **Image Analysis**

The gastric antrum, pylorus, and the proximal duodenum were segmented from the lumen-enhanced MRI images by using a custom-built pipeline in Matlab (Mathworks, Massachusetts, USA) developed previously. Gastric volumes obtained at different times were rigidly co-registered to the first volume to minimize motion-induced displacements. To quantify antral motility, 16 cross-sectional planes that are perpendicular to the antral axis were defined at various locations

(from 0 to 7.5mm distant to pylorus) along the axis. The segmented voxels within each cross-sectional plane were summed over all slices to quantify the cross-sectional area (CSA) of the lumen. As illustrated in Figure 5.2A, a time series that represent the temporal change of CSA was obtained at every location along the antral axis (herein referred to the contraction time series). When an occlusive contraction wave arrived at a cross-sectional plane, a minimal CSA was attained. Due to irregular sampling caused by respiratory gating, the contraction time series were further resampled to 0.5Hz. For almost every rat studied in this work, occlusive contractions only occurred along the less curvature, whereas the greater curvature only exhibited non-occlusive contractions.

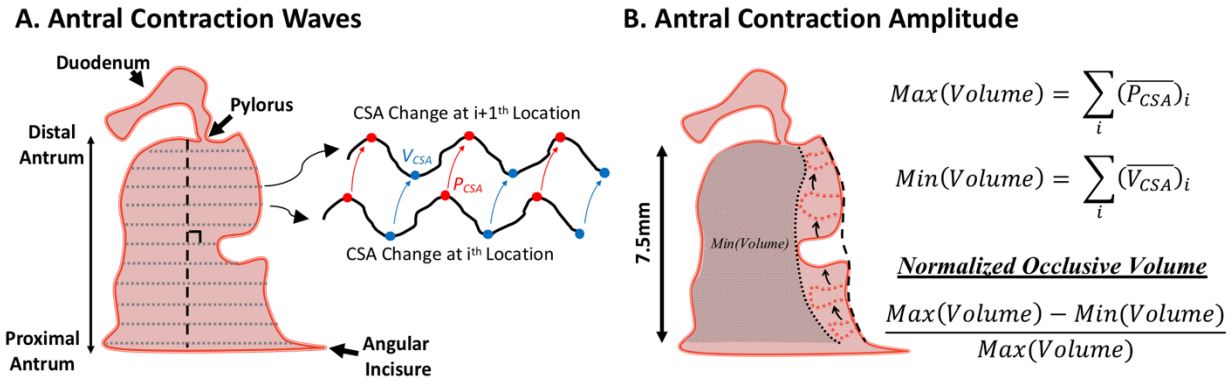

Figure 5.2 **Image analysis of antral motility. A.** Cross-sectional areas (CSAs) along the long axis of the antrum (0 to 7.5mm distant from the pylorus, which correspond to 16 cross-sectional planes) were computed from the 3-D antral volume. The temporal change of CSAs at different locations of the antrum exhibits phase differences, revealing the propagation of antral contraction waves. When an occlusive contraction wave arrives at a cross-sectional plane, the minimal CSA is attained (V_{CSA}). On the other hand, when the occlusive contraction wave is fully away from a cross-sectional plane, the maximal CSA is attained (P_{CSA}) **B.** Calculation of antral contraction amplitude. The contraction amplitude is defined as the normalized difference between the maximum and minimum antral volume, which represents the percentage occlusion of the antral volume. The maximum antral volume is defined as the sum of the temporal mean of peak values over all 16 cross-sectional planes, whereas the minimum antral volume is defined as the sum of the temporal mean of valley values over the 16 cross-sectional planes.

To compute the frequency of antral contraction waves, Fourier analysis was applied to all 16 contraction time series thus each of their power spectral density (PSD) was derived. After averaging the 16 PSDs, the contraction frequency could be identified from the largest peak in the spectrum. To quantify the amplitude of antral contraction waves, a volumetric approach was proposed as shown in Figure 5.2B. During the 1-min interval of VNS application, the peaks and

the valleys from all contraction time series were automatically detected. The peaks and the valleys correspond to the maximal and minimal CSA of a cross-sectional plane, respectively. The maximum antral volume was then defined as the sum of the temporal mean of peak values over all 16 cross-sectional planes, whereas the minimum antral volume was defined as the sum of the temporal mean of valley values over the 16 cross-sectional planes. Finally, the percentage occlusion of the antral volume (herein referred to the antral contraction amplitude) was defined as the normalized difference between the maximum and minimum antral volume.

Next, pyloric motility was quantified as the area under the curve (AUC) of changes in luminal CSA at the pyloric sphincter. To compute luminal CSA at the pyloric sphincter, a distance transform-based approach was applied [111]. Specifically, distance transformation was first applied to the binary, segmented gut images. The distance transform map describes the distance from every luminal voxel to their closest boundary. Next, the medial axis of the GI tract was computed by applying a thinning algorithm (Matlab *bwmorph* function) that iteratively eroded pixels from the boundary until no more thinning was possible. Here, the distance-transformed values along the medial axis are the local maxima that represent the radius of the maximum inscribed circle, as illustrated in Figure 5.3A. The cross-sectional diameter could be calculated and thus the luminal CSA was approximated by summing the product of diameter and slice thickness over all slices. Lastly, an integral analysis was applied to the contraction time series at the pylorus to obtain the AUC, as illustrated in Figure 5.3B. Similarly, the contraction time series were resampled to 0.5Hz for further frequency and amplitude analysis.

5.2.7 **Data Analysis**

For each stimulation group, antral motility (i.e. contraction amplitude) and pyloric motility (i.e. AUC) were computed for each stimulus parameter setting during the 1-min ON period. The motility measurements were normalized against their baseline values over the 3-5 minutes immediately preceding the onset of the first VNS setting. The results were expressed as percentage increase/decrease from baseline. Further, a linear regression analysis was performed to characterize the association between stimulus dose and gastric motility. The independent variable used for the regression model was the logarithm-transformed stimulus dose, and the dependent variable was the mean antral contraction amplitude change or mean pyloric motility change. The

linear regression analysis was conducted separately for the two stimulation frequencies (i.e. 5Hz and 10Hz).

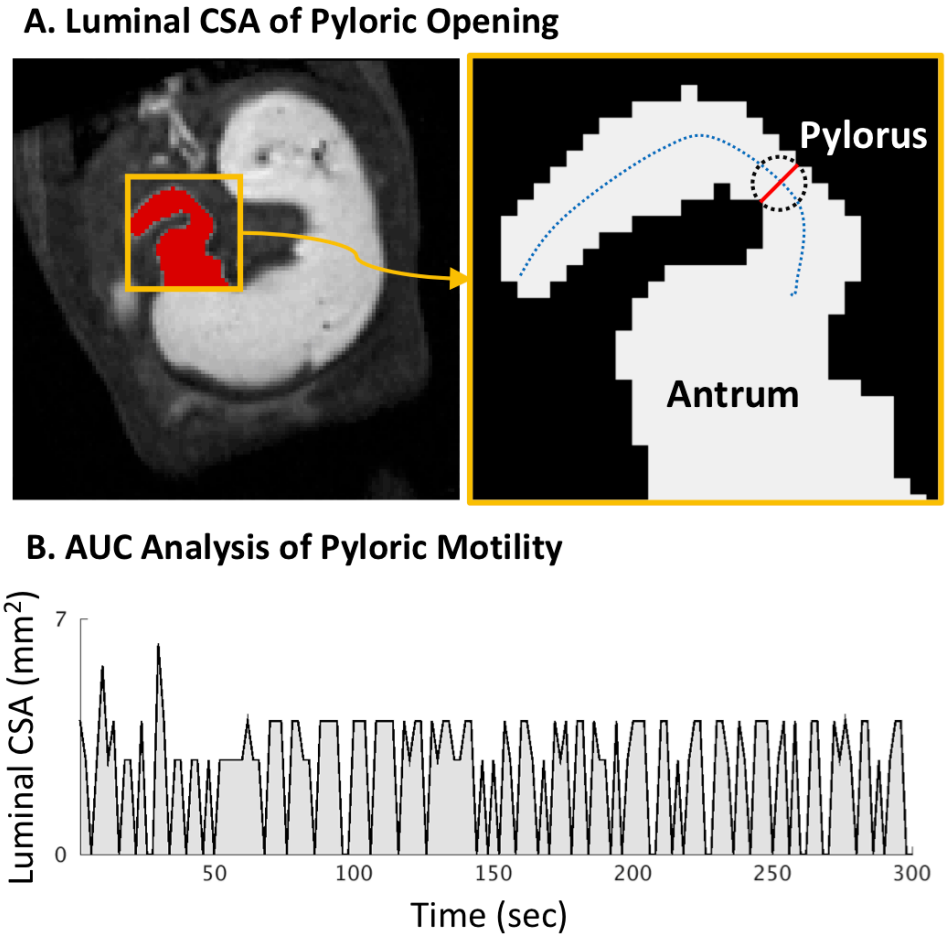

Figure 5.3 **Image analysis of pyloric motility. A.** After the antropyloroduodenal region was segmented, the medial axis (blue dashed line) of the GI tract was computed, and the radius of the maximum inscribed circle (black dashed circle) along the medial axis was calculated from the distance-transformed binary segmented GI tract. The luminal CSA at the pylorus was quantified by summing the product of cross-sectional diameter (red line) and slice thickness over all slices. **B.** The pyloric motility was defined as the area under the curve (AUC) of changes in luminal CSA of pyloric opening.

5.2.8 **Statistics**

All data are expressed as mean (SEM). A paired-sample Student's t-test was conducted to compare motility measurements during each VNS setting to the same variable obtained during the baseline condition. A Student's t-test was applied to the slope obtained from regression analysis

to test the goodness of fit of the regression model. Pearson correlations between the stimulus dose and the motility measurements were calculated as well. Values of $p<0.05$ were considered statistically significant.

5.3 Results

Here I report the use of contrast-enhanced MRI to investigate the effect of left cervical VNS on GI motility in rats under a wide range of stimulus parameters. The effect of afferent versus efferent stimulation was dissociated, if not entirely, by configuring the placement of the cathode (i.e. the polarity) on the bipolar electrode. The combined effect of afferent and efferent VNS was further ascertained by delivering electrical pulses with alternating polarity to the vagus. Each VNS setting was delivered for one minute, followed by another minute of rest without stimulation, during which dynamic gastric MRI was performed continuously. The order of VNS settings was randomized within and across animals to counterbalance any causal effects.

Table 5.1 **Mean motility measurements in rats under baseline period.** Data are presented in Mean (SEM).

Group	Antral Motility			Pyloric Motility	
	Frequency (CPM)	Amplitude (% Occlusion)	Velocity (mm/s)	Frequency (CPM)	AUC ($mm^2 \cdot s$)
Afferent VNS (N=7)	4.46 (0.06)	17.0 (0.8)	0.77 (0.02)	4.86 (0.25)	0.59 (0.04)
Efferent VNS (N=5)	5.25 (0.10)	21.1 (2.0)	0.85 (0.03)	5.27 (0.18)	0.74 (0.05)

Table 5.2 **Mean percentage change in motility for each set of VNS parameters for the 3 conditions.** Data are presented in Mean (SEM). An asterisk indicates a significant value ($p<0.05$).

Group	PA (mA)	PW (ms)	% Change in antral contraction amplitude		% Change in pyloric motility (AUC)	
			PF (Hz)		PF (Hz)	
			5	10	5	10
Afferent VNS (N=7)	0.13	0.13	84.49 (21.31)*	118.24 (27.84)*	55.47 (46.16)	52.43 (62.71)
		0.25	121.87 (27.74)*	89.22 (18.29)*	18.91 (18.09)	28.35 (55.44)
		0.5	95.21 (26.67)*	52.74 (26.18)	46.17 (59.74)	41.82 (42.65)
	0.25	0.13	68.69 (26.08)	93.81 (21.38)*	34.43 (34.54)	13.49 (48.87)
		0.25	96.92 (18.61)*	97.14 (22.03)*	36.06 (57.09)	60.14 (52.72)
		0.5	128.08 (45.63)*	72.23 (23.73)	121.53 (64.72)	64.13 (59.07)
	0.5	0.13	118.54 (26.63)*	100.73 (21.50)*	-10.42 (28.87)	13.21 (32.94)
		0.25	106.88 (32.70)*	97.79 (34.99)	37.17 (41.08)	61.88 (46.25)
		0.5	113.52 (25.81)*	55.50 (28.00)	59.44 (52.52)	153.88 (75.17)
	1	0.13	84.58 (29.84)	99.58 (33.14)*	110.30 (77.99)	75.85 (57.45)
		0.25	71.82 (25.22)*	55.50 (34.92)	66.27 (44.68)	93.88 (33.27)
		0.5	95.37 (33.90)*	34.77 (31.78)	181.25 (115.69)	88.69 (97.75)
Efferent VNS (N=5)	0.13	0.13	51.23 (28.67)	24.00 (19.52)	41.07 (38.04)	91.00 (71.20)
		0.25	72.00 (42.72)	31.19 (21.95)	54.00 (41.45)	55.22 (64.19)
		0.5	-5.04 (18.13)	22.93 (49.18)	143.14 (114.83)	155.38 (115.30)
	0.25	0.13	12.89 (12.29)	16.43 (22.35)	58.00 (29.25)	84.25 (76.81)
		0.25	32.10 (56.75)	-20.19 (27.46)	172.19 (76.20)	72.83 (49.21)
		0.5	-10.96 (30.54)	-16.59 (35.00)	119.96 (92.36)	134.72 (108.93)
	0.5	0.13	18.19 (25.52)	8.40 (27.08)	130.88 (79.29)	176.35 (56.82)*
		0.25	6.10 (19.66)	-8.22 (45.11)	93.63 (47.85)	147.46 (99.23)
		0.5	-26.80 (33.14)	-17.87 (33.92)	179.30 (83.63)	189.15 (70.03)
	1	0.13	-15.80 (27.50)	-29.28 (15.53)	167.18 (86.42)	201.29 (93.16)
		0.25	-9.16 (23.11)	-35.84 (13.49)	95.13 (83.47)	89.15 (93.54)
		0.5	-17.64 (11.89)	-4.36 (15.69)	138.19 (94.06)	51.64 (40.87)
Combined Afferent & Efferent VNS (N=7)	0.13	0.13	40.27 (24.51)	43.91 (29.53)	-7.74 (17.95)	62.42 (59.31)
		0.25	45.82 (33.73)	56.98 (25.96)	45.22 (66.85)	55.90 (35.71)
		0.5	26.87 (19.34)	50.72 (23.34)	71.34 (65.40)	63.01 (54.16)
	0.25	0.13	40.72 (32.05)	18.94 (23.21)	108.32 (59.30)	57.69 (57.98)
		0.25	52.67 (17.50)*	46.88 (32.53)	142.46 (106.76)	89.48 (88.27)
		0.5	32.99 (30.45)	-1.09 (18.84)	184.24 (76.07)*	105.54 (85.82)
	0.5	0.13	26.78 (29.84)	17.85 (21.05)	74.58 (88.25)	136.31 (99.20)
		0.25	2.14 (22.35)	4.89 (26.57)	187.21 (92.38)	161.92 (99.96)
		0.5	-19.79 (19.99)	-23.65 (11.68)	202.90 (100.20)	177.54 (102.76)
	1	0.13	1.22 (26.39)	-1.60 (20.75)	140.06 (79.22)	64.37 (59.23)
		0.25	-17.03 (16.44)	-25.90 (14.58)	185.31 (82.14)*	98.31 (45.76)
		0.5	9.43 (28.42)	-24.54 (18.28)	220.59 (118.40)	142.94 (68.90)

The occlusive amplitude of antral contraction waves and the tone of pyloric opening were measured as a function of stimulus settings. No significant change was observed in antral and pyloric contraction frequency across conditions. Table 5.1 shows the baseline motility measurements and Table 5.2 shows the VNS-evoked motility changes for each set of VNS parameters. Note that one rat from the afferent VNS group was excluded due to abnormal respiratory pattern during imaging and thus degraded image quality.

5.3.1 **VNS Effects on Antral Motility**

For afferent VNS, the 24 sets of parameters primarily induced excitatory effect on antral contraction amplitude to various degree (Figure 5.4A). At a stimulation frequency of 5Hz, there was a significant, positive change in contraction amplitude from baseline values under most stimulus settings. A non-significant increase ($p=0.80$) in contraction amplitude was found when increasing the stimulus dose (Q: product of pulse amplitude and pulse width) at this frequency. However, at the stimulus frequency of 10Hz, the contraction amplitude continued to fall as the pulse width was increased up to 0.5ms. In this circumstance, an increase of VNS dose induced a significant ($t=-3.54$, $p<0.01$, $R^2=0.56$) decrease in contraction amplitude, but the amplitude was overall still greater than baseline values.

Efferent VNS imposed two different effects on antral motility: one being excitatory and the other being inhibitory, as illustrated in Figure 5.4B. At both stimulus frequencies, lower doses of VNS promoted contraction amplitude, with 5Hz being more pronounced than 10Hz. However, the results from linear regression ($t=-4.08$, $p<0.01$, $R^2=0.63$ for 5Hz; $t=-3.11$, $p<0.05$, $R^2=0.49$ for 10Hz) indicated a significant, proportional decrease in contraction amplitude as the stimulus dose increased, highlighting the recruitment of inhibitory fibers in the efferent pathway. A cut-off value Q was defined when the regression line crossed the zero-percentage change. The cut-off was higher for the stimulus frequency at 5Hz ($Q=0.13\mu C$) than at 10Hz ($Q=0.08\mu C$), suggesting that the threshold for activating inhibitory fibers was lower at 10Hz than at 5Hz.

Interestingly, when afferent and efferent VNS were performed alternately, the stimulus-response relations show an additive effect of afferent and efferent VNS, with the effect of efferent VNS being more dominant over afferent VNS (Figure 5.4C). Combined afferent and efferent VNS could promote antral contraction amplitude under a wider range of low dose VNS settings than by performing efferent VNS alone. Regression analysis revealed a significant decrease in contraction

amplitude as the stimulus dose increased ($t=-3.51$, $p<0.01$, $R^2=0.55$ for 5Hz; $t=-4.80$, $p<0.001$, $R^2=0.70$ for 10Hz). Similarly, a higher cut-off Q was found for the stimulus frequency at 5Hz (Q=0.25μC) than at 10Hz (Q=0.15μC).

5.3.2 **Effects of Strong VNS Dose on Gastric Physiology**

As revealed in Figure 5.4, I found that high dose efferent (as well as combined afferent & efferent VNS) dampened antral contraction amplitude. To further demonstrate the effect, I additionally performed high dose efferent VNS (1mA, 0.5ms, 10Hz) with 30 seconds on, 30 seconds off duty cycle in one animal. As illustrated in Figure 5.5A, when efferent VNS at supramaximal intensity was applied to the left cervical vagus nerve, gastric secretion was induced, resulting in an enlarged corporal and antral volume. Furthermore, antral contraction waves were ceased during the ON period, highlighting the inhibitory effect of efferent VNS. Fig. 5B shows an example CSA change extracted from middle antrum before, during and after efferent VNS. At the onset of each VNS, an abrupt change in CSA can be observed, reflecting the enlargement of antral volume caused by relaxation of the antrum and the infused secretory volume. The propagation of antral contraction waves ceased during efferent VNS. Such inhibitory effect on antral contraction was immediately followed by intensive, rebound contractions when the VNS was turned off. The effect was reproducible over multiple cycles.

5.3.3 **VNS Effects on Pyloric Motility**

Regardless of the directionality of VNS, the vagal innervation on pyloric sphincter was found to be mostly relaxatory (corresponding to a decrease in pyloric tone, or equivalently to an increase in AUC). For afferent VNS at 5Hz, the maximum response was induced either at the highest PA (1mA) or the highest PW (0.5ms) utilized in this study. When stimulating at 10Hz, the greatest response was observed at PA=0.5mA and PW=0.5ms, and the effective settings for promoting pyloric motility were of wider range than that of 5Hz. An increase in stimulus dose induced a significant increase in pyloric AUC at both stimulus frequencies ($t=2.30$, $p<0.05$, $R^2=0.35$ for 5Hz; $t=3.02$, $p<0.05$, $R^2=0.50$ for 10Hz), as shown in Figure 5.6A.

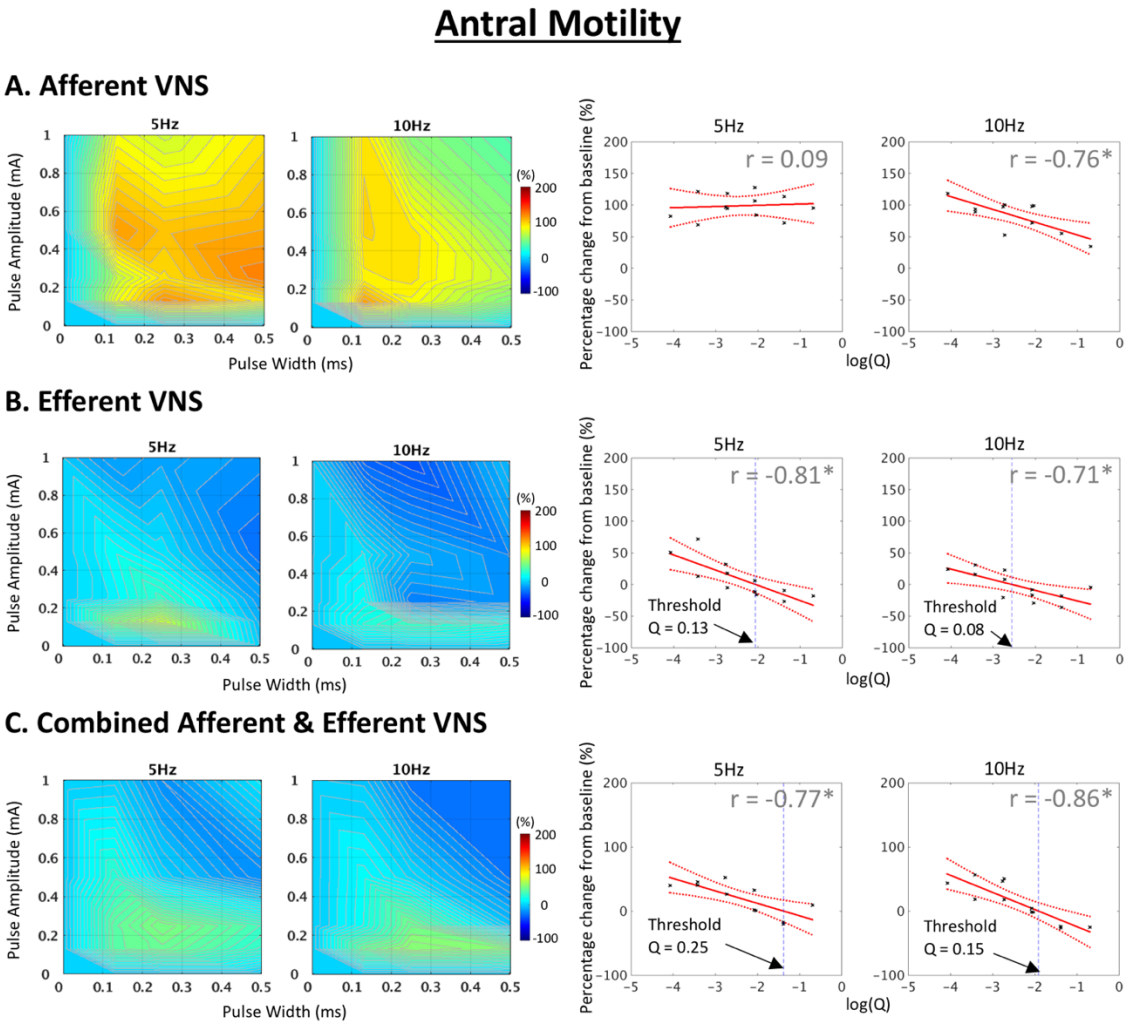

Figure 5.4 **Effects of VNS parameters and directionality of VNS on antral motility. A.** Afferent VNS. **B.** Efferent VNS. **C.** Combined Afferent and Efferent VNS. Left panel: Effect of VNS on antral contraction amplitude under different VNS parameters. Right panel: Linear regression analysis of changes in antral contraction amplitude as a function of log-transformed VNS dose (Q: pulse amplitude x pulse width). Afferent VNS seems to promote antral contraction amplitude more effectively than efferent VNS. Meanwhile, high dose efferent VNS inhibits antral contraction. For both efferent and combined afferent and efferent VNS, a cut-off value Q (dotted blue line) is defined when the regression line crossed the zero-percentage change. The cut-off is higher for the stimulus frequency at 5Hz than at 10Hz. The color bar indicates percentage change of antral contraction amplitude from baseline values. Dotted red lines: 95% confidence interval of regression. r: Pearson correlation coefficient. *p<0.05.

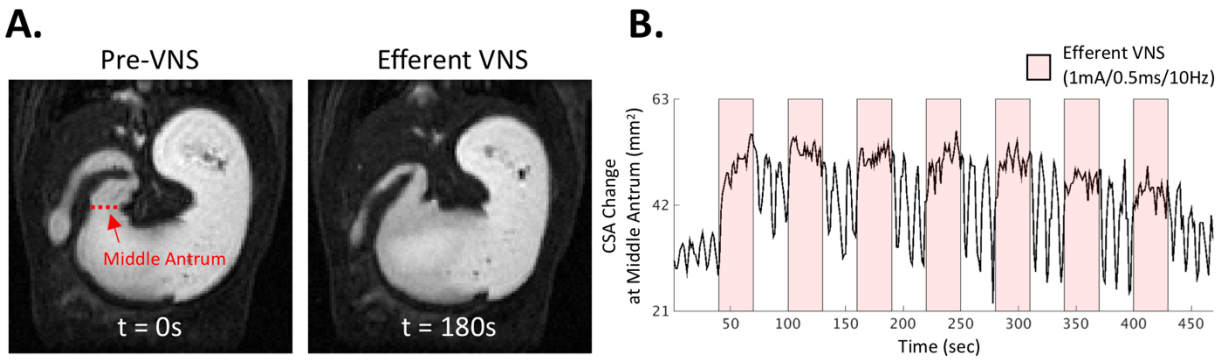

Figure 5.5 **High dose efferent VNS retards antral peristalsis and induces gastric secretion. A.** Example gastric images before and during high dose efferent VNS (PA=1mA, PW=0.5ms, PF = 10Hz). Efferent VNS under this parameter setting ceased antral contraction wave while inducing excessive secretory volume into the corpus and the antrum. **B.** A CSA change taken from the middle antrum as indicated in panel A. The onset of high dose efferent VNS significantly increases the CSA, followed by little or no phasic change in CSA. There is a large rebound, intensive contraction on the offset of efferent VNS.

On the other hand, efferent VNS was found to promote pyloric opening more effectively under a wider spectrum of VNS settings than afferent VNS (Figure 5.6B). This effect once again elaborates the activation of inhibitory fibers in the efferent pathway. However, depending on the strength of the stimulus, efferent VNS induced a marginally significant increase and a slight, non-significant increase in pyloric AUC for 5Hz and 10Hz, respectively ($t=2.16$, $p=0.06$, $R^2=0.32$ for 5Hz; $t=0.66$, $p=0.52$, $R^2=0.04$ for 10Hz).

A marked increase in pyloric motility was found when performing combined afferent and efferent VNS at high dose and at 5Hz (Figure 5.6C). The stimulus-response relations again show additive effect of afferent and efferent VNS. A stimulus frequency of 5Hz was found to promote pyloric motility more effectively than 10Hz. Finally, a significant linear regression indicated a proportional increase in pyloric motility as the stimulus dose increased ($t=6.26$, $p<0.001$, $R^2=0.80$ for 5Hz; $t=2.59$, $p<0.05$, $R^2=0.40$ for 10Hz).

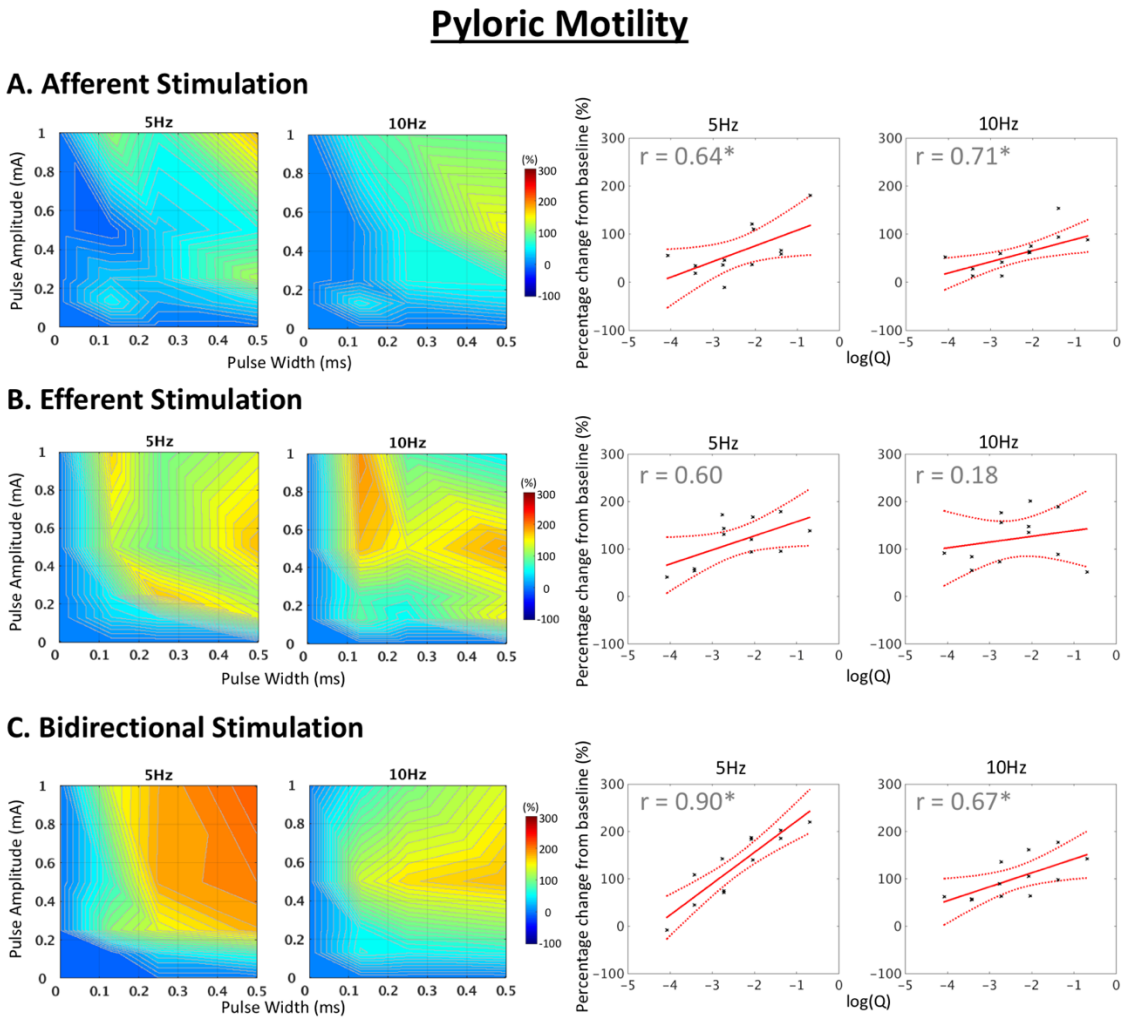

Figure 5.6 **Effects of VNS parameters and directionality of VNS on pyloric motility. A.** Afferent VNS. **B.** Efferent VNS. **C.** Combined Afferent and Efferent VNS. Left panel: Effect of VNS on pyloric motility under different VNS parameters. Right panel: Linear regression analysis of changes in pyloric motility as a function of log-transformed VNS dose (Q: pulse amplitude x pulse width). An increase in stimulus dose promotes pyloric motility, indicating an increase in AUC of pyloric opening or equivalently a decrease in pyloric tone. The color bar indicates percentage change of AUC of pyloric opening from baseline values. Dotted red lines: 95% confidence interval of regression. r: Pearson correlation coefficient. *p<0.05.

5.4 Discussion

In this study, I characterized the effect of different cervical VNS settings on gastric motility in anesthetized rats. To my knowledge, this is the first animal study that utilizes gastric MRI to non-invasively assess postprandial gastric motility under VNS with a wide range of parameters. The impact of directionality of VNS was studied by configuring the cathode on the bipolar cuff

electrode. Gastric MRI revealed that electrical activation of the afferent pathway may promote antropyloric motility more effectively then directly activating the efferent pathway. A reduction in antral contraction amplitude and relaxation of pyloric sphincter under efferent VNS highlighted the inhibitory pathway of the motor limb of the vagovagal circuitry. Further, efferent stimulation was typically accompanied with undesirable off-target effects such as bradycardia and bradypnea, which were in line with the observations from previous VNS studies [211], [212].

5.4.1 **Efferent VNS Induces Multiple Effects on Gastric Physiology**

Previous studies on vagal control of gastric motility have largely focused on the efferent parasympathetic innervation of the GI tract [171], [172], [186], [201]. The modulatory role of efferent VNS with different stimulus parameters on gastric motility was discovered by Veach [213] over a hundred years ago. In a cat model, he found that the stronger the stimulus strength and/or the higher the stimulus frequency, the more prominent the inhibitory effect on gastric motility. The general opinion that there are two groups of efferent fibers that influence gastric motility: one being excitatory and the other being inhibitory [6], is supported by the present finding. In line with previous studies [171], [214], the activation threshold for the two groups of fibers seems to be different, which was dependent on the stimulus strength (pulse amplitude and pulse width) as well as the rate at which these pulses were applied (frequency). Here, I found that lower pulse amplitude and/or lower pulse width produced excitatory response on antral contraction amplitude. However, when I kept increasing the pulse amplitude and pulse width over a certain level, the amplitude of antral contraction waves became smaller and eventually, the contraction waves ceased at supramaximal intensity. The phenomenon confirms the presence of efferent fibers with two different calibers; the fiber caliber for inducing excitatory response is perhaps larger than the fiber caliber for inducing inhibitory response, where the activation threshold is lower for the former than the latter. The two fiber groups are likely unmyelinated fibers, as the activation thresholds for the two groups were suggested to be both higher than that needed for inducing cardiac response [188], [215], under which the heart is primarily mediated by efferent B-fibers. My experimental observation is also consistent with the finding that there are only a few myelinated fibers in the abdominal vagi [216]. Notably, the pulse amplitude and pulse width required for inducing inhibitory response are generally smaller than the previously reported parameters, though different animal species were used [171], [201]. Speculatively, the difference in experimental condition (i.e.

pre-prandial versus post-prandial state) may be the underlying cause, as the basal gastric tone should vary across the two states. Interestingly, the threshold for producing inhibitory response on antral motility was slightly higher at 5Hz than at 10Hz. It was suggested that the stimulus frequency could be responsible for selective activation of the efferent excitatory (cholinergic) and inhibitory [non-adrenergic, non-cholinergic (NANC)] effects [217] (i.e. 5Hz for acetylcholine release and 10Hz for vasoactive intestinal peptide release). Nevertheless, a clear cut on frequency-specificity was not apparent in the present study, as the two frequencies could both produce excitatory and inhibitory response.

The excessive secretion induced by efferent VNS observed in the present study is in complete agreement with previous findings [172], [202], [218], [219]. The effect was most visually pronounced at the supramaximal intensity, regardless of the two stimulus frequency utilized in this study. This finding is perhaps not too surprising, as gastric parietal cells in the rat are mainly innervated by unmyelinated C-fibers [202], [203], therefore a larger stimulus dose is required trigger vagally mediated secretory response. On the other hand, the inhibitory motility pattern induced by high dose efferent VNS consists of two phases. The first phase was a rapid relaxation of the antrum at the onset of stimulus, followed by intensive, rebound contractions on cessation of the stimulation. As reported and discussed elsewhere [201], [220], the rebound contractions could be of purinergic origin and the release of prostaglandins by NANC terminals may account for this post-stimulus pattern.

The influence of efferent VNS on pyloric motility appeared to be primarily inhibitory. This observation coincides with previous findings that VNS does not seem to impose a strong tonic influence on pyloric resistance; VNS was shown to decrease pyloric resistance through the NANC pathways and thus increase transpyloric flow [185]. However, the seemingly pure inhibitory effect could depend on the choice of stimulus frequency, as it was suggested in a canine study that low-frequency stimulation (0.2-0.5Hz) exerted tonic contractions, whereas higher frequency (>0.7 Hz) of stimulation could inhibit both phasic and tonic contractions [189]. Further experiments are needed to evaluate the potentially excitatory effect of efferent VNS on pyloric tone with a wider range of stimulus frequency.

In sum, my results suggest that stimulating the vagal efferent nerves could induce multiple effects on gastric physiology. These effects heavily, if not entirely, on the dose and the frequency of the stimulus. The likelihood that both excitatory and inhibitory efferent fibers are unmyelinated

fibers pose technical difficulty in selective activation of one but not the other fiber group. As a result, efferent VNS employ complex and heterogeneous neural signaling to the gut, which may lead to undesired, mixed gastric response. Furthermore, a promotion of antropyloric coordination seems to be hard to achieve, because there exists no parameter setting that can maximally increase antral motility while reducing pyloric tone.

5.4.2 **Reflex Excitation on Gastric Motility via Afferent VNS**

While most studies utilized electrical stimulation of the peripheral end of the sectioned vagal nerve, the effect of afferent VNS on gastric motility has received considerably less attention. Here, I performed afferent VNS at the cervical level to mimic the vagovagal reflex occurred in the physiological state. The vagal afferents carry signals from stretch receptors [9], [73] and chemoreceptors [221] to dorsal vagal complex in the brainstem, resulting in downstream, coordinated signals to different segments of the GI tract [5], [60]. It has been widely demonstrated the reflex excitation on antral motility [201], [204] and pyloric relaxation [222] via fundic distention. On the other hand, balloon distension of the duodenum could inhibit antral motility and increase pyloric tone [223], [224]. Speculatively, activation of different branches of the vagal afferents may result in selective and choreographic gastric motility. Indeed, I found that afferent VNS at 5Hz significantly promoted antral motility under a wide range of stimulus settings. This finding may suggest that the afferent fibers that are responsible for delivering excitatory response to the antrum are recruited under this stimulus frequency. When the stimulus frequency was increased to 10Hz, a higher stimulus dose resulted in a decrease in contraction amplitude, suggesting that a second group of fibers has been recruited. The second group of vagal afferents may convey reflex signals that go back to the stomach to activate relaxation of the smooth muscle via inhibitory vagal efferents, as similar finding was reported previously [225], [226]. Such relaxatory response is also consistent with my finding that a decrease in pyloric tone could be achieved at a similar stimulus dose. Taken together, electrical activation of the vagal afferent pathway into the central nervous system could potentially result in a more coordinated, physiological downstream signaling to different segments of the GI tract than direct efferent VNS.

5.4.3 **Limitations and Future Directions**

There are several limitations in this study. Firstly, the directionality of VNS was controlled by the placement of the cathode on the bipolar cuff electrode. This approach relies on the phenomenon known as “anodal block”, where the anode should be theoretically hyperpolarized and thus blocking the propagating CNAP evoked at the cathode. However, whether or not the evoked CNAP was indeed unidirectional was not confirmed in all rats. Although the stimulus-response maps show differential patterns between conditions within (afferent vs. combined afferent & efferent) and across (afferent vs. efferent) animals, I cannot rule out the possibility that the stimulation was not fully unidirectional. Additional experimentations (e.g. vagotomy, chemical nerve blockade, etc.) is required to affirm the directionality of VNS in future experiments.

Secondly, a majority of VNS-gastric studies were conducted on fasted animals. The pattern of pre-prandial gastric physiology is relatively more stable and predictable. However, postprandial gastric motility is a dynamic process that includes complex feedforward, feedback and local reflexes during digestion of a meal. It is therefore not unlikely that the VNS-induced gastric response observed in the present study might be biased by spontaneous changes from the gastric emptying process. Although the sequence of 24 VNS settings was randomized across animals so that the impact of spontaneous gastric activity could be counterbalanced, it remains an experimental challenge for screening the effect of various VNS parameters on the same animal within a single imaging session.

6. SUMMARY

6.1 Conclusion

Since the first use of MRI in imaging GI motility back in 1988, gastric MRI has demonstrated the potential in providing non-invasive, comprehensive assessments of gastric physiology and pathophysiology. Recent technical advances in the development of high-field MRI, rapid imaging sequences and multi-channel receive coils have allowed gastric MRI to provide further insights into mechanisms of symptoms and to characterize the efficacy of therapeutics. However, gastric MRI remains rarely used in clinical routine due to practical and technical reasons. There is currently no standardized test meal and imaging protocol, sufficient validation of outcome metrics, or automated postprocessing software that enables analysis of vast quantities of data. Moreover, the absence of animal gastric MRI severely limits its throughput in refinement and optimization of this technology and elucidating the mode of action of new therapeutics. To address these critical needs, I have first established 1) a highly-benign feeding protocol for rats to spontaneously consume a nutritionally complete meal, 2) a free-breathing MR imaging protocol that captures the digestive process in near real-time, and (3) algorithms for segmentation and quantification of stomach emptying and motility with extremely high temporal and spatial resolution [124]. The imaging protocol and analytical algorithms are readily translatable and applicable for human gastric MRI. Through open source (https://github.com/libilab/GastricMRI) and data sharing, this dissertation also delivers a public resource to gastric physiology and imaging communities. I expect the experimental and analytical protocols to become a standard in preclinical and clinical settings for assessing gastric physiology in health and diseases or when exposed to different therapeutics.

With the newly established gastric MRI protocol and analysis tools, I was able to characterize physiological changes in gastric emptying rate, antral motility, degree of pyloric opening, intestinal filling and absorption as the organ responded to vagus nerve stimulation. Although our understanding about the neuroanatomy of vagovagal circuitry has expanded substantially over the past three decades, the therapeutic potential of electrical stimulation of the vagus nerve in modulating gastric physiology has long been elusive due to the lack of appropriate physiological readout. In this regard, I revealed that stimulating the vagus nerve at the cervical level could

promote gastric emptying rate by enlarging the pyloric opening wider and longer measured with MRI [158]. The effect of vagal stimulation on gastric motility was further characterized under a wide range of stimulus settings. The MRI-based, non-invasive assessment provided new insights into the differential effects of afferent versus efferent VNS on gastric motility. Importantly, the findings presented in this dissertation converged to the general opinions on vagal effects on the enteric system. Taken together, I expect this experimental protocol could shed light on the use of gastric MRI for guiding and ultimately optimizing individualized neuromodulation protocol for treating gastric disorders.

6.2 Perspectives

Here, I will raise some important issues as well as challenges and opportunities that deserve future development and investigation.

6.2.1 Awake vs. Anesthetized Animal Model

The use of anesthetics is perhaps the only but the largest physiologically confounding factor in the current experimental setup; all animals were sedated with dexmedetomidine and low-dose Isoflurane (<0.5%). Anesthesia could have an impact on the excitability of the nerve and thus might have modulated gastric motility. Dexmedetomidine, also known as an agonist of α2-adrenergic receptors, has an inhibitory effect on the sympathetic system [222]. While the sympathetic nervous system primarily plays an inhibitory role on gastric motility [5], reducing sympathetic innervations on the GI tract may potentially alter the pattern of normal as well as VNS-induced gastric responses. Further experiments may be of interest to evaluate the VNS effect on animals under different anesthetics. Notably, recent developments in awake animal model for neuroimaging (e.g. functional MRI) [156], [157] highlight the opportunity and feasibility of conducting gastric MRI in conscious rats, thereby eliminating the confounding effect of anesthetics on gastric physiology.

6.2.2 4-Dimensional (3D+Time) Assessment of the Entire GI Tract

In addition to gastric emptying and motility, small bowel motility, bowel flow, colonic function and total gut transit are also important aspects of GI physiology and pathophysiology. Although intestinal MRI has been applied to humans [107], [175], the imaging strategy is often

limited to a single-slice method due to much faster intestinal motility (>10 cycles/min) than gastric motility (~3 cycles/min). The single-slice imaging approach could at best characterize the temporal information about the peristaltic and segmental activity in the small intestines, with the volumetric details being poorly informed. Small intestinal MRI is even more challenging to apply to animals because their intestinal motility are typically two to three folds faster than that in humans (e.g. 20~25 cycles/min in rats). Thanks to recent advances in parallel imaging and in-plane acceleration techniques, one of the future research directions should focus on more rapid MRI acquisition techniques in order to simultaneously survey the entire GI tract with sufficient spatial coverage and temporal resolution. As a result, one could not only examine gastric functions by utilizing the technology proposed in this dissertation but also expand and stimulate efforts in developing next-generation automated analysis of intestinal MRI data.

REFERENCES

[1] N. I. H. Department of Health and Human Services, "Opportunities and Challenges in Digestive Diseases Research: Recommendations of the National Commission on Digestive Diseases," *NIH Publ.*, pp. 08–6514, 2009.

[2] J. E. Everhart, "The burden of digestive diseases in the United States," *Bethesda, MD Natl. Inst. Diabetes Dig. Kidney Dis. US Dept Heal. Hum. Serv.*, 2008.

[3] T. L. Abell, V. K. Bernstein, T. Cutts, G. Farrugia, J. Forster, W. L. Hasler, R. W. McCallum, K. W. Olden, H. P. Parkman, and C. R. Parrish, "Treatment of gastroparesis: a multidisciplinary clinical review," *Neurogastroenterol. Motil.*, vol. 18, no. 4, pp. 263–283, 2006.

[4] R. A. Travagli, G. E. Hermann, K. N. Browning, and R. C. Rogers, "Brainstem Circuits Regulating Gastric Function," *Annu. Rev. Physiol.*, vol. 68, no. 1, pp. 279–305, 2006.

[5] K. N. Browning and R. A. Travagli, "Central nervous system control of gastrointestinal motility and secretion and modulation of gastrointestinal functions," *Compr. Physiol.*, vol. 4, no. 4, pp. 1339–1368, 2014.

[6] R. A. Travagli and L. Anselmi, "Vagal neurocircuitry and its influence on gastric motility," *Nat. Rev. Gastroenterol. Hepatol.*, vol. 13, no. 7, pp. 389–401, 2016.

[7] J. Zhang and J. D. Z. Chen, "Systematic review: applications and future of gastric electrical stimulation," *Aliment. Pharmacol. Ther.*, vol. 24, no. 7, pp. 991–1002, 2006.

[8] L. Sherwood, *Human physiology: from cells to systems*. 2015.

[9] T. L. Powley, E. A. Baronowsky, J. M. Gilbert, C. N. Hudson, F. N. Martin, J. K. Mason, J. L. McAdams, and R. J. Phillips, "Vagal afferent innervation of the lower esophageal sphincter," *Auton. Neurosci. Basic Clin.*, vol. 177, no. 2, pp. 129–142, 2013.

[10] H.-R. B. And and Terry L. Powley, "Vagal afferent innervation of the rat fundic stomach: Morphological characterization of the gastric tension receptor," *J. Comp. Neurol.*, vol. 319, no. 2, pp. 261–276, 1992.

[11] R. C. Rogers, D. M. McTigue, and G. E. Hermann, "Vagovagal reflex control of digestion: afferent modulation by neural and 'endoneurocrine' factors," *Am. J. Physiol. Liver Physiol.*, vol. 268, no. 1, pp. G1–G10, 1995.

[12] O. Al-Shboul, “The importance of interstitial cells of cajal in the gastrointestinal tract,” *Saudi J. Gastroenterol.*, vol. 19, no. 1, p. 3, 2013.

[13] T. H. H. Wang, P. Du, T. R. Angeli, N. Paskaranandavadivel, J. C. Erickson, T. L. Abell, L. K. Cheng, and G. O’Grady, “Relationships between gastric slow wave frequency, velocity, and extracellular amplitude studied by a joint experimental-theoretical approach,” *Neurogastroenterol. Motil.*, vol. 30, no. 1, pp. 1–9, 2018.

[14] M. M. Wolfe and A. H. Soll, “The Physiology of Gastric Acid Secretion,” *N. Engl. J. Med.*, vol. 319, no. 26, pp. 1707–1715, 1988.

[15] J. Keller, G. Bassotti, J. Clarke, P. Dinning, M. Fox, M. Grover, P. M. Hellström, M. Ke, P. Layer, C. Malagelada, H. P. Parkman, S. M. Scott, J. Tack, M. Simren, H. Törnblom, and M. Camilleri, “Expert consensus document: Advances in the diagnosis and classification of gastric and intestinal motility disorders,” *Nat. Rev. Gastroenterol. Hepatol.*, vol. 15, no. 5, pp. 291–308, 2018.

[16] P. Vanden Berghe, P. Janssen, S. Kindt, R. Vos, and J. Tack, “Contribution of different triggers to the gastric accommodation reflex in humans,” *Am. J. Physiol. Liver Physiol.*, vol. 297, no. 5, pp. G902–G906, 2009.

[17] F. Azpiroz and J. R. Malagelada, “Physiological variations in canine gastric tone measured by an electronic barostat,” *Am. J. Physiol.*, vol. 248, no. 2 Pt 1, 1985.

[18] M. M.J., H. P.J., and P. E.R., “Central vagal stimulation evokes gastric volume changes in mice: A novel technique using a miniaturized barostat,” *Neurogastroenterol. Motil.*, vol. 16, no. 1, pp. 5–11, 2004.

[19] M. L. Rouzade, J. Fioramonti, and L. Bueno, “Decrease in gastric sensitivity to distension by 5-HT1Areceptor agonists in rats,” *Dig. Dis. Sci.*, vol. 43, no. 9 SUPPL., pp. 2048–2054, 1998.

[20] J. Zhao, D. Liao, and H. Gregersen, “Tension and stress in the rat and rabbit stomach are location- and direction-dependent,” *Neurogastroenterol. Motil.*, vol. 17, no. 3, pp. 388–398, 2005.

[21] T. L. Abell, M. Camilleri, K. Donohoe, W. L. Hasler, H. C. Lin, A. H. Maurer, R. W. McCallum, T. Nowak, M. L. Nusynowitz, H. P. Parkman, P. Shreve, L. A. Szarka, W. J. Snape, and H. A. Ziessman, "Consensus recommendations for gastric emptying scintigraphy: A joint report of the American neurogastroenterology and motility society and the society of nuclear medicine," *Am. J. Gastroenterol.*, vol. 103, no. 3, pp. 753–763, 2008.

[22] D. M. Tang and F. K. Friedenberg, "Gastroparesis: Approach, Diagnostic Evaluation, and Management," *Disease-a-Month*, vol. 57, no. 2, pp. 74–101, 2011.

[23] B. Braden, S. Adams, L. P. Duan, K. H. Orth, F. D. Maul, B. Lembcke, G. Hör, and W. F. Caspary, "The [13C]acetate breath test accurately reflects gastric emptying of liquids in both liquid and semisolid test meals," *Gastroenterology*, vol. 108, no. 4, pp. 1048–1055, 1995.

[24] Y. F. Ghoos, B. D. Maes, B. J. Geypens, G. Mys, M. I. Hiele, P. J. Rutgeerts, and G. Vantrappen, "Measurement of gastric emptying rate of solids by means of a carbon-labeled octanoic acid breath test," *Gastroenterology*, vol. 104, no. 6, pp. 1640–1647, 1993.

[25] R. J. Fraser, M. Horowitz, A. F. Maddox, and J. Dent, "Postprandial antropyloroduodenal motility and gastric emptying in gastroparesis - effects of cisapride," *Gut*, vol. 35, no. 2, pp. 172–178, 1994.

[26] J. Desipio, F. K. Friedenberg, A. Korimilli, J. E. Richter, H. P. Parkman, and R. S. Fisher, "High-resolution solid-state manometry of the antropyloroduodenal region," *Neurogastroenterol. Motil.*, vol. 19, no. 3, pp. 188–195, 2007.

[27] L. A. Szarka and M. Camilleri, "Methods for measurement of gastric motility," *Am. J. Physiol. Liver Physiol.*, vol. 296, no. 3, pp. G461–G475, 2009.

[28] T. Hausken, S. Ødegaard, K. Matre, and A. Berstad, "Antroduodenal motility and movements of luminal contents studied by duplex sonography," *Gastroenterology*, vol. 102, no. 5, pp. 1583–1590, 1992.

[29] O. H. Gilja, T. Hausken, S. Ødegaard, and A. Berstad, "Ultrasonography and three-dimensional methods of the upper gastrointestinal tract," *Eur. J. Gastroenterol. Hepatol.*, vol. 17, no. 3, pp. 277–282, 2005.

[30] P. M. King, R. D. Adam, A. Pryde, W. N. McDicken, and R. C. Heading, "Relationships of human antroduodenal motility and transpyloric fluid movement: Non-invasive observations with real-time ultrasound," *Gut*, vol. 25, no. 12, pp. 1384–1391, 1984.

[31] C. Stendal, *Practical guide to gastrointestinal function testing*. 1997.

[32] A. J. Pullan, J. U. Egbuji, P. Du, L. K. Cheng, G. O'Grady, J. A. Windsor, and W. J. E. P. Lammers, "Origin and propagation of human gastric slow-wave activity defined by high-resolution mapping," *Am. J. Physiol. Liver Physiol.*, vol. 299, no. 3, pp. G585–G592, 2010.

[33] J. D. Z. Chen, Z. Lin, J. Pan, and R. W. Mccallum, "Abnormal gastric myoelectrical activity and delayed gastric emptying in patients with symptoms suggestive of gastroparesis," *Dig. Dis. Sci.*, vol. 41, no. 8, pp. 1538–1545, 1996.

[34] M. A. L. Edelbroek and M. A. L. Edelbroek, "Relationship between surface electrogastrography and antropyloric pressures," *Am. Physiol. Soc.*, vol. 268, no. 3, pp. G424–G430, 1995.

[35] B. Pfaffenbach, B. Wedmann, R. Adamek, and M. Wegener, "The significance of electrogastrographically determined amplitudes--is there a correlation to sonographically measured antral mechanical contractions?," *Z. Gastroenterol.*, vol. 33, no. 2, pp. 103–107, 1995.

[36] E. Rey, R. S. Choung, C. D. Schleck, A. R. Zinsmeister, N. J. Talley, and G. R. Locke, "Prevalence of hidden gastroparesis in the community: The gastroparesis 'iceberg,'" *J. Neurogastroenterol. Motil.*, vol. 18, no. 1, pp. 34–42, 2012.

[37] H. P. Parkman, "Idiopathic Gastroparesis," *Gastroenterol. Clin. North Am.*, vol. 44, no. 1, pp. 59–68, 2015.

[38] I. Soykan, B. Sivri, I. Sarosiek, B. Kiernan, and R. W. Mccallum, "Demography, clinical characteristics of patients with gastroparesis_1998_DDS.pdf," vol. 43, no. 11, pp. 2398–2404, 1998.

[39] H. Vittal, G. Farrugia, G. Gomez, and P. J. Pasricha, "Mechanisms of Disease: The pathological basis of gastroparesis - A review of experimental and clinical studies," *Nat. Clin. Pract. Gastroenterol. Hepatol.*, vol. 4, no. 6, pp. 336–346, 2007.

[40] J. G. Moore, P. E. Christian, J. A. Brown, C. Brophy, F. Datz, A. Taylor, and N. Alazraki, "Influence of meal weight and caloric content on gastric emptying of meals in man," *Dig. Dis. Sci.*, vol. 29, no. 6, pp. 513–519, 1984.

[41] J. G. Moore, P. E. Christian, and R. E. Coleman, "Gastric emptying of varying meal weight and composition in man," *Dig. Dis. Sci.*, vol. 26, no. 1, pp. 16–22, 2005.

[42] E. T. A. Friend and P. T. Page, "Gastroparesis and Diabetes," *Book*, pp. 1–7, 2006.

[43] A. Lee and B. Kuo, “Metoclopramide in the treatment of diabetic gastroparesis,” *Expert Rev. Endocrinol. Metab.*, vol. 5, no. 5, pp. 653–662, 2010.

[44] D. Silvers, M. Kipnes, V. Broadstone, D. Patterson, E. M. M. Quigley, R. McCallum, N. K. Leidy, C. Farup, Y. Liu, and A. Joslyn, “Domperidone in the management of symptoms of diabetic gastroparesis: efficacy, tolerability, and quality-of-life outcomes in a multicenter controlled trial,” *Clin. Ther.*, vol. 20, no. 3, pp. 438–453, 1998.

[45] R. Dhir and J. E. Richter, “Erythromycin in the short-and long-term control of dyspepsia symptoms in patients with gastroparesis,” *J. Clin. Gastroenterol.*, vol. 38, no. 3, pp. 237–242, 2004.

[46] J. Chen, P. Yeaton, and R. W. McCallum, “Effect of erythromycin on gastric myoelectrical activity in normal human subjects.,” *Am. J. Physiol.*, vol. 263, no. 1 Pt 1, pp. G24-8, 1992.

[47] O. H. Nielsen, K. Hvid-Jacobsen, P. Lund, and E. Langholz, “Gastric emptying and subjective symptoms of nausea: lack of effects of a 5-hydroxytryptamine-3 antagonist ondansetron on gastric emptying in patients with gastric stasis syndrome,” *Digestion*, vol. 46, no. 2, pp. 89–96, 1990.

[48] H. P. Parkman, W. L. Hasler, and R. S. Fisher, “American Gastroenterological Association medical position statement: diagnosis and treatment of gastroparesis,” *Gastroenterology*, vol. 127, no. 5, pp. 1589–1591, 2004.

[49] M. Camilleri, H. P. Parkman, M. A. Shafi, T. L. Abell, and L. Gerson, “Clinical guideline: management of gastroparesis,” *Am. J. Gastroenterol.*, vol. 108, no. 1, p. 18, 2013.

[50] S. Kim, I. Shin, J. Kim, H. Kang, J. Mun, S. Yang, and J. Yoon, “Mirtazapine for severe gastroparesis unresponsive to conventional prokinetic treatment,” *Psychosomatics*, vol. 47, no. 5, pp. 440–442, 2006.

[51] A. Patrick and O. Epstein, “Review article: gastroparesis,” *Aliment. Pharmacol. Ther.*, vol. 27, no. 9, pp. 724–740, Feb. 2008.

[52] R. J. Fontana and J. L. Barnett, “Jejunostomy tube placement in refractory diabetic gastroparesis: a retrospective review.,” *Am. J. Gastroenterol.*, vol. 91, no. 10, 1996.

[53] C. H. Kim and D. K. Nelson, “Venting percutaneous gastrostomy in the treatment of refractory idiopathic gastroparesis,” *Gastrointest. Endosc.*, vol. 47, no. 1, pp. 67–70, 1998.

[54] P. J. Pasricha, W. J. Ravich, and A. N. Kalloo, “Effects of intrasphincteric botulinum toxin on the lower esophageal sphincter in piglets,” *Gastroenterology*, vol. 105, no. 4, pp. 1045–1049, 1993.

[55] C. Montecucco and J. Molgó, “Botulinal neurotoxins: revival of an old killer,” *Curr. Opin. Pharmacol.*, vol. 5, no. 3, pp. 274–279, 2005.

[56] G.-Q. Song, Y. Lei, X. Xu, and J. D. Z. Chen, “Gastric electrical stimulation with long pulses in humans and animals: can data obtained in animals be replicated in humans?,” *Neuromodulation Technol. Neural Interface*, vol. 13, no. 2, pp. 87–92, 2010.

[57] T. L. Abell, J. Chen, A. Emmanuel, C. Jolley, A. I. Sarela, and H. Törnblom, “Neurostimulation of the gastrointestinal tract: Review of recent developments,” *Neuromodulation*, vol. 18, no. 3, pp. 221–227, 2015.

[58] J. Heckert, A. Sankineni, W. B. Hughes, S. Harbison, and H. Parkman, “Gastric Electric Stimulation for Refractory Gastroparesis: A Prospective Analysis of 151 Patients at a Single Center,” *Dig. Dis. Sci.*, vol. 61, no. 1, pp. 168–175, 2016.

[59] J. B. Frøkjær, S. Bergmann, C. Brock, A. Madzak, A. D. Farmer, J. Ellrich, and A. M. Drewes, “Modulation of vagal tone enhances gastroduodenal motility and reduces somatic pain sensitivity,” *Neurogastroenterol. Motil.*, vol. 28, no. 4, pp. 592–598, 2016.

[60] R. C. Rogers, G. E. Hermann, and R. A. Travagli, *Brainstem Control of Gastric Function*, First Edit., vol. 1. Elsevier Inc., 2006.

[61] R. A. Travagli, B. Neurosciences, and B. Sciences, “Novel transmitters in brainstem vagal neurocircuitry : new players on the pitch,” no. 717, 2018.

[62] P. Mabo, J.-L. Bonnet, C. Henry, D. Ojeda, A. Bel, H. Romero Ugalde, G. Carrault, C. Gallet, V. Le Rolle, and A. I. Hernández, “Acute effect of Vagus nerve stimulation parameters on cardiac chronotropic, inotropic, and dromotropic responses,” no. November 2017, p. 77, 2017.

[63] F. Giordano, A. Zicca, C. Barba, R. Guerrini, and L. Genitori, “Vagus nerve stimulation: Surgical technique of implantation and revision and related morbidity,” *Epilepsia*, 2017.

[64] V. A. . Pavlov and K. J. . Tracey, “The vagus nerve and the inflammatory reflex-linking immunity and metabolism,” *Nat. Rev. Endocrinol.*, vol. 8, pp. 743–754, 2012.

[65] F. A. Koopman, S. S. Chavan, S. Miljko, S. Grazio, S. Sokolovic, P. R. Schuurman, A. D. Mehta, Y. A. Levine, M. Faltys, R. Zitnik, K. J. Tracey, and P. P. Tak, "Vagus nerve stimulation inhibits cytokine production and attenuates disease severity in rheumatoid arthritis," *Proc. Natl. Acad. Sci.*, vol. 113, no. 29, pp. 8284–8289, 2016.

[66] K. W. Hatton and B. G. Fahy, "Vagal Nerve Stimulation and Reflux," *Anesth. Analg.*, vol. 105, no. 3, 2007.

[67] S. Ikramuddin, R. P. Blackstone, A. Brancatisano, J. Toouli, S. N. Shah, B. M. Wolfe, K. Fujioka, J. W. Maher, J. Swain, F. G. Que, J. M. Morton, D. B. Leslie, R. Brancatisano, L. Kow, R. W. O'Rourke, C. Deveney, M. Takata, C. J. Miller, M. B. Knudson, K. S. Tweden, S. A. Shikora, M. G. Sarr, and C. J. Billington, "Effect of Reversible Intermittent Intra-abdominal Vagal Nerve Blockade on Morbid Obesity," *Jama*, vol. 312, no. 9, p. 915, 2014.

[68] K. N. Browning, "Role of central vagal 5-HT3 receptors in gastrointestinal physiology and pathophysiology," *Front. Neurosci.*, vol. 9, no. OCT, pp. 1–10, 2015.

[69] T. L. Powley and R. J. Phillips, "Morphology and topography of vagal afferents innervating the GI tract," *Am. J. Physiol. Liver Physiol.*, 2002.

[70] H. Berthoud, N. R. Carlson, and T. L. Powley, "Topography of efferent vagal innervation of the rat gastrointestinal tract," *Am. J. Physiol. Integr. Comp. Physiol.*, vol. 260, no. 1, pp. R200–R207, 1991.

[71] T. L. Powley, J. C. Prechtl, E. A. Fox, and H.-R. Berthoud, "Anatomical considerations for surgery of the rat abdominal vagus: distribution, paraganglia and regeneration," *J. Auton. Nerv. Syst.*, no. 9, 1983.

[72] J. C. Prechtl and T. L. Powley, "The Fiber Composition of the Abdominal Vagus of the Rat," *Anat. Embryol. (Berl).*, vol. 181, no. 2, pp. 101–115, 1990.

[73] T. L. Powley, C. N. Hudson, J. L. Mcadams, E. A. Baronowsky, and R. J. Phillips, "Vagal Intramuscular Arrays: The Specialized Mechanoreceptor Arbors That Innervate the Smooth Muscle Layers of the Stomach Examined in the Rat," *J. Comp. Neurol.*, vol. 524, no. 4, pp. 713–737, 2016.

[74] D. J. Lomas, R. R. Sood, M. J. Graves, R. Miller, N. R. Hall, and A. K. Dixon, "Colon carcinoma: MR imaging with CO2 enema—pilot study," *Radiology*, vol. 219, no. 2, pp. 558–562, 2001.

[75] M. J. Graves, D. J. Lomas, E. Sala, I. J. Joubert, and S. H. Habib, "CO2 as a distending medium for gastric and small bowel MRI: a feasibility study," *Eur. Radiol.*, vol. 15, no. 4, pp. 672–676, 2005.

[76] D. J. Lomas and M. J. Graves, "Small bowel MRI using water as a contrast medium.," *Br. J. Radiol.*, vol. 72, no. 862, pp. 994–997, 1999.

[77] C. Tu, E. A. Osborne, and A. Y. Louie, "Activatable T 1 and T 2 magnetic resonance imaging contrast agents," *Ann. Biomed. Eng.*, vol. 39, no. 4, pp. 1335–1348, 2011.

[78] H.-J. Weinmann, R. C. Brasch, W.-R. Press, and G. E. Wesbey, "Characteristics of gadolinium-DTPA complex: a potential NMR contrast agent," *Am. J. Roentgenol.*, vol. 142, no. 3, pp. 619–624, 1984.

[79] F. Bloch, "Nuclear induction," *Phys. Rev.*, vol. 70, no. 7–8, p. 460, 1946.

[80] D. H. Carr, J. Brown, G. M. Bydder, R. E. Steiner, H. J. Weinmann, U. Speck, A. S. Hall, and I. R. Young, "Gadolinium-DTPA as a contrast agent in MRI: initial clinical experience in 20 patients," *Am. J. Roentgenol.*, vol. 143, no. 2, pp. 215–224, 1984.

[81] W. Schwizer, R. Fraser, H. Maecke, K. Siebold, R. Funck, and M. Fried, "Gd-DOTA as a gastrointestinal contrast agent for gastric emptying measurements with MRI," *Magn. Reson. Med.*, 1994.

[82] D. F. Evans, M. K. Stehling, G. Lamont, R. Coxon, A. M. Howseman, R. J. Ordridge, J. D. Hardcastle, and P. Mansfield, "INVESTIGATION OF GASTROINTESTINAL MOTILITY WITH ECHO PLANAR MAGNETIC-RESONANCE IMAGING (EPI)," in *Gut*, 1988, vol. 29, no. 10, pp. A1452–A1452.

[83] M. K. Stehling, D. F. Evans, G. Lamont, R. J. Ordidge, A. M. Howseman, B. Chapman, R. Coxon, P. Mansfield, J. D. Hardcastle, and R. E. Coupland, "Gastrointestinal tract: dynamic MR studies with echo-planar imaging.," *Radiology*, vol. 171, no. 1, pp. 41–46, 1989.

[84] J. Wright, D. Evans, P. Gowland, and P. Mansfield, "Validation of antroduodenal motility measurements made by echo-planar magnetic resonance imaging," no. August 1998, pp. 19–25, 1999.

[85] R. Treier, A. Steingoetter, D. Weishaupt, O. Goetze, P. Boesiger, M. Fried, and W. Schwizer, "Gastric motor function and emptying in the right decubitus and seated body position as assessed by magnetic resonance imaging," *J. Magn. Reson. Imaging*, vol. 23, no. 3, pp. 331–338, 2006.

[86] L. Marciani, P. a Gowland, R. C. Spiller, P. Manoj, R. J. Moore, P. Young, and a J. Fillery-Travis, "Effect of meal viscosity and nutrients on satiety, intragastric dilution, and emptying assessed by MRI.," *Am. J. Physiol. Gastrointest. Liver Physiol.*, vol. 280, no. 6, pp. G1227–G1233, 2001.

[87] M. A. Kwiatek, D. Menne, A. Steingoetter, O. Goetze, Z. Forras-Kaufman, E. Kaufman, H. Fruehauf, P. Boesiger, M. Fried, W. Schwizer, and M. R. Fox, "Effect of meal volume and calorie load on postprandial gastric function and emptying: studies under physiological conditions by combined fiber-optic pressure measurement and MRI," *AJP Gastrointest. Liver Physiol.*, vol. 297, no. 5, pp. G894–G901, 2009.

[88] A. Steingoetter, M. Fox, R. Treier, D. Weishaupt, B. Marincek, P. Boesiger, M. Fried, and W. Schwizer, "Effects of posture on the physiology of gastric emptying: A magnetic resonance imaging study," *Scand. J. Gastroenterol.*, vol. 41, no. 10, pp. 1155–1164, 2006.

[89] L. M. A. Ni, T. Y. A. No, S. Y. A. M. Ki, P. A. Gowland, S. Sciences, R. Centre, P. R. Unit, D. Division, and M. P. Corporation, "Effect of a novel 5-HT 3 receptor agonist MKC-733 on upper gastrointestinal motility in humans," *Aliment. Pharmacol. Ther.*, no. Mmc, pp. 1039–1048, 2003.

[90] I. M. de Zwart, B. Mearadji, H. J. Lamb, P. H. C. Eilers, A. A. M. Masclee, A. de Roos, and P. Kunz, "Gastric Motility: Comparison of Assessment with Real-Time MR Imaging or Barostat Measurement—Initial Experience," *Radiology*, vol. 224, no. 2, pp. 592–597, Aug. 2002.

[91] W. Schwizer, A. Steingoetter, and M. Fox, "Magnetic resonance imaging for the assessment of gastrointestinal function," *Scand. J. Gastroenterol.*, vol. 41, no. 11, pp. 1245–1260, 2006.

[92] P. Boulby, P. Gowland, V. Adams, and R. C. Spiller, "Use of echo planar imaging to demonstrate the effect of posture on the intragastric distribution and emptying of an oil/water meal," *Neurogastroenterol. Motil.*, vol. 9, no. 1, pp. 41–47, Mar. 1997.

[93] W. Schwizer, H. Maecke, and F. Michael, "Measurement of gastric emptying by magnetic resonance imaging in humans," *Gastroenterology*, vol. 103, no. 2, pp. 369–376, 1992.

[94] C. Feinle, P. Kunz, P. Boesiger, M. Fried, and W. Schwizer, "Scintigraphic validation of a magnetic resonance imaging method to study gastric emptying of a solid meal in humans," *Gut*, vol. 44, no. 1, p. 106 LP-111, Jan. 1999.

[95] C. L. Hoad, H. Parker, N. Hudders, C. Costigan, E. F. Cox, A. C. Perkins, P. E. Blackshaw, L. Marciani, R. C. Spiller, M. R. Fox, and P. A. Gowland, "Measurement of gastric meal and secretion volumes using magnetic resonance imaging," *Phys. Med. Biol.*, vol. 60, no. 3, pp. 1367–1383, 2015.

[96] O. Goetze, R. Treier, M. Fox, A. Steingoetter, M. Fried, P. Boesiger, and W. Schwizer, "The effect of gastric secretion on gastric physiology and emptying in the fasted and fed state assessed by magnetic resonance imaging," *Neurogastroenterol. Motil.*, vol. 21, no. 7, pp. 725–734, 2009.

[97] J. Fidler, A. E. Bharucha, M. Camilleri, J. Camp, D. Burton, R. Grimm, S. J. Riederer, R. A. Robb, and A. R. Zinsmeister, "Application of magnetic resonance imaging to measure fasting and postprandial volumes in humans," *Neurogastroenterol. Motil.*, vol. 21, no. 1, pp. 42–51, Jan. 2009.

[98] W. Ajaj, S. C. Goehde, N. Papanikolaou, G. Holtmann, S. G. Ruehm, J. F. Debatin, and T. C. Lauenstein, "Real time high resolution magnetic resonance imaging for the assessment of gastric motility disorders," *Gut*, vol. 53, no. 9, pp. 1256–1261, 2004.

[99] J. Borovicka, R. Lehmann, P. Kunz, R. Fraser M.B.B.S, C. Kreiss, G. Crelier, P. Boesiger, G. A. Spinas, M. Fried, and W. Schwizer, "Evaluation of gastric emptying and motility in diabetic gastroparesis with magnetic resonance imaging: effects of cisapride," *Am. J. Gastroenterol.*, vol. 94, no. 10, pp. 2866–2873, 1999.

[100] Y. Zhang, M. Brady, and S. Smith, "Segmentation of Brain MR Images Through a Hidden Markov Random Field Model and the Expectation-Maximization Algorithm," 2001.

[101] D. N. Greve and B. Fischl, "Accurate and robust brain image alignment using boundary-based registration," *Neuroimage*, vol. 48, no. 1, pp. 63–72, Oct. 2009.

[102] S. M. Smith, M. Jenkinson, M. W. Woolrich, C. F. Beckmann, T. E. J. Behrens, H. Johansen-Berg, P. R. Bannister, M. De Luca, I. Drobnjak, and D. E. Flitney, "Advances in functional and structural MR image analysis and implementation as FSL," *Neuroimage*, vol. 23, pp. S208–S219, 2004.

[103] R. W. Cox, "AFNI: software for analysis and visualization of functional magnetic resonance neuroimages," *Comput. Biomed. Res.*, vol. 29, no. 3, pp. 162–173, 1996.

[104] S. Banerjee, S. Dixit, M. Fox, and A. Pal, “Validation of a rapid, semiautomatic image analysis tool for measurement of gastric accommodation and emptying by magnetic resonance imaging,” *Am. J. Physiol. - Gastrointest. Liver Physiol.*, vol. 308, no. 8, pp. G652–G663, 2015.

[105] C. L. Hoad, H. Parker, N. Hudders, C. Costigan, E. F. Cox, A. C. Perkins, P. E. Blackshaw, L. Marciani, R. C. Spiller, M. R. Fox, and P. A. Gowland, “Measurement of gastric meal and secretion volumes using magnetic resonance imaging,” *Phys. Med. Biol.*, vol. 60, no. 3, pp. 1367–1383, 2015.

[106] S. Bickelhaupt, J. M. Froehlich, R. Cattin, S. Raible, H. Bouquet, U. Bill, and M. A. Patak, “Software-supported evaluation of gastric motility in MRI: A feasibility study,” *J. Med. Imaging Radiat. Oncol.*, vol. 58, no. 1, pp. 11–17, 2014.

[107] A. Menys, C. Hoad, R. Spiller, S. M. Scott, D. Atkinson, L. Marciani, and S. A. Taylor, “Spatio-temporal motility MRI analysis of the stomach and colon,” *Neurogastroenterol. Motil.*, vol. 0, no. 0, p. e13557, Feb. 2019.

[108] C. S. de Jonge, A. J. P. M. Smout, A. J. Nederveen, and J. Stoker, “Evaluation of gastrointestinal motility with MRI: Advances, challenges and opportunities,” *Neurogastroenterology and Motility*. 2018.

[109] X. Wan, P. Wedeking, and M. F. Tweedle, “Sources of heterogeneous contrast enhancement in the gastrointestinal tract,” *Magn. Reson. Imaging*, vol. 12, no. 7, pp. 1009–1012, 1994.

[110] X. Wan, P. Wedeking, and M. F. Tweedle, “MRI evaluation of potential gastrointestinal contrast media,” *Magn. Reson. Imaging*, vol. 13, no. 2, pp. 215–218, 1995.

[111] A. C. Ailiani, T. Neuberger, J. G. Brasseur, G. Banco, Y. Wang, N. B. Smith, and A. G. Webb, “Quantitative analysis of peristaltic and segmental motion in vivo in the rat small intestine using dynamic MRI,” *Magn. Reson. Med.*, vol. 62, no. 1, pp. 116–126, 2009.

[112] A. C. Ailiani, T. Neuberger, J. G. Brasseur, G. Banco, Y. Wang, N. B. Smith, and A. G. Webb, “Quantifying the effects of inactin vs Isoflurane anesthesia on gastrointestinal motility in rats using dynamic magnetic resonance imaging and spatio-temporal maps,” *Neurogastroenterol. Motil.*, vol. 26, no. 10, pp. 1477–1486, 2014.

[113] J. Liu, X. Qiao, and J. D. Z. Chen, “Vagal afferent is involved in short-pulse gastric electrical stimulation in rats.,” *Dig. Dis. Sci.*, vol. 49, no. 5, pp. 729–37, 2004.

[114] Y. Masuda, T. Tanaka, N. Inomata, N. Ohnuma, S. Tanaka, Z. Itoh, H. Hosoda, M. Kojima, and K. Kangawa, "Ghrelin stimulates gastric acid secretion and motility in rats," *Biochem. Biophys. Res. Commun.*, vol. 276, no. 3, pp. 905–908, 2000.

[115] C. D. R. Murray, N. M. Martin, M. Patterson, S. A. Taylor, M. A. Ghatei, M. A. Kamm, C. Johnston, S. R. Bloom, and A. V Emmanuel, "Ghrelin enhances gastric emptying in diabetic gastroparesis: a double blind, placebo controlled, crossover study," *Gut*, vol. 54, no. 12, pp. 1693–1698, 2005.

[116] G. J. Dockray, "Gastrointestinal hormones and the dialogue between gut and brain," *J. Physiol.*, vol. 592, no. 14, pp. 2927–2941, Jul. 2014.

[117] S. Murray, A. Tulloch, M. S. Gold, and N. M. Avena, "Hormonal and neural mechanisms of food reward, eating behaviour and obesity," *Nat. Rev. Endocrinol.*, vol. 10, no. 9, p. 540, 2014.

[118] T. Ishiguchi, S. Nishioka, and T. Takahashi, "Inhibitory neural pathway regulating gastric emptying in rats," *J. Auton. Nerv. Syst.*, vol. 79, no. 1, pp. 45–51, 2000.

[119] G. Krolczyk, D. Zurowski, J. Sobocki, M. P. Slowiaczek, J. Laskiewicz, A. Matyja, K. Zaraska, W. Zaraska, and P. J. Thor, "Effects of continuous microchip (MC) vagal neuromodulation on gastrointestinal function in rats," *J. Physiol. Pharmacol.*, vol. 52, no. 4 I, pp. 705–715, 2001.

[120] K. Ataka, A. Inui, A. Asakawa, I. Kato, and M. Fujimiya, "Obestatin inhibits motor activity in the antrum and duodenum in the fed state of conscious rats," *AJP Gastrointest. Liver Physiol.*, vol. 294, no. 5, pp. G1210–G1218, 2008.

[121] J. Jordi, F. Verrey, and T. A. Lutz, "Simultaneous assessment of gastric emptying and secretion in rats by a novel computed tomography-based method," *AJP Gastrointest. Liver Physiol.*, vol. 306, no. 3, pp. G173–G182, 2014.

[122] L. Marciani, "Assessment of gastrointestinal motor functions by MRI: A comprehensive review," *Neurogastroenterol. Motil.*, vol. 23, no. 5, pp. 399–407, 2011.

[123] A. E. Bharucha, R. A. Karwoski, J. Fidler, D. R. Holmes, R. A. Robb, S. J. Riederer, and A. R. Zinsmeister, "Comparison of manual and semiautomated techniques for analyzing gastric volumes with MRI in humans," *AJP Gastrointest. Liver Physiol.*, vol. 307, no. 5, pp. G582–G587, 2014.

[124] K.-H. Lu, J. Cao, S. Oleson, T. L. Powley, and Z. Liu, "Contrast Enhanced Magnetic Resonance Imaging of Gastric Emptying and Motility in Rats," *IEEE Trans. Biomed. Eng.*, vol. 9294, no. c, pp. 1–1, 2017.

[125] J. E. Thomas, "Mechanics and regulation of gastric emptying," *Physiol. Rev.*, vol. 37, no. 4, pp. 453–474, 1957.

[126] H. P. Parkman, W. L. Hasler, and R. S. Fisher, "American Gastroenterological Association technical review on the diagnosis and treatment of gastroparesis," *Gastroenterology*, vol. 127, no. 5, pp. 1592–1622, 2004.

[127] S. C. Woods and R. J. Seeley, "Understanding the physiology of obesity: review of recent developments in obesity research," *Int. J. Obes.*, vol. 26, no. S4, p. S8, 2002.

[128] H. B. El–Serag, "Time trends of gastroesophageal reflux disease: a systematic review," *Clin. Gastroenterol. Hepatol.*, vol. 5, no. 1, pp. 17–26, 2007.

[129] O. Couturier, C. Bodet-Milin, S. Querellou, T. Carlier, A. Turzo, and Y. Bizais, "Gastric scintigraphy with a liquid–solid radiolabelled meal: performances of solid and liquid parameters," *Nucl. Med. Commun.*, vol. 25, no. 11, pp. 1143–1150, 2004.

[130] H. U. De Schepper, F. Cremonini, D. Chitkara, and M. Camilleri, "Assessment of gastric accommodation: overview and evaluation of current methods," *Neurogastroenterol. Motil.*, vol. 16, no. 3, pp. 275–285, 2004.

[131] F. Azpiroz and J.-R. Malagelada, "Gastric tone measured by an electronic barostat in health arid postsurgical gastroparesis," *Gastroenterology*, vol. 92, no. 4, pp. 934–943, 1987.

[132] I. M. de Zwart, J. J. L. Haans, P. Verbeek, P. H. C. Eilers, A. de Roos, and A. A. M. Masclee, "Gastric accommodation and motility are influenced by the barostat device: assessment with magnetic resonance imaging," *Am. J. Physiol. Liver Physiol.*, vol. 292, no. 1, pp. G208–G214, 2007.

[133] E. S. Björnsson and H. Abrahamsson, "Interdigestive gastroduodenal manometry in humans. Indication of duodenal phase III as a retroperistaltic pump," *Acta Physiol. Scand.*, vol. 153, no. 3, pp. 221–230, 1995.

[134] C. Feinle, P. Kunz, P. Boesiger, M. Fried, and W. Schwizer, "Scintigraphic validation of a magnetic resonance imaging method to study gastric emptying of a solid meal in humans," *Gut*, vol. 44, no. 1, pp. 106–111, 1999.

[135] D. M. Mudie, K. Murray, C. L. Hoad, S. E. Pritchard, M. C. Garnett, G. L. Amidon, P. A. Gowland, R. C. Spiller, G. E. Amidon, and L. Marciani, "Quantification of gastrointestinal liquid volumes and distribution following a 240 mL dose of water in the fasted state," *Mol. Pharm.*, vol. 11, no. 9, pp. 3039–3047, 2014.

[136] S. Baba, A. Sasaki, J. Nakajima, T. Obuchi, K. Koeda, and G. Wakabayashi, "Assessment of gastric motor function by cine magnetic resonance imaging," *J. Gastroenterol. Hepatol.*, vol. 24, no. 8, pp. 1401–1406, 2009.

[137] J. C. Bezdek, R. Ehrlich, and W. Full, "FCM: The fuzzy c-means clustering algorithm," *Comput. Geosci.*, vol. 10, no. 2–3, pp. 191–203, 1984.

[138] S. Lankton and A. Tannenbaum, "Localizing region-based active contours," *IEEE Trans. image Process.*, vol. 17, no. 11, pp. 2029–2039, 2008.

[139] S. G. Willet and J. C. Mills, "Stomach organ and cell lineage differentiation: from embryogenesis to adult homeostasis," *Cell. Mol. Gastroenterol. Hepatol.*, vol. 2, no. 5, pp. 546–559, 2016.

[140] N. Otsu, "A threshold selection method from gray-level histograms," *IEEE Trans. Syst. Man. Cybern.*, vol. 9, no. 1, pp. 62–66, 1979.

[141] L. Marciani, P. Young, J. Wright, R. Moore, N. Coleman, P. A. Gowland, and R. C. Spiller, "Antral motility measurements by magnetic resonance imaging," *Neurogastroenterol. Motil.*, vol. 13, no. 5, pp. 511–518, 2001.

[142] W. Schwizer, R. Fraser, H. Maecke, K. Siebold, R. Funck, and M. Fried, "Gd-DOTA as a gastrointestinal contrast agent for gastric emptying measurements with MRI," *Magn. Reson. Med.*, vol. 31, no. 4, pp. 388–393, 1994.

[143] P. Caravan, J. J. Ellison, T. J. McMurry, and R. B. Lauffer, "Gadolinium (III) chelates as MRI contrast agents: structure, dynamics, and applications," *Chem. Rev.*, vol. 99, no. 9, pp. 2293–2352, 1999.

[144] M. Rogosnitzky and S. Branch, "Gadolinium-based contrast agent toxicity: a review of known and proposed mechanisms," *Biometals*, vol. 29, no. 3, pp. 365–376, 2016.

[145] A. P. Brown, N. Dinger, and B. S. Levine, "Stress produced by gavage administration in the rat," *J. Am. Assoc. Lab. Anim. Sci.*, vol. 39, no. 1, pp. 17–21, 2000.

[146] S. Damsch, G. Eichenbaum, A. Tonelli, L. Lammens, K. Van den Bulck, B. Feyen, J. Vandenberghe, A. Megens, E. Knight, and M. Kelley, "Gavage-related reflux in rats: identification, pathogenesis, and toxicological implications," *Toxicol. Pathol.*, vol. 39, no. 2, pp. 348–360, 2011.

[147] M. Bonnichsen, N. Dragsted, and A. K. Hansen, "The welfare impact of gavaging laboratory rats," *Anim. WELFARE-POTTERS BAR THEN WHEATHAMPSTEAD-*, vol. 14, no. 3, p. 223, 2005.

[148] I. Kunstyr, K. Peters, and K. Gärtner, "Investigations on the function of the rat forestomach.," *Lab. Anim. Sci.*, vol. 26, no. 2 Pt l, pp. 166–170, 1976.

[149] K. Gärtner, "The forestomach of rats and mice, an effective device supporting digestive metabolism in muridae," *J. Exp. Anim. Sci.*, vol. 42, no. 1, pp. 1–20, 2002.

[150] M. Sauter, J. Curcic, D. Menne, O. Goetze, M. Fried, W. Schwizer, and A. Steingoetter, "Measuring the interaction of meal and gastric secretion: A combined quantitative magnetic resonance imaging and pharmacokinetic modeling approach," *Neurogastroenterol. Motil.*, vol. 24, no. 7, 2012.

[151] T. Asai, W. W. Mapleson, and I. Power, "Differential effects of clonidine and dexmedetomidine on gastric emptying and gastrointestinal transit in the rat.," *Br. J. Anaesth.*, vol. 78, no. 3, pp. 301–307, 1997.

[152] M. C. Torjman, J. I. Joseph, C. Munsick, M. Morishita, and Z. Grunwald, "Effects of Isoflurane on gastrointestinal motility after brief exposure in rats," *Int. J. Pharm.*, vol. 294, no. 1–2, pp. 65–71, 2005.

[153] H. Lu, Q. Zou, H. Gu, M. E. Raichle, E. A. Stein, and Y. Yang, "Rat brains also have a default mode network," *Proc. Natl. Acad. Sci.*, vol. 109, no. 10, pp. 3979–3984, 2012.

[154] L.-M. Hsu, X. Liang, H. Gu, J. K. Brynildsen, J. A. Stark, J. A. Ash, C.-P. Lin, H. Lu, P. R. Rapp, and E. A. Stein, "Constituents and functional implications of the rat default mode network," *Proc. Natl. Acad. Sci.*, vol. 113, no. 31, pp. E4541–E4547, 2016.

[155] J. Grandjean, A. Schroeter, I. Batata, and M. Rudin, "Optimization of anesthesia protocol for resting-state fMRI in mice based on differential effects of anesthetics on functional connectivity patterns," *Neuroimage*, vol. 102, pp. 838–847, 2014.

[156] Z. Liang, J. King, and N. Zhang, "Uncovering intrinsic connectional architecture of functional networks in awake rat brain," *J. Neurosci.*, vol. 31, no. 10, pp. 3776–3783, 2011.

[157] N. Zhang, P. Rane, W. Huang, Z. Liang, D. Kennedy, J. A. Frazier, and J. King, "Mapping resting-state brain networks in conscious animals," *J. Neurosci. Methods*, vol. 189, no. 2, pp. 186–196, 2010.

[158] K. H. Lu, J. Cao, S. Oleson, M. P. Ward, R. J. Phillips, T. L. Powley, and Z. Liu, "Vagus nerve stimulation promotes gastric emptying by increasing pyloric opening measured with magnetic resonance imaging," *Neurogastroenterol. Motil.*, vol. 30, no. 10, 2018.

[159] M. Camilleri, J. Toouli, M. F. Herrera, B. Kulseng, L. Kow, J. P. Pantoja, R. Marvik, G. Johnsen, C. J. Billington, F. G. Moody, M. B. Knudson, K. S. Tweden, M. Vollmer, R. R. Wilson, and M. Anvari, "Intra-abdominal vagal blocking (VBLOC therapy): Clinical results with a new implantable medical device," *Surgery*, vol. 143, no. 6, pp. 723–731, 2008.

[160] M. G. Sarr, C. J. Billington, R. Brancatisano, A. Brancatisano, J. Toouli, L. Kow, N. T. Nguyen, R. Blackstone, J. W. Maher, S. Shikora, D. N. Reeds, J. C. Eagon, B. M. Wolfe, R. W. O'Rourke, K. Fujioka, M. Takata, J. M. Swain, J. M. Morton, S. Ikramuddin, M. Schweitzer, B. Chand, and R. Rosenthal, "The EMPOWER Study: Randomized, prospective, double-blind, multicenter trial of vagal blockade to induce weight loss in morbid obesity," *Obes. Surg.*, vol. 22, no. 11, pp. 1771–1782, 2012.

[161] R. W. McCallum, I. Sarosiek, H. P. Parkman, W. Snape, F. Brody, J. Wo, and T. Nowak, "Gastric electrical stimulation with Enterra therapy improves symptoms of idiopathic gastroparesis," *Neurogastroenterol. Motil.*, vol. 25, no. 10, p. 815, 2013.

[162] P. L. R. Andrews and G. J. Sanger, "Abdominal vagal afferent neurones: An important target for the treatment of gastrointestinal dysfunction," *Curr. Opin. Pharmacol.*, vol. 2, no. 6, pp. 650–656, 2002.

[163] R. A. Travagli, G. E. Hermann, K. N. Browning, R. C. Rogers, R. Travagli, G. E. Alberto, K. N. Hermann, R. C. R. Browning, and R. Alberto, "Musings on the Wanderer: What's New in our Understanding of Vago-Vagal Reflexes? III. Activity-dependent plasticity in vago-vagal reflexes controlling the stomach," 2003.

[164] C. Qin, Y. Sun, J. D. Z. Chen, and R. D. Foreman, "Gastric electrical stimulation modulates neuronal activity in nucleus tractus solitarii in rats," *Auton. Neurosci.*, vol. 119, no. 1, pp. 1–8, 2005.

[165] E. Ben-Menachem, “Vagus-nerve stimulation for the treatment of epilepsy,” *Lancet Neurol.*, vol. 1, no. 8, pp. 477–482, 2002.

[166] M. S. George, H. A. Sackeim, A. J. Rush, L. B. Marangell, Z. Nahas, M. M. Husain, S. Lisanby, T. Burt, J. Goldman, and J. C. Ballenger, “Vagus nerve stimulation: a new tool for brain research and therapy,” *Biol. Psychiatry*, vol. 47, no. 4, pp. 287–295, 2000.

[167] G. M. De Ferrari, H. J. G. M. Crijns, M. Borggrefe, G. Milasinovic, J. Smid, M. Zabel, A. Gavazzi, A. Sanzo, R. Dennert, and J. Kuschyk, “Chronic vagus nerve stimulation: a new and promising therapeutic approach for chronic heart failure,” *Eur. Heart J.*, vol. 32, no. 7, pp. 847–855, 2010.

[168] B. A. Malow, J. Edwards, M. Marzec, O. Sagher, and G. Fromes, “Effects of vagus nerve stimulation on respiration during sleep A pilot study,” *Neurology*, vol. 55, no. 10, pp. 1450–1454, 2000.

[169] W. J. de Jonge, E. P. van der Zanden, F. O. The, M. F. Bijlsma, D. J. van Westerloo, R. J. Bennink, H.-R. Berthoud, S. Uematsu, S. Akira, R. M. van den Wijngaard, and G. E. Boeckxstaens, “Stimulation of the vagus nerve attenuates macrophage activation by activating the Jak2-STAT3 signaling pathway,” *Nat. Immunol.*, vol. 6, no. 8, pp. 844–851, 2005.

[170] K. J. Tracey, L. V. Borovikova, S. Ivanova, M. Zhang, H. Yang, G. I. Botchkina, L. R. Watkins, H. Wang, N. Abumrad, and J. W. Eaton, “Vagus nerve stimulation attenuates the systemic inflammatory response to endotoxin.,” *Nature*, vol. 405, no. 6785, pp. 458–462, 2000.

[171] J. Martinson, “The Effect of Graded Stimulation of Efferent Vagal Nerve Fibres on Gastric Motility,” *Acta Physiol. Scand.*, vol. 62, no. 3, pp. 256–262, 1964.

[172] D. Grundy and T. Scratcherd, “Effect of Stimulation of the Vagus Nerve in Bursts on Gastric Acid Secretion and Motility in the Anaesthetized Ferret,” *Jour. Physiol.*, vol. 333, pp. 451–461, 1982.

[173] J. C. Eagon and K. A. Kelly, “Effect of electrical stimulation on gastric electrical activity, motility and emptying,” *Neurogastroenterol. Motil.*, vol. 7, no. 1, pp. 39–45, 1995.

[174] J. Curcic, M. Sauter, W. Schwizer, M. Fried, P. Boesiger, and A. Steingoetter, "Validation of a golden angle radial sequence (GOLD) for abdominal T1 mapping during free breathing: Demonstrating clinical feasibility for quantifying gastric secretion and emptying," *J. Magn. Reson. Imaging*, vol. 41, no. 1, pp. 157–164, 2015.

[175] A. Menys, S. A. Taylor, A. Emmanuel, A. Ahmed, A. A. Plumb, F. Odille, A. Alam, S. Halligan, and D. Atkinson, "Global Small Bowel Motility: Assessment with Dynamic MR Imaging," *Radiology*, vol. 269, no. 2, pp. 443–450, 2013.

[176] I. Locatelli, A. Mrhar, and M. Bogataj, "Gastric emptying of pellets under fasting conditions: A mathematical model," *Pharm. Res.*, vol. 26, no. 7, pp. 1607–1617, 2009.

[177] J. J. Gleysteen and E. G. Gohlke, "The antrum can control gastric emptying of liquid meals," *J. Surg. Res.*, vol. 26, no. 4, pp. 381–391, 1979.

[178] T. J. Stemper, "Gastric emptying and its relationship to antral contractile activity.," *Gastroenterology*, vol. 69, no. 3, pp. 649–653, 1975.

[179] U. T. Strunz and M. I. Grossman, "Effect of intragastric pressure on gastric emptying and secretion.," *Am. J. Physiol. Metab.*, vol. 235, no. 5, p. E552, 1978.

[180] K. A. Kelly, "Gastric emptying of liquids and solids: roles of proximal and distal stomach," *Am. J. Physiol. Liver Physiol.*, vol. 239, no. 2, pp. G71–G76, 1980.

[181] H. J. Ehrlein, "Inductographic studies on the pyloric sphincter," *Commun. Soil Sci. Plant Anal.*, vol. 1008, p. 493, 1992.

[182] R. Edin, H. Ahlman, and J. Kewenter, "The Vagal Control of the Feline Pyloric Sphincter," *Acta Physiol. Scand.*, vol. 107, no. 2, pp. 169–174, 1979.

[183] R. Edin, "The vagal control of the pyloric motor function: a physiological and immunohistochemical study in cat and man.," *Acta Physiol. Scand. Suppl.*, vol. 485, pp. 1–30, 1980.

[184] S. S. Mir, G. L. Telford, G. R. Mason, and H. S. Ormsbee, "Noncholinergic nonadrenergic inhibitory innervation of the canine pylorus," *Gastroenterology*, vol. 76, no. 6, pp. 1443–1448, 1979.

[185] C. H. Malbert, C. Mathis, and J. P. Laplace, "Vagal control of pyloric resistance," *Am. J. Physiol. Liver Physiol.*, vol. 269, no. 4, pp. G558–G569, 1995.

[186] T. Takahashi and C. Owyang, “Vagal control of nitric oxide and vasoactive intestinal polypeptide release in the regulation of gastric relaxation in rat.,” *J. Physiol.*, vol. 484, no. 2, pp. 481–492, 1995.

[187] J. Martinson, “Vagal Relaxation of the Stomach Experimental Re-investigation of the Concept of the Transmission Mechanism,” *Acta Physiol.*, vol. 64, no. 4, pp. 453–462, 1965.

[188] J. Martinson and A. Muren, “Excitatory and Inhibitory Effects of Vagus Stimulation on Gastric Motility in the Cat,” *Acta Physiol. Scand.*, vol. 57, no. 4, pp. 309–316, 1963.

[189] H.-D. Allescher, E. E. Daniel, J. Dent, J. E. T. Fox, and F. Kostolanska, “Extrinsic and Intrinsic Neural Control of Pyloric,” *J. Physiol.*, vol. 401, pp. 17–38, 1988.

[190] J. H. Szurszewski, “Modulation of smooth muscle by nervous activity: a review and a hypothesis,” in *Federation proceedings*, 1977, vol. 36, no. 10, pp. 2456–2461.

[191] J.-P. Miolan and C. Roman, “Discharge of efferent vagal fibers supplying gastric antrum: indirect study by nerve suture technique.,” *Am. J. Physiol. Metab.*, vol. 235, no. 4, p. E366, 1978.

[192] T. Wang, P. Du, T. R. Angeli, N. Paskaranandavadivel, J. C. Erickson, T. L. Abell, L. K. Cheng, and G. O’Grady, “Relationships between gastric slow wave frequency, velocity, and extracellular amplitude studied by a joint experimental-theoretical approach,” *Neurogastroenterol. Motil.*, vol. 30, no. 1, 2018.

[193] R. C. Rogers, G. E. Hermann, and R. A. Travagli, “Brainstem pathways responsible for oesophageal control of gastric motility and tone in the rat,” *J. Physiol.*, vol. 514, no. 2, pp. 369–383, 1999.

[194] A. Stengel and Y. Taché, “Neuroendocrine control of the gut during stress: corticotropin-releasing factor signaling pathways in the spotlight,” *Annu. Rev. Physiol.*, vol. 71, pp. 219–239, 2009.

[195] J. Zheng, A. Dobner, R. Babygirija, K. Ludwig, and T. Takahashi, “Effects of repeated restraint stress on gastric motility in rats,” *Am. J. Physiol. Integr. Comp. Physiol.*, vol. 296, no. 5, pp. R1358–R1365, 2009.

[196] M. Uchida and C. Iwamoto, “Influence of amino acids on gastric adaptive relaxation (accommodation) in rats as evaluated with a barostat,” *J. Smooth Muscle Res.*, vol. 52, pp. 56–65, 2016.

[197] O. H. Gilja, T. Hausken, I. Wilhelmsen, and A. Berstad, “Impaired accommodation of proximal stomach to a meal in functional dyspepsia,” *Dig. Dis. Sci.*, vol. 41, no. 4, pp. 689–696, 1996.

[198] C. C. Horn, J. L. Ardell, and L. E. Fisher, “Electroceutical Targeting of the Autonomic Nervous System,” *Physiology*, vol. 34, no. 2, pp. 150–162, 2019.

[199] N. Stakenborg, A. M. Wolthuis, P. J. Gomez-Pinilla, G. Farro, M. Di Giovangiulio, G. Bosmans, E. Labeeuw, M. Verhaegen, I. Depoortere, A. D’Hoore, G. Matteoli, and G. E. Boeckxstaens, “Abdominal vagus nerve stimulation as a new therapeutic approach to prevent postoperative ileus,” *Neurogastroenterol. Motil.*, vol. 29, no. 9, pp. 1–11, 2017.

[200] G. Jansson and J. Martinson, “Some Quantitative Considerations on Vagally Induced Relaxation of the Gastric Smooth Muscle in the Cat,” *Acta Physiol. Scand.*, vol. 63, no. 3, pp. 351–357, 1965.

[201] P. L. Andrews and T. Scratcherd, “The Gastric Motility Patterns Induced by Direct and Reflex Excitation of the Vagus Nerves in the Anaesthetized Ferret.,” *J. Physiol.*, vol. 302, no. 1, pp. 363–378, 1980.

[202] H. R. Berthoud, W. B. Laughton, and T. L. Powley, “Vagal Stimulation-Induced Gastric Acid Secretion in the Anesthetized Rat,” *J. Auton. Nerv. Syst.*, vol. 16, no. 3, pp. 193–204, 1986.

[203] H.-R. Berthoud, E. A. Fox, and T. L. Powley, “Abdominal Pathways and Central Origin of Rat Vagal Fibers That Stimulate Gastric Acid,” *Gastroenterology*, vol. 100, pp. 627–637, 1991.

[204] P. L. R. Andrews, D. Grundy, and T. Scratcherd, “Reflex excitation of antral motility induced by gastric distension in the ferret,” *J. Physiol.*, vol. 298, pp. 79–84, 1980.

[205] J. Burneo, E. Faught, R. Knowlton, R. Morawetz, and R. Kuzniecky, “Weight loss associated with vagus nerve stimulation,” *Neurology*, vol. 59, no. 3, pp. 463–464, 2002.

[206] J. V. Pardo, S. A. Sheikh, M. A. Kuskowski, C. Surerus-Johnson, M. C. Hagen, J. T. Lee, B. R. Rittberg, and D. E. Adson, “Weight loss during chronic, cervical vagus nerve stimulation in depressed patients with obesity: An observation,” *Int. J. Obes.*, vol. 31, no. 11, pp. 1756–1759, 2007.

[207] S. C. Cork, “The role of the vagus nerve in appetite control: Implications for the pathogenesis of obesity,” *J. Neuroendocrinol.*, vol. 30, no. 11, pp. 1–10, 2018.

[208] K. N. Browning, S. Verheijden, and G. E. Boeckxstaens, “The Vagus Nerve in Appetite Regulation, Mood, and Intestinal Inflammation,” *Gastroenterology*, vol. 152, no. 4, pp. 730–744, 2017.

[209] J. S. Bodenlos, K. L. Schneider, J. Oleski, K. Gordon, A. Rothschild, and S. L. Pagoto, “Vagus nerve stimulation and food intake: Effect of body mass index,” *J. Diabetes Sci. Technol.*, vol. 8, no. 3, pp. 590–595, 2014.

[210] G. S. Brindley and M. D. Craggs, “A technique for anodally blocking large nerve fibres through chronically implanted electrodes,” *J. Neurol. Neurosurg. Psychiatry*, vol. 43, no. 12, pp. 1083–1090, 1980.

[211] B. Zaaimi, R. Grebe, and F. Wallois, “Animal model of the short-term cardiorespiratory effects of intermittent vagus nerve stimulation,” *Auton. Neurosci. Basic Clin.*, vol. 143, no. 1–2, pp. 20–26, 2008.

[212] H. M. Stauss, “Differential hemodynamic and respiratory responses to right and left cervical vagal nerve stimulation in rats,” *Physiol. Rep.*, 2017.

[213] H. O. Veach, “Studies on the innervation of smooth muscle. I. Vagus effects on the lower end of the esophagus, cardia and stomach of the cat, and the stomach and lung of the turtle in relation to Wedensky inhibition.,” *Am. J. Physiol.*, vol. 71, no. 2, pp. 229–264, 1925.

[214] Y. Aihara, H. Nakamura, A. Sato, and S. A., “Relations Between Various Fiber Groups of Vagal and Spanchnic Nerves and Gastric Motility in Rats,” *Neurosci. Lett.*, vol. 10, pp. 281–286, 1978.

[215] K. M. Wasilczuk, K. Y. Qing, P. P. Irazoqui, M. P. Ward, P. P. Vlachos, C. J. Goergen, and E. H. Phillips, “B fibers are the best predictors of cardiac activity during Vagus nerve stimulation,” *Bioelectron. Med.*, vol. 4, no. 1, pp. 1–11, 2018.

[216] G. Gabella and H. L. Pease, “Number of axons in the abdominal vagus of the rat,” *Brain Res.*, vol. 58, no. 2, pp. 465–469, 1973.

[217] I. Bockx, K. Verdrengh, I. Vander Elst, J. van Pelt, F. Nevens, W. Laleman, and D. Cassiman, “High-frequency vagus nerve stimulation improves portal hypertension in cirrhotic rats,” *Gut*, vol. 61, no. 4, pp. 604–612, 2012.

[218] J. Martinson, “The Effect of Graded Vagal Stimulation on Gastric Motility, Secretion and Blood Flow in the Cat,” *Acta Physiol. Scand.*, vol. 65, no. 4, pp. 300–309, 1965.

[219] H. R. Berthoud and T. L. Powley, “Characteristics of gastric and pancreatic responses to vagal stimulation with varied frequencies: evidence for different fiber calibers?,” *J. Auton. Nerv. Syst.*, vol. 19, no. 1, pp. 77–84, 1987.

[220] M. C. Baccari, F. Calamai, and G. Staderini, “The influence of the vagally induced rebound contractions on the non-adrenergic, non-cholinergic (NANC) inhibitory motility of the rabbit stomach and the role of prostaglandins,” *J. Auton. Nerv. Syst.*, vol. 37, no. 2, pp. 125–135, 1992.

[221] H. R. Berthoud and W. L. Neuhuber, “Functional and chemical anatomy of the afferent vagal system,” *Auton. Neurosci. Basic Clin.*, vol. 85, no. 1–3, pp. 1–17, 2000.

[222] T. Ishiguchi, M. Nakajima, H. Sone, H. Tada, A. K. Kumagai, and T. Takahashi, “Gastric distension-induced pyloric relaxation: central nervous system regulation and effects of acute hyperglycaemia in the rat,” *J. Physiol.*, vol. 533, no. 3, pp. 801–813, 2004.

[223] A. Shafik, “Effect of duodenal distension on the pyloric sphincter and antrum and the gastric corpus: Duodenopyloric reflex,” *World J. Surg.*, vol. 22, no. 10, pp. 1061–1064, 1998.

[224] P. J. Treacy, G. G. Jamieson, and J. Dent, “the Effect of Duodenal Distension Upon Antro-Pyloric Motility and Liquid Gastric Emptying in Pigs,” *ANZ J. Surg.*, vol. 66, no. 1, pp. 37–40, 2008.

[225] D. S., B. M., and R. J.P., “Inhibition of antral and pyloric electrical activity by vagal afferent stimulation in the rabbit,” *J. Auton. Nerv. Syst.*, vol. 19, no. 1, pp. 13–20, 1987.

[226] S. Deloof, D. Croix, and G. Tramu, “The role of vasoactive intestinal polypeptide in the inhibition of antral and pyloric electrical activity in rabbits,” *J. Auton. Nerv. Syst.*, vol. 22, no. 2, pp. 167–173, 1988.

VITA

Kun-Han Lu is a Ph.D. candidate in the School of Electrical and Computer Engineering at Purdue University, West Lafayette, Indiana. He received his B.S. and M.S. degrees from National Taiwan University, Taipei, Taiwan in 2012 and 2014, respectively. He joined the Laboratory of Integrated Brain Imaging at Purdue University in August 2014. His research focus is on neural engineering, magnetic resonance imaging, image processing and bioelectric medicine. He has had multiple years of interdisciplinary training in conducting translational MRI research.

His primary research interest is in studying the interactions between the central nervous system and the peripheral organs. He has led and contributed to the development and dissemination of MR imaging techniques and analysis software for non-invasive assessment of brain and gut functions in human and animals. He has participated in several cross-institutional projects including the Stimulating Peripheral Activity to Relieve Conditions (SPARC) and the Defense Advanced Research Projects Agency (DARPA) Electrical Prescriptions (ElectRx) initiatives. His work has continuously been published in a number of first-author and co-authored peer-reviewed articles. His work has also won awards at the International Society for Magnetic Resonance in Medicine (ISMRM).

PUBLICATIONS

Peer-reviewed Journal Articles

1. **Lu K-H**, Cao J, Phillips R, Powley TL, Liu Z., "Differential Effects of Afferent and Efferent Vagus Nerve Stimulation on Gastric Motility Assessed with Magnetic Resonance Imaging," [In preparation]
2. **Lu K-H**, Cao J, Oleson S, Ward MP, Phillips R, Powley TL, Liu Z., "Vagus nerve stimulation promotes gastric emptying by increasing pyloric opening measured with magnetic resonance imaging," Neurogastroenterology & Motiliy, e13380, 2018. **[Cover Article]**
3. **Lu K-H**, Cao J, Oleson S, Powley TL, Liu Z, "Contrast enhanced magnetic resonance imaging of gastric emptying and motility in rats," IEEE Transactions on Biomedical Engineering, 64(11): 2546-2554, 2017. **[Feature Article]**
4. **Lu K-H**, Jeong J-H, Wen H, Liu Z, "Spontaneous activity in the visual cortex is organized by visual streams," Human Brain Mapping, 38(9): 4613-4630, 2017.
5. **Lu K-H**, Hung S, Wen H, Marussich L, Liu Z, "Influences of high-level features, gaze, and scene transitions on the reliability of BOLD responses to natural movie stimuli," PLoS ONE, 11(8): e0161797, 2016.
6. Lynch L, **Lu K-H**, Wen H, Zhang Y, Saykin AJ, Liu Z., "Task-evoked functional connectivity does not explain functional connectivity differences between rest and task conditions," Human Brain Mapping, 39: 4939-4948, 2018.
7. Somann J, Albors G, Neihouser K, **Lu K-H**, Liu Z, Durkes A, Robinson J, Powley TL, Irazoqui, P, "Chronic cuffing of cervical vagus nerve inhibits efferent fiber integrity in rat model," Journal of Neural Engineering, 15(3): 036018, 2018.
8. Cao J, **Lu K-H**, Powley TL, Liu Z, "Vagal nerve stimulation triggers widespread responses and alters large-scale functional connectivity in the rat brain," PLoS ONE, 12(2): e0189518, 2017.
9. Zhang Y, Chen G, Wen H., **Lu K-H**, Liu Z, "Musical imagery involves Wernicke's area in bilateral and anti-correlated network interactions in musicians," Scientific Reports, 7: 17066, 2017.

10. Oleson ST, **Lu K-H**, Liu Z, Durkes AC, Sivasankar PM, "Proton density weighted laryngeal MRI in systemically dehydrated rats," Laryngoscope, doi: 10.1002/lary.26978, 2017.
11. Wen H, Shi J, Zhang Y, **Lu K-H**, Cao J, Liu Z, "Neural encoding and decoding with deep learning for dynamic natural vision," Cerebral Cortex, doi: 10.1093/cercor/bhx268, 2017.
12. Marussich L, **Lu K-H**, Wen H, Liu Z, "Mapping white-matter functional organization at rest and during naturalistic visual perception," NeuroImage, 146: 1128-1141, 2017.
13. Cao J, **Lu K-H**, Oleson S, Phillips R, Jaffey D, Hendren C, Powley T, Liu Z., "Gastric Stimulation Drives Fast BOLD Responses of Neural Origin," [under review by NeuroImage]
14. Han K, Wen H, Shi J, **Lu K-H**, Liu Z., "Variational auto-encoder: an unsupervised model for modeling and decoding brain activity in visual cortex," [under review by NeuroImage]
15. Oleson ST, Duan C, **Lu K-H**, Calve S, Liu Z, Sivasankar PM, Durkes AC, "In Vivo Magnetic Resonance Imaging of Rat Vocal Fold Dehydration and Rehydration," [under review by Laryngoscope]

Conference Proceedings

Oral presentations

1. **Lu K-H**, Cao J, Phillips RJ, Powley TL, Liu Z, "Contrast-enhanced MRI reveals differential effects of afferent and efferent vagus nerve stimulation on gastric motility," the Scientific Meeting of the International Society of Magnetic Resonance for Medicine, 2019.
2. **Lu K-H**, Cao J, Phillips RJ, Powley TL, Liu Z, "Differential effects of afferent and efferent vagus nerve stimulation on gastric motility assessed with magnetic resonance imaging," International Society for Autonomic Neuroscience (ISAN), 2019.
3. **Lu K-H**, Cao J, Oleson S, Ward MP, Phillips RJ, Powley TL, Liu Z, "Vagus nerve stimulation promotes gastric emptying by increasing pyloric opening measured with magnetic resonance imaging," International Society for Autonomic Neuroscience (ISAN), 2019.

4. **Lu K-H**, Cao J, Oleson S, Ward MP, Powley TL, Liu Z, "Vagus nerve stimulation promotes gastric emptying in rat measured by magnetic resonance imaging," the Scientific Meeting of the International Society of Magnetic Resonance for Medicine, 2018. **[Magna Cum Laude Award]**
5. **Lu K-H**, Jeong JY, Wen H, Liu Z, "Spontaneous activity patterns reveal non-retinotopic functional parcellation and organization of human visual cortex," the Scientific Meeting of the International Society of Magnetic Resonance for Medicine, 2017. **[Summa Cum Laude Award]**
6. **Lu K-H**, Cao J, Marussich L, Hu TC, Liu Z, "Mapping abdominal inflammatory response using manganese-enhanced MRI (MEMRI)," the Scientific Meeting of the International Society of Magnetic Resonance for Medicine, 2017. **[Magna Cum Laude Award]**
7. Cao J, **Lu K-H**, Hendren C, Phillips RJ, Jaffey DM, Powley TL, Liu Z, "The Predominant Role of the Vagus Nerve in Gastric Electrical Stimulation Evoked Gut-Brain Axis," the Scientific Meeting of the International Society of Magnetic Resonance for Medicine, 2019.
8. Mandal R, Babaria N, Cao J, **Lu K-H**, Liu Z, "MRI Powered and Triggered Current Stimulator for Concurrent Stimulation and MRI," the Scientific Meeting of the International Society of Magnetic Resonance for Medicine, 2019.
9. Cao J, **Lu K-H**, Phillips R, Powley TL, Liu Z, "Visceral stimulation triggers high-frequency BOLD responses in the rat brain," the Scientific Meeting of the International Society of Magnetic Resonance for Medicine, 2018. **[Magna Cum Laude Award]**
10. Cao J, **Lu K-H**, Powley TL, Liu Z, "Vagus nerve stimulation evokes widespread BOLD responses in the rat brain," the Scientific Meeting of the International Society of Magnetic Resonance for Medicine, 2018. **[Magna Cum Laude Award]**
11. Oleson S, **Lu K-H**, Cao J, Liu Z, "In-vivo vagus nerve to central nervous system tracing using manganese enhanced magnetic resonance imaging," the Scientific Meeting of the International Society of Magnetic Resonance for Medicine, 2018.
12. Malandraki GA, Mourão LF, **Lu K-H**, Friel KM, Luchesi KF, Sheppard JJ, Gordon AM, Liu Z, "Functional and structural connectivity in children with unilateral cerebral palsy and clinical dysphagia: a multimodal neuroimaging study," the Annual European Society for Swallowing Disorders (ESSD) Congress, 2017. **[Best Abstract Award]**

13. Wen H, Shi J, **Lu K-H**, Zhang Y, Marussich L, Liu Z, “Decode cortical fMRI activity to reconstruct naturalistic movie via deep learning,” the Annual Meeting of the Organization for Human Brain Mapping, 2016. **[Merit Abstract Award]**

Poster presentations

1. **Lu K-H**, Wen H, Liu Z, “Fine-scale ICA Reveals Retinotopic Organization in the Visual Cortex under Natural Vision,” the Annual Meeting of the Organization for Human Brain Mapping, 2018.
2. **Lu K-H**, Wen H, Liu Z, “Sources of reliable fMRI responses to natural movie stimuli,” the Annual Meeting of the Organization for Human Brain Mapping, 2016.
3. Cao J, Mandal R, **Lu K-H**, Hendren C, Phillips RJ, Powley TL, Liu Z, “The brain responds to gastric electric stimulation with orientation selectivity,” International Society for Autonomic Neuroscience (ISAN), 2019.
4. Oleson S, **Lu K-H**, Cao J, Powley TL, Liu Z, “In-vivo Tracing of Vagal Projections to the Brain with Manganese Enhanced Magnetic Resonance Imaging,” International Society for Autonomic Neuroscience (ISAN), 2019.
5. Sclocco R, Nguyen C, Staley R, Fisher H, Garcia R, Hubbard C, Mendez A, **Lu K-H**, Liu Z, Ward MP, Powley TL, Kuo B, Napadow V, “In-vivo Tracing of Vagal Projections to the Brain with Manganese Enhanced Magnetic Resonance Imaging,” International Society for Autonomic Neuroscience (ISAN), 2019.
6. Lynch LK, **Lu K-H**, Wen H, Zhang Y, Saykin AJ, Liu Z, “Task-Evoked FC Does Not Explain FC Differences Between Rest and Task Conditions”, the Annual Meeting of the Organization for Human Brain Mapping, 2018.
7. Zhang Y, Wen H, **Lu K-H**, Liu Z, " Common and Distinct Cortical Network Bases of Musical Perception and Imagery," the Annual Meeting of the Organization for Human Brain Mapping, 2017.
8. Han K, Wen H, Shi J, **Lu K-H**, Liu Z, "Decoding Cortical Activity with Variational Autoencoder Supports Direct Visual Reconstruction," the Annual Meeting of the Organization for Human Brain Mapping, 2017.

9. Cao J, **Lu K-H**, Ward MP, Powley TP, Liu Z, "Neural and physiological responses to vagus nerve stimulation in rats," the Scientific Meeting of the International Society of Magnetic Resonance for Medicine, 2017. **[Magna Cum Laude Award]**
10. Marussich L, Lu K-H, Wen H, Liu Z, "Hierarchical clusters of white-matter fMRI are coupled with cortical visual networks," the Annual Meeting of the Organization for Human Brain Mapping, 2016.
11. Marussich L, Jeong JY, **Lu K-H**, Hung S-C, Liu Z, "Natural vision task partially reorganizes resting state networks," the Annual Meeting of the Organization for Human Brain Mapping, 2015.
12. Jeong JY, Druzbicki J, **Lu K-H**, Wen H, Liu Z, "Functional relevance of spatial ICA and k-means clustering," the Scientific Meeting of the International Society of Magnetic Resonance for Medicine, 2015.